TECHNICAL REPORT DOCUMENTATION PAGE

1. Report No. (FHWA-RD-95-###)	2. Government Accession No.	3. Recipient's Catalog No.
4. Title Shear strength of horizontally curved steel I-girders		5. Report Date: 6. Performing Organization Code:
7. Author(s): A. Zureick, D. White, N. Phoawanich, J. Park		8. Performing Organization Rpt. No.
9. Performing Organization Name and Address: Georgia Institute of Technology Structural Engineering, Mechanics, and Materials School of Civil and Environmental Engineering Atlanta, GA 30332-0355		10. Work Unit No. (TRAIS) (NCP number goes here) 11. Contract or Grant No.
12. Sponsoring Agency Name and Address		13. Type of Report / Period Covered 14. Sponsoring Agency Code

15. Supplementary Notes

Contracting Officer's Technical Representative (COTR) -- name of FHWA staff member, routing code)

16. Abstract

This report presents the results of four full-scale curved steel I girder component tests conducted to examine their shear behavior and to determine their maximum shear strengths. A web depth D of 1219 mm (48 in) and AASHTO M270 Grade 345 steel is selected for all of these girders. The nominal web thickness for the shear tests is selected as 8 mm (5/16 in), resulting in a nominal web slenderness D/t_w of 154. Two of the girders, referred to as S1 and S1-S, have a radius R = 63 630 mm (208.75 ft) and transverse stiffener spacing such that the ratio d_o/D is 3 for S1 and 1.5 for S1-S (producing d_o/R = 0.0575 and 0.0287 respectively). The other two test components, labeled as S2 and S2-S, are identical to S1 and S1-S except that their radii are 36 580 mm (120 ft), resulting in d_o/R = 0.10 and 0.050. All of the girders are braced against radial deflections at intervals of 3658 mm (12 ft) along the girder arc. Therefore, the ratio L_b/R is equal to 0.0575 for S1 and S1-S and 0.10 for S2 and S2-S, where L_b is the distance between the brace points along the girder arc. The above girders are instrumented to determine their maximum shear resistance as well as the mechanisms associated with the development of their shear strengths. Of particular interest is the extent to which the curved webs are capable of developing postbuckling strength, and the influence of the horizontal curvature and panel aspect ratio on the development of this strength.

17. Key Words	18. Distribution Statement		
Rehabilitation, strengthening, polymer, carbon fibers, composites, Testing			
19. Security Classif. (of this report)	20. Security Classif. (of this page)	21. No. of Pages (inc. front matter) 96	22. Price

LIST OF FIGURES

LIST OF FIGURES

LIST OF FIGURES

LIST OF TABLES

CHAPTER I - INTRODUCTION

With the increased usage of horizontally curved steel I girder bridges, the interest in understanding the behavior of and developing rational design guidelines for these types of structures has grown rapidly. One particular interest is the shear strength of curved I girders, an issue that has been studied analytically and experimentally by a number of investigators.

Prior research has shown that the elastic buckling strength of a curved web panel is greater than that of a straight girder panel with the same aspect ratio, material properties, web slenderness ratio, and boundary conditions (Mozer et al. 1970, 1971 and 1975; Mariani et al. 1973, Abdel-Sayed 1973; Davidson 1996; Lee and Yoo 1999b; White et al. 2001). However the increase in strength due to horizontal curvature is typically small relative to the shear capacity, and thus the *Guide Specifications for Horizontally Curved Highway Bridges* (AASHTO 2001a), hereafter referred to as the *2001 Guide Specifications*, ignore this benefit and utilize the same shear buckling strength equations as in the AASHTO Standard and LRFD provisions for straight I girders (AASHTO 2000, 2001b).

The experimental work of Mozer et al. (1970, 1971 and 1975) also indicated that horizontal curvature reduces the maximum shear strength of curved web panels from that of straight panels; however, the reduction for cases of practical values of horizontal curvature (e.g., $L_b/R \leq 0.10$) was found to be insignificant. Lee and Yoo (1999b) and White et al. (2001) have confirmed these findings analytically.

Despite the available analytical and numerical studies on the shear behavior and strength of curved I girders, no experimental tests of transversely-stiffened I girders with web slenderness $D/t_w > 70$ and panel aspect ratio $d_o/D > 1.33$ have been conducted. Mozer and Culver (1970) did

test girders with ($D/t_w = 188$, $d_o/D = 1$) and with ($D/t_w = 150$, $d_o/D = 1.33$), and I girders with similar parameters have been tested in Japan. These test limits appear to be related to the fact that the AASHTO design specifications in effect for straight I girders at the time of the early research on curved I girder bridges limited the panel aspect ratio to $d_o/D \leq 1$. As a result, the *2001 Guide Specifications* place the following significant restrictions on the design of curved I girder webs:

- The maximum web slenderness is limited to

$$\frac{D}{t_w} \leq 100 \tag{1}$$

for curved girders with unstiffened web panels (defined by $d_o/D > 1$) and a radius of curvature less than 213 m (700 ft). This restriction is relaxed to $D/t_w \leq 150$ for $R \geq 610$ m (2000 ft), with a linear transition in the D/t_w limit between these two radii, i.e., for $R \geq 213$ m,

$$\frac{D}{t_w} \leq 100 + 0.125(R - 213) \leq 150 \tag{2}$$

where R is expressed in m. The limit $D/t_w \leq 150$ is the maximum web slenderness permitted for unstiffened web panels in the LRFD straight girder Specifications (AASHTO 2001b), and is intended to facilitate handling during fabrication and erection. The limit of 100 is selected to satisfy approximately the web compactness provisions in AASHTO LRFD for $F_y = 345$ MPa (50 ksi), which is the maximum F_y allowed for the use of compact flange flexural strength equations in the *Guide Specifications* (AASHTO 2001a).

- The ratio d_o/D is restricted to be less than or equal to one in girders designed with stiffened web panels.

- The maximum web flexural stresses are limited to the elastic bend buckling stress under all loading conditions. Also, potential postbuckling contributions to the shear strength are neglected.

Hall et al. (1999) state in their discussion of new recommended research:

> **"Relief from this requirement [the limit of $d_o/D \leq 1$] for some curvatures can be justified with additional testing. Neither fatigue behavior nor strength of curved-girder webs is well understood at this time, and it would be risky to reduce the stiffening requirements without further analytical and experimental research.... Reduction of required web stiffening is one area where gains are possible.... Investigation of various types of web stiffening should be expanded for bending, shear, and combined bending and shear conditions.... The effect of stiffener spacing on the bend-buckling strength of curved girders with varying details is needed."**

1.1 OBJECTIVE AND SCOPE

This report presents the results of four full-scale curved steel I girder component tests conducted to examine their shear behavior and to determine their maximum shear strengths. A web depth D of 1219 mm (48 in) and AASHTO M270 Grade 345 steel is selected for all of these girders to match that of eight bending component specimens tested at the FHWA Turner Fairbank Laboratory (Hartmann and Wright 2001). The nominal web thickness for the shear tests is selected as 8 mm (5/16 in), resulting in a nominal web slenderness D/t_w of 154. Two of the girders, referred to as S1 and S1-S, have a radius R = 63 630 mm (208.75 ft) and transverse stiffener spacing such that the ratio d_o/D is 3 for S1 and 1.5 for S1-S (producing $d_o/R = 0.0575$ and 0.0287 respectively). The other two test components, labeled as S2 and S2-S, are identical to S1 and S1-S except that their radii are 36 580 mm (120 ft), resulting in $d_o/R = 0.10$ and 0.050. All of the girders are braced against radial deflections at intervals of 3658 mm (12 ft) along the

girder arc. Therefore, the ratio L_b/R is equal to 0.0575 for S1 and S1-S and 0.10 for S2 and S2-S, where L_b is the distance between the brace points along the girder arc.

The above girders are instrumented to determine their maximum shear resistance as well as the mechanisms associated with the development of their shear strengths. Of particular interest is the extent to which the curved webs are capable of developing postbuckling strength, and the influence of the horizontal curvature and panel aspect ratio on the development of this strength.

1.2 ORGANIZATION

The following chapter provides a detailed review of prior research on curved I girder web behavior and existing specification provisions for proportioning of horizontally curved I girder web panels. Although the complete range of issues associated with curved I girder web design is beyond the scope of this specific research, it is essential to understand the broad context within which the current research on maximum shear strength of curved I girder webs fits. This is followed in Chapter 3 by an overview of the geometry and boundary conditions for the four shear strength tests conducted in this research, and a detailed summary of the measured geometry and material properties for the test girders. Chapter 4 then describes the test apparatus and procedure. Chapter 5 discusses the test results, including comparisons with several strength models and their predictions, and conclusions are provided in Chapter 6.

CHAPTER II BACKGROUND

Requirements for proportioning of horizontally curved I girder web panels have been established in the past based essentially either on maximum elastic stress limits (including consideration of fatigue) or maximum strength considerations. Prior work concerning these requirements is reviewed below.

2.1 ELASTIC STRESS BASED WEB SLENDERNESS LIMITS (INCLUDING CONSIDERATION OF FATIGUE)

Culver et al. (1972a, b) were the first to develop recommended web slenderness limits for curved I girder webs. These investigators determined the values of D/t_w at various curvatures, quantified by the parameter d_o/R, to limit calculated web longitudinal plate bending stresses at transverse stiffeners to the same magnitude as in imperfect straight girder web panels with the same panel aspect ratio d_o/D, web slenderness $D/t_w = 200$, and out-of-flatness representative of AWS (1966) fabrication tolerances. Straight girders with a web slenderness of 200 were selected as a base in these studies since this value was approximately the upper limit on the web slenderness of straight girders at the time of the research. Culver et al. analyzed a range of cylindrically-curved web panels in doubly-symmetric girders with D/t_w up to 300, d_o/D from 0.67 to 1.5 and d_o/R up to 0.167. The resulting equation for the maximum D/t_w allowable within curved web panels can be written as

$$\frac{D}{t_w} \le 6.78 \sqrt{\frac{E}{F_y}} \left[1 - 8.6\frac{d_o}{R} + 34\left(\frac{d_o}{R}\right)^2 \right] \tag{3}$$

In the limit that R goes to infinity, this equation reduces to the restriction on the maximum slenderness of straight I girder webs within the AASHTO straight girder Specifications (AASHTO 2000, 2001b), which defines an upper bound below which fatigue due to excessive web lateral deflections is not a consideration. This limit is based on the research by Yen and Muller (1966) and Muller and Yen (1968). The dependency of Eq. (3) on F_y indirectly reflects the tendency of bridges designed with higher yield strength steels to be subjected to larger applied stresses. Culver et al. (1972a) stated that, "Until fatigue test data are obtained for curved girders, this reduction [Eq. (3)] or essentially limiting D/t_w for highly curved girders to existing limits in the working stress portion of the AASHO specifications appears to be warranted."

In the analyses conducted by Culver et al. (1972a, b), the web panel was modeled as a series of isolated unit cylindrical strips on an elastic foundation, subjected to a radial pressure loading per (Wachowiak 1967) to simulate the effect of horizontal curvature. The radial displacements at the web boundaries were assumed to be zero. An extension of this work was published a year later, when Culver et al. (1973) used a shell model to examine the accuracy of the cylindrical strip idealization. This work also included consideration of longitudinal stiffeners. In both (Culver 1972) and (Culver et al. 1973), the investigators showed that the magnitude of the longitudinal web plate bending stresses was significantly affected by the spring constant of the equivalant elastic foundation associated with the plate action between the girder flanges (or the flanges and the longitudinal stiffeners). Also, both (Culver et al. 1972a and 1973) show a significant increase in the calculated longitudinal web plate bending stresses at the transverse stiffeners with decreasing panel aspect ratio d_o/D. However, they found that the required reduction in D/t_w (for the above stresses to be the same magnitude in curved web panels as in imperfect straight web panels with the same d_o/D) to be insensitive to the spring constant and the value of d_o/D.

Nevertheless, their computed web plate bending stresses ranged from as low as nine percent to as high as 44 percent of the yield strength of A36 steel (for $d_o/D = 1.5$ and the largest spring constant versus $d_o/D = 0.67$ and the smallest spring constant) (Culver et al. 1973). Since the web fatigue behavior should be related to the stress magnitudes, it is possible that a more rational assessment of fatigue might be attained with a basis different than that of equating web plate bending stresses in curved and straight web panels without regard for the magnitude of the stresses, as in the above.

Daniels and Herbein (1980) conducted the only experimental research in the U.S. regarding fatigue of curved steel bridge I girders. These investigators studied the performance of thin webs in a number of homogeneous noncomposite doubly-symmetric I girders. Based on this research, Daniels et al. (1980) concluded that Eq. (3) was too severe and proposed the following more liberal equations (expressed here in a nondimensionalized form):

$$\frac{D}{t_w} \le 4.27 \sqrt{\frac{E}{f_b}} \left[1 - 4\frac{d_o}{R} \right] \le 170 \tag{4}$$

for allowable stress design and

$$\frac{D}{t_w} \le 6.78 \sqrt{\frac{E}{F_y}} \left[1 - 4\frac{d_o}{R} \right] \le 192 \tag{5}$$

for load factor design.

Daniels et al. (1980) arrived at Eqs. (4) and (5) by observing that the radial deflections at the web-to-flange boundaries in curved I girders tend to reduce the relative web transverse displacements and the corresponding plate bending stresses. The analyses by Culver et al. (1972a, b, 1973) did not consider these effects. The girders tested by Daniels and Herbein (1980) exceeded the Eq. (3) limits in all cases, but no fatigue crack developed along the web boundaries. The web

slenderness D/t_w ranged from 139 to 192 and the panel aspect ratio d_o/D ranged from to 2.03 to 2.36 in these girders. In the development of their design recommendations Daniels et al. (1980) state, "To estimate the lateral deflections of the web boundaries would be mathematically highly involved, if not impossible. Thus, a rigorous reexamination of the web boundary bending stresses is not warranted for the sake of establishing web slenderness ratios. A relatively simple although empirical way to liberate the slenderness reduction factor is to reduce the (CURT) adopted initial out-of-straightness." Daniels et al. (1980) developed Eqs. (4) and (5) simply by assuming an initial web out-of-straightness of one-half that assumed by Culver et al. (1972a, b, 1973). Equation (4) is adopted within the allowable stress design portion of the *AASHTO Guide Specifications for Horizontally Curved Highway Bridges* (AASHTO 1993). However, the load factor design portion of these specifications still retains Eq. (3).

More recently, Davidson et al. (1999) developed a conservative multiplier that can be applied to the stress at the web-flange juncture of a curved I girder (calculated by beam theory as $f = -My/I$) to obtain an estimate of the maximum von Mises stress in the web, located at the web-flange juncture, including geometric nonlinear plate bending effects. This multiplier takes the form

$$\psi_w = \left[1 + 1.5\sqrt{\frac{D_c}{R}}\right]\sqrt{1 + 0.161\frac{D_c}{t_w}\frac{D_c}{R} + 0.128\left(\frac{D_c}{t_w}\right)^2\left(\frac{D_c}{R}\right)^2} \tag{6}$$

where D_c is the depth of the web in compression. Davidson et al. (1999) also propose a reduction factor on the web slenderness D/t_w that can be applied as an alternative to the bracketed terms in Eqs. (3) through (5) by taking the inverse square root of Eq. (6), i.e.,

$$R_s = \sqrt{\frac{1}{\psi_w}} \tag{7}$$

Although there is no theoretical basis for this equation, it fits closely with the reduction proposed by Daniels et al. (1980) and with a separate equation for the maximum D/t_w in curved I girders proposed in (Nakai et al. 1986; Nakai and Yoo 1988). The D/t_w limit proposed by Nakai et al. (1986) is based on equating the plate bending stresses within curved and equivalent imperfect straight girder web panels, similar to the basis for the equations proposed by Culver et al. (1972a, b, 1973). The analyses by Davidson et al. (1999) were conducted on isolated curved web panels with the vertical bending moments applied as an idealized linear stress distribution through the depth of the cross-section at the ends of the panel.

Davidson et al. (2000) extended the above research on behavior of curved webs subjected to uniform vertical bending to include the effects of combined bending and shear. The shearing in the web was induced by applying shear tractions along the four panel edges. They found that the addition of shear tends to give a small increase in the transverse "bulging" displacements within the panel and the maximum stress at the top of the web, along with a further reduction in the girder moment at first yield (with first yield calculated including the effect of plate bending stresses). However, since the increase in the maximum stress due to added shear was small, they found that Eq. (6) from (Davidson et al. 1999) was still conservative.

The general trends observed by (Davidson et al. 1999 and 2000) were also observed by Mikami and Furunishi (1984), who also studied the nonlinear behavior of isolated cylindrical web panels subjected to uniform vertical bending and combined bending and shear edge tractions. In summary, both Davidson and Mikami and Furnishi found that:

- The web membrane stress associated with the overall bending of the girder tends to decrease as the horizontal curvature increases, and as a result, the bending moment carried by the web panel is reduced.

- A web panel subjected to combined bending and shear has smaller web membrane stresses due to vertical bending compared with the same panel under uniform vertical bending.
- The web plate bending stresses under combined bending and shear are larger than those under uniform vertical bending.

Unfortunately, Davidson et al. (1999 and 2000) apply Eq. (6) in calculating the maximum girder flexural strength, effectively basing the vertical bending strength of the curved I girder on a criterion that the localized maximum von Mises stress at the web flange juncture (including the plate bending stresses, but neglecting contributions of residual stresses due to cutting and welding of the web plate) should never exceed the yield strength of the material. Their approach for estimating web plate bending stresss may be valuable for assessment of fatigue. However, in the view of the authors, there is no reason why an I girder web needs to be limited to nominal first yield under maximum strength loading conditions. It can be shown that generally, the overall contribution of the web to both vertical and lateral bending is relatively small compared to that of the flanges of an I girder. It should be possible to allow some yielding within a noncompact or slender curved web at maximum strength load levels without any significant detriment to the overall girder vertical and/or lateral bending capacity. This issue is addressed within the context of curved homogenous I girders in the parametric studies by White et al. (2001). Also, an analogy can be drawn with the design of straight hybrid I girders. In hybrid I girder design, the web is allowed to yield under the maximum design loading conditions, regardless of whether it is compact or not (Schilling and Frost 1964; Schilling 1968; ASCE 1968). The reduction in the flexural capacity due to web yielding and web bend buckling is accounted for within the hybrid R_h and load-shedding R_b factors of the AASHTO (2001b) Specifications. The capacity of a hybrid girder does not need to be limited to first yielding of the web.

The *Guide Specifications* (AASHTO 2001a) do not adopt any of the above equations for a maximum allowable D/t_w. Rather, these specifications limit the nominal web stress due to vertical bending of the I girder to the web bend buckling stress, and the limit the web shear force to the elastic or inelastic shear buckling load. Hall et al. (1999) evaluated the prior research pertaining to the fatigue of curved I girder webs, and concluded that fatigue issues due to web plate bending can be avoided if the web stresses are maintained below these buckling strengths (Hall 2000). There is precedent for limiting the web to its elastic bend buckling and elastic/inelastic shear buckling strength to avoid fatigue issues in straight I girder webs (Patterson et al. 1970, Galambos et al. 1977, Fisher et al. 1979, Montgomery 1987, Nowak et al. 1993, Okura et al. 1993 and AASHTO 2001b). Duchene and Maquoi (1985) and Remadi et al. (1985) show a clear correlation between significant increases in the maximum surface stresses perpendicular to the flange or to the transverse stiffeners at the web boundaries and exceeding of the web critical stress in models of straight I girder webs. However, the *Guide Specifications* restrict the web to these buckling strengths under all loading combinations, whereas the LRFD Specifications (AASHTO 2001b) apply this limit only under fatigue loading conditions.

The theoretical web elastic bend buckling stress is expressed in the *2001 Guide Specifications* as

$$f_{bw} \le \left[\frac{\pi^2 Ek}{12(1-\nu^2)\left(\frac{D}{t_w}\right)^2} = \frac{0.9Ek}{\left(\frac{D}{t_w}\right)^2} \right] \le F_y \tag{8}$$

where

$$k = 7.2\left(\frac{D}{D_c}\right)^2 \ge 7.2 \tag{9}$$

for unstiffened webs and

$$k = 9\left(\frac{D}{D_c}\right)^2 \geq 7.2 \tag{10}$$

for stiffened web panels. The multiplier 7.2 in Eq. (5) results in a bend-buckling coefficient of 28.8 for doubly symmetric girders. This is close to the theoretical value of k = 24 for webs with $D_c = D/2$ and simply supported boundary conditions on their longitudinal edges. The multiplier 9 in Eq. (6) gives a k of 36 for a doubly symmetric girder, which is approximately 80 percent of the difference between the buckling coefficient for simply supported and fully restrained longitudinal edge conditions. Equation (5) is used implicitly in the current AASHTO LRFD Specifications for representation of the bend-buckling resistance within the load-shedding parameter R_b for sections with $D_c > D/2$, and Eq. (6) gives the bend-buckling coefficient implicitly used within R_b for sections with $D_c \leq D/2$. Hall et al. (1999) explain that the smaller bend-buckling coefficient is used for unstiffened webs to account conservatively for potential moment-shear interaction effects. Also, they explain that the more liberal value is utilized for stiffened web panels since the reserve postbuckling strength of the panel in bending and in shear is ignored. The lower limit of 7.2 on the value of k is approximately equal to the theoretical buckling coefficient for a web plate under uniform compression assuming clamped boundary conditions at the flanges (SSRC 1998).

For $d_o/D \leq 1$, the limit on D/t_w based on Eq. (8), applied to all loading conditions, is typically more restrictive than the Daniels et al. (1980) load factor design equation (Eq. (5)). However, for $d_o/D > 1$, the Daniels et al. equation can be more restrictive than the (AASHTO 2001a) limits on D/t_w. The reader can verify these observations by assuming $f_{bw} = F_y = 345$ MPa (50 ksi) under the maximum strength loading conditions along with Eq. (8), and comparing

the result to Eq. (5). By restricting the web slenderness based on Eq. (8), the *2001 Guide Specifications* (AASHTO 2001a) consider directly the effect of girder monosymmetry in limiting the web slenderness that can be used in design. It should be noted that although Eq. (5) can be more restrictive than Eq. (8) for $d_o/D > 1$, Eqs. (1) and (2) still can be more critical than Eq. (5).

The current LRFD Specifications (AASHTO 2001b) limit the web in straight I girders to the elastic bend or shear buckling strength only under fatigue loading conditions. With further research, it may be possible to liberalize the limits specified by the *2001 Guide Specifications* and by Daniels et al. (1980). For instance, it may be possible to avoid fatigue issues by restricting the web stresses to the elastic buckling stress only under fatigue loading conditions up to some curvature limit. However, combined shear and bending may need to be considered, e.g., by using a reduced value for the buckling coefficient as in Eq. (5), if fatigue issues are to be addressed based on an elastic buckling limit under fatigue loading conditions only.

2.2 WEB REQUIREMENTS BASED ON STRENGTH

The issues associated with horizontally curved I girder web panels and maximum strength include:

- The shedding of flexural stresses due to bend buckling type deformations of the curved web panels.
- The distortion of thin webs associated with flange raking, and the resulting potential reduction in the lateral-torsional stiffness and resistance.
- Shear buckling of curved web panels and the potential development of postbuckling tension field action.

- Potential interactions between the actions associated with the flexural and shear strengths. For instance, it is possible that the shear capacity of a curved I girder could be reduced because of the loss of lateral restraint and/or tension field anchorage from a compression flange subjected to high vertical and/or lateral bending. Conversely, the vertical bending capacity of an I girder might be reduced due to destabilization of the compression flange associated with the buckling and/or postbuckling response of the web in shear.
- Bending of transverse stiffeners due to the tendency of the curved web to deflect outward, for girders designed based on a web shear buckling limit, and due to potential additional demands associated the development of postbuckling strengths, if tension field action is utilized in the calculation of the design shear strength.

With respect to the first issue, Culver et al. (1972) show in Table 1 of their paper that, for doubly-symmetric I girders, the reduction in the yield moment capacity M_y due to web plate bending is approximately the same as that predicted by Basler's (1961) web load shedding parameter for straight girders R_b. White et al. (2001) performed a finite element parametric study of a wide range of doubly and monosymmetric curved I girders with $2D_c/t_w$ values up to 208 and reviewed experimental tests with $2D_c/t_w$ up to 188. They proposed unified flexural strength equations which involve a simple extension of current LRFD (AASHTO 2001b) straight I girder strength formulas, and found that these equations adequately predict the maximum flexural capacities with the direct use of the current LRFD load shedding factor, R_b (with F_y used in the R_b equation instead of f_b, for simplicity of the design calculations).

Regarding the second issue, there is some evidence that transverse stiffeners can improve the bending resistance of curved I girders (Mozer et al. 1970, 1971 and 1975; Nakai et al. 1984). White et al. (2001) considered this aspect parametrically for girders with $D/t_w = 160$, and found

that the increase in the flexural resistance with decreasing d_o/D (for $d_o/D = 1$, 2 and 3) is noticeable in some cases, but that it is generally small. However, they noted that the transverse stiffeners were not attached to the tension flange in their analyses, and that the effects of close stiffener spacing may be more significant for smaller D/t_w values. White et al. (2001) included the effects of flange raking and the associated web distortion in their finite element parametric studies. Overall, they found that their proposed flexural strength predictor equations are reasonably insensitive to potential increases in the flange lateral bending due to web distortion. It is believed that, in large part, this is due to (1) the use of the actual unsupported length L_b within the flexural resistance equations, rather than a smaller effective length, and (2) limiting the use of these equations in members with sustained flange lateral bending moments to the length L_r, where L_r is the unsupported length associated with the transition from inelastic to elastic lateral torsional buckling in the equivalent straight girder strength equations. This corresponds approximately to the limit on L_b/b_f of 25 in (AASHTO 2001a).

The third issue is the primary subject of this research. Lee and Yoo (1999b) recently considered the strength of curved web panels subjected to pure shear loading, via finite element analysis. Similar to Davidson (2000), they applied the web shear to isolated panels by shear tractions along the four panel edges. Based on their studies, Lee and Yoo concluded that shear strength models developed for straight I girders, including postbuckling resistance, are also adequate for estimating the nominal strength of curved web panels when the curvature parameter

$$c = \frac{d_o^2}{8Rt_w} \tag{11}$$

is less than or equal to one. This limit is the maximum value of c considered in their studies; also, $c = 1$ was considered as a practial upper bound by Nakai (1981). Furthermore, Lee and

Yoo (1999b) found that the elastic shear buckling strength of curved girder web panels for practical I girder proportions is much higher than that associated with traditional shear buckling equations based on equivalent flat plates with simply supported edge conditions. However, these strengths are only slightly greater than those calculated using an equation suggested for straight girder web panels by Lee et al. (1996). Lee et al. (1996) developed a simple set of formulas for calculation of the web shear buckling coefficient, accounting for realistic restraint conditions from the girder flanges. Bradford (1996) independently derived web shear buckling charts that predict essentially the same shear strengths as the equations of Lee et al. Based on the research by Lee and Yoo (1999b; 1998) and Lee et al. (1996), it is clear that the assumption that web panels are simply supported at all four edges is typically quite conservative in both flat and curved web panels, particularly for panels with d_o/D significantly greater than one.

Regarding the postbuckling strength under pure shear, Lee and Yoo (1999) showed that curved girder web panels with $c \leq 1$ can support shear loadings well beyond the elastic buckling limit, similar to the levels supported by straight I girder webs, despite the presence of out-of-plane bending from the inception of the loading.

White et al. (2001) studied parametrically the shear strength of complete curved I girders with the same support and loading conditions as utilized in the experimental shear tests addressed in this report. The results of their parametric study indicate that:

- The current AASHTO LRFD shear strength equations provide a reasonably good characterization of the maximum shear strength for girders with D/t_w up to 160 and $L_b/R \leq 0.10$, even though Basler's model is not very realistic in characterizing the physical shear strength behavior.

- The accuracy of the AASHTO LRFD shear strength equations is improved by basing the web shear buckling coefficient on the equations developed by Lee et al. (1996). Although the strengths for slightly less than half of 133 girders considered in their parametric study are overpredicted when the equations developed by Lee et al. (1996) are used for the shear buckling coefficient in the LRFD shear strength formulas, the standard deviation of the ratio between the predicted and the finite element based strengths is significantly reduced by the use of the more refined shear buckling coefficient.
- The shear buckling coefficient equations developed by Lee and Yoo (1996) provide an accurate characterization of shear buckling loads obtained by elastic linear buckling finite element analyses.
- The typical increases in the web elastic shear buckling strength and decreases in the ultimate shear capacity due to horizontal curvature are small compared to the effects of various other factors that lead to variability in design equation predictions relative to experimental tests and refined finite element models.
- Based solely on maximum strength considerations, the maximum limit on transverse stiffener spacing of $d_o/D = 3$ in the AASHTO LRFD straight girder Specifications is also sufficient for horizontally curved I girders with $L_b/R \leq 0.10$.

Of the shear strength equations considered by White et al. (2001), the AASHTO LRFD equations with the shear buckling coefficient calculated per the equations proposed by Lee et al. (1996) give the most accurate predictions relative to refined finite element strength predictions. In the interest of maintaining levels of simplicity similar to those of the current AASHTO provisions, White et al. (2001) limited their study to formulas that do not require consideration of girder flange proportions and flexural stresses. Therefore, they focused on the current

(AASHTO 2001b) equations, the equations proposed by Lee and Yoo (1998a, b, 1999b), and the current AASHTO equations modified by use of the Lee's shear buckling coefficient formulas. Chapter II of White et al. (2001a) provides detailed discussions of the concepts associated with these different strength predictors, and discusses their individual strengths and limitations.

The fourth issue, potential interaction between web shear strength and the I girder flexural capacity was also addressed in the parametric studies by White et al. (2001). These authors found that curved I girder capacities can be predicted adequately by the combination of the AASHTO (2001b) or modified AASHTO shear strength equations discussed above with flexural resistance equations proposed in their research, without the need for consideration of any interaction between these strengths. In fact, the flexural strength equations proposed in their research, which include the effect of lateral flange bending due to any source (i.e., horizontal curvature as well as applied loadings and torsion within curved and/or straight I girder bridges), tend to give conservative predictions of the flexural capacity in cases involving high shear and high moment, when the strength is controlled by flexure. This is not surprising once it is understood that the combination of moment gradient (equal to the web shear force) and smaller flange lateral bending moments (because of the rapid reduction in vertical bending moment as we move away from the maximum moment location, due to the high shear) tends to increase the flexural capacity in high-shear high-moment loading cases. Also, the maximum moment occurs at a brace location in the high-shear high-moment tests studied by White et al. (2001), as well as in typical cases of high-shear high-moment in bridge structures.

In (White et al. 2001), the unsupported length and flange proportions in some of the girders subjected to high-shear low-moment loadings (i.e., loaded such that an inflection point occurs at the middle of the test segment) were such that significant lateral flange bending was evident at

their maximum strength limit state. The strengths of these girders were adequately predicted by the combined flexural and shear strength equations proposed by White et al. (2001), without any requirement for consideration of moment-shear strength interaction. Also, White et al. (2001) found that for girders in which the calculated resistance is controlled by the suggested shear strength equations, the statistical distribution of the predicted to the finite element based strengths is similar for high shear with high or with low bending moment. In girders controlled by the proposed flexural strength equations, the strengths tend to be predicted more conservatively for high-moment high-shear than for uniform vertical bending cases, i.e., zero shear.

It should be noted that Nakai and Yoo (1988) and Fukumoto (1997) summarize high-shear high-moment test results for horizontally curved I girders that indicate significant moment-shear interaction. However, the strengths of these girders are predicted adequately with the equations proposed by White et al. (2001), albeit the shear strengths are predicted conservatively in these girders due to the fact that the AASHTO shear strength equations do not directly include a contribution to the shear strength from the flanges. ****The above statement needs to be verified****

The fifth issue listed above, failure of transverse stiffeners, was addressed originally by Culver et al. (1972c) and Mariani (1973). These researchers studied curved web panels under pure shear analytically using the Donnell shell equation and the Galerkin method. They concluded that the required stiffener rigidity for a curved web is less than that for a straight web if the panel aspect ratio d_o/D is less than 0.78. However, for $0.78 \leq d_o/D \leq 1$, they found that the required stiffener rigidity increases with the curvature by the ratio

$$X = 1 + \frac{1}{1775}\left(\frac{d_o}{D} - 0.78\right)Z^4 \qquad (12)$$

where Z is a curvature parameter defined as

$$Z = \frac{d_o^2}{Rt_w}\sqrt{1-\nu^2} \tag{13}$$

for $d_o/D \leq 1$. This study was limited to $0 \leq Z \leq 10$. Its design recommendations were limited to $d_o/D \leq 1$, although panel aspect ratios up to $d_o/D = 1.5$ were considered. The limit of $d_o/D \leq 1$ appears to be related to: (a) the fact that the AASHTO Standard Specifications in effect at the time of the research limited the panel aspect ratios of transversely-stiffened straight I girders to this value and (b) their study indicated that a function different than Eq. (12) would be needed for $d_o/D = 1.5$. Their studies with girders having a $d_o/D = 1.5$ indicate that a maximum rigidity of 2.4 times that required for the corresponding straight-girder web is necessary at $Z = 5.0$, but that this required rigidity reduces to the same requirement as for transverse stiffeners in straight girder webs as Z approaches 0.0 or 10.0. Equation (12) gives a required value of $X = 2.24$ for $d_o/D = 1$ and $Z = 10$, and therefore the maximum rigidity requirement determined in this research for panels with $d_o/D = 1.5$ was not significantly larger than that for $d_o/D = 1$.

Only the development of the web buckling strength was addressed in the above research; web postbuckling behavior and its influence on the transverse stiffeners was not considered. Equations (10) and (11) are adopted within the *2001 Guide Specifications*.

Based on analytical studies, Nakai et al. (1984b, 1985c) developed a beam-column model to estimate the strength of transverse stiffeners in curved I girders, including the influence of web tension-field action. Their analytical results were compared to experiments conducted by Nakai et al. (1984a), which led to a recommendation that the relative rigidity parameter β, defined as the ratio between the required rigidity of a transverse stiffener in a horizonally curved girder to that in an equivalent straight girder, must be the following:

For stiffeners attached to one side of the web plate:

$$\beta = \begin{cases} 1.0 + (\alpha - 0.69)Z[9.38\alpha - 7.67 - (1.49\alpha - 1.78)Z] & \text{for} \quad 0.69 \le \alpha \le 1.0 \\ 1.0 \quad \text{for} \quad \alpha < 0.69 \end{cases} \tag{14}$$

and for stiffeners attached to both sides of the web:

$$\beta = \begin{cases} 1.0 + (\alpha - 0.65)Z[12.67\alpha - 10.42 - (1.99\alpha - 2.49)Z] & \text{for} \quad 0.65 \le \alpha \le 1.0 \\ 1.0 \quad \text{for} \quad \alpha < 0.65 \end{cases} \tag{15}$$

where $\alpha = d_o/D$.

Nakai and Yoo (1988) state that in deriving the above limits, the aspect ratio of the web panel d_o/D is limited to a value less than or equal to one because the required rigidity of the transverse stiffeners is too large for use in design practice unless this condition is imposed. Also, they state that the same conclusion has been reached by Mariani et al. (1973). The (Mariani et al. 1973) paper does not contain any evidence of this conclusion. For $Z = 10$ and $\alpha = 1.0$, Eq. (14) gives a required value for β of 15.3. Although this is a significant additional requirement beyond that for transverse stiffeners in a straight I girders, these more stringent requirements can often be met with reasonable stiffener proportions.

CHAPTER III - TEST GIRDERS

Four curved I girder test components, labeled hereafter as S1, S1-S, S2 and S2-S, were fabricated from AASHTO M270 Grade 345 steel. All the test girders had an total arc length of 11,580 mm (38 ft) and a doubly-symmetric cross section with nominally 544.5 x 22.2 mm (21 7/16 x 7/8 in) flange plates curve cut and 1219 x 8 mm (48 x 5/16 in) web plates heat curved. The radii R were 63,630 mm (208.75 ft) for S1 and S1-S and 36,580 mm (120 ft) for S2 and S2-S. All the girders had four 229 x 25.4 mm (9 x 1 in) bearing stiffeners placed in pairs at 305 mm (1 ft) from their ends and at 3,660 mm (12 ft) intervals along their length. Dimensions of these test girders are shown in Figure 1 and Figure 2 . The objectives of each of these tests are summarized.

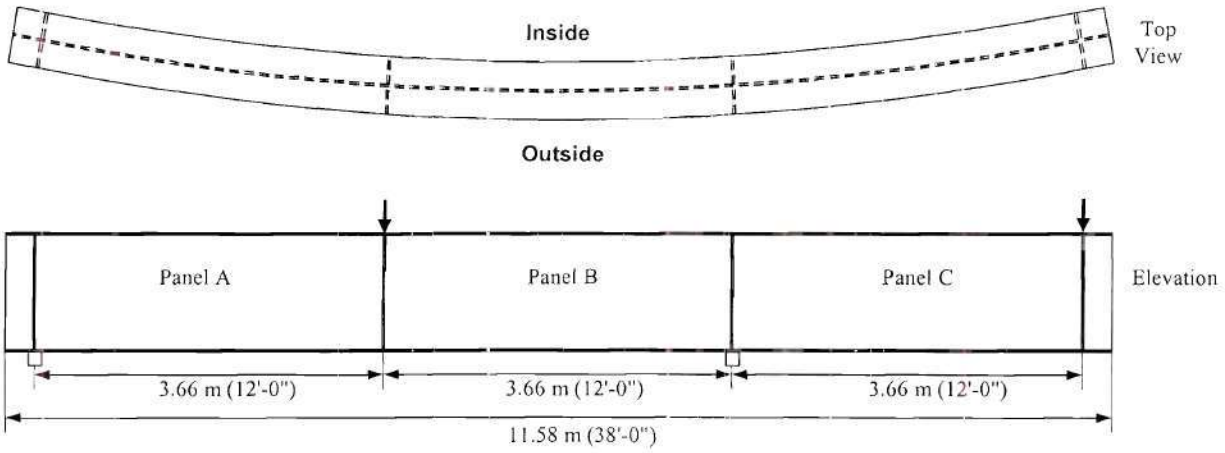

Figure 1 Dimensions of test girders S1 and S2

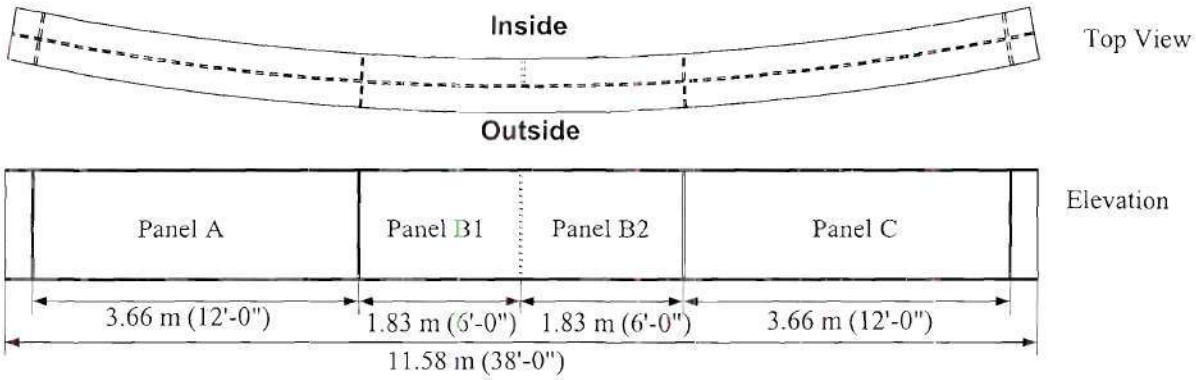

Figure 2 Dimensions of test girders S1-S and S2-S

Girder S1: The objective of this test was to examine the shear strength of a curved web panel having an aspect ratio $d_o/D = 3$, a ratio of the web panel length to the radius of curvature of $d_o/R = 0.0575$, and a subtended angle between the cross frame locations of $L_b/R = 0.0575$, which is slightly greater than one-half of the maximum value 0.10 permitted by the *2001 AASHTO Guide Specifications*. The web of this girder had only the four bearing stiffeners described above without any intermediate transverse stiffeners between.

Girder S1-S: This girder was identical in length and curvature to S1, but had an additional 165 x 16 mm (6-1/2 x 5/8 in) intermediate transverse stiffener located at the center of each panel between the bearing stiffeners. The intermediate transverse stiffeners were cut back 25.4 mm (1 in) from one of the flanges, and were placed on the side of the web closest to the center of curvature only. The resulting web panel aspect ratio for this girder was 1.5, and the value of d_o/R was 0.0287. Although the above transfer stiffner has very reasonable proportions relative to the girder geometry, it has moment of inertia about its edge in contact with the web plate of 52 times

that required by the AASHTO LRFD (2000) Specifications. The stiffner requirements for curved webs discussed in Chapter 2 do not apply for $d_o/D > 1.0$.

Girder S2: This test girder was similar to S1 in that it only had bearing stiffeners at 3658 mm (12 ft) intervals along its length and a resulting panel aspect ratio of $d_o/D = 3$. However, this girder differed from S1 in that it had a radius of 36 580 mm (120 ft), thus representing a case in which $L_b/R = 0.10$, the maximum subtended angle between the cross frame locations allowed by the *2001 AASHTO Guide Specifications*. The corresponding d_o/R for this girder was 0.10.

Girder S2-S: This girder was identical to S1-S, but with a radius of 36 580 mm (120 ft). Therefore, its normalized dimensional parameters were $d_o/D = 1.5$, $d_o/R = 0.050$ and $L_b/R = 0.10$.

Table 1 presents a matrix of nondimensional test parameters associated with these four tests, including the parameters c and Z given by Eqs. (11) and (13), calculated using the nominal thickness $t_w = 8$ mm (5/16 in). It can be observed that the value of c for all but one of these designs is significantly greater than one. This is due to the use of large panel aspect ratios d_o/D and web slenderness D/t_w relative to current practice, as reflected in the *2001 Guide Specifications* and in Nakai (1981).

Table 1 Summary of test girder nondimensional parameters.

Girder	L_b/R	d_o/D	d_o/R	$c = d_o^2/8Rt_w$	$Z = d_o^2\sqrt{1-\upsilon^2}/Rt_w$
S1	0.0575	3	0.0575	3.31	25.3
S1-S	0.0575	1.5	0.0287	0.83	6.3
S2	0.10	3	0.1000	5.76	44.0
S2-S	0.10	1.5	0.0500	1.44	11.0

3.1 MEASURED DIMENSIONS

The top and bottom flange widths and thicknesses were measured at seven locations along the length of the test girders using a precision caliper. These measurements were taken adjacent to each of the four bearing stiffeners, and at the middle of each of the three unsupported lengths. The flange thicknesses were measured at the flange tips on each side of the web at each of these locations, giving a total of 14 thickness measurements for each flange. The web thicknesses were measured with an ultrasonic time-of-flight device at the same seven locations as above, and at approximately 1/3 and 2/3 of the web height, giving a total of 14 web thickness measurements for each girder. The web thickness measurements from the ultrasonic device were checked versus direct measurements using a precision caliper at three locations through the web depth at both ends of the girders. The ratio of the average web thickness measured by the ultrasonic device and by the caliper for these 24 locations was 1.007. The web depths were measured with a tape at the ends of the girders and at each of the interior bearing stiffener locations. The total girder depth, including the flange thicknesses, was measured at the centerline of the flanges at the girder ends. This depth was measured at the flange tips on each side of the web at the interior bearing stiffener locations, and the total depth at the centerline of the flanges was then estimated by taking the average of these two depths. The depth of the web plate D was then calculated by subtracting the average flange thickness measured at each of these locations from the total depth.

The data from the above cross-section measurements are summarized in Table 2. The flange widths b_f at the girder ends were consistently about 1.5 mm (0.06 in) smaller in Girders S1 and S1-S and about 5 mm (0.20 in) smaller in Girders S2 and S2-S than the average of the flange widths measured at the other locations. Therefore, the end measurements for the flange widths are not included within the statistics reported in the table.

The radial distance from a straight chord between the tips of the flanges closest to the center of curvature at the locations of the end bearing stiffners and the corresponding tip of the flanges at the mid-length of the test girders is reported and compared to its nominal value based on the specified radii in Table 3. This distance was estimated by pulling a wire taught between the flange tips at the locations of the end bearing stiffners, and then measuring the distance from this wire to the closest flange tip at the girder mid-length by a scale. In addition, the corresponding radial distances from a straight chord between the flange tips at the locations of the interior bearing stiffners are reported in the table.

Lastly, Table 4 shows the values for the maximum out-of-flatness of the web relative to a straight chord between the top and the bottom of web panel. These imperfections were estimated by placing a straight edge between the top and bottom of the web in a vertical position at various locations along the length, and measuring the gap between the straight edge and the web panel with a scale. The ratio of these out-of-flatness values to the web thickness, and to the maximum value permitted by the AWS Bridge Welding Code (AWS 1995) in interior girders with one-sided stiffeners, (equal to d/67 where d is the least panel dimension), are also shown in the table.

Table 2 Measured cross-section dimensions

Girder		D (mm)	t_w (mm)	Top Flange		Bottom Flange	
				b_f (mm)	t_f (mm)	b_f (mm)	t_f (mm)
S1	Average	1217	8.53	546.6	22.99	546.4	23.04
	COV (%)	0.08	0.78	0.15	0.22	0.09	0.25
	Maximum	1218	8.64	547.9	23.06	546.9	23.14
	Median	1217	8.53	546.4	23.01	546.4	23.01
	Minimum	1216	8.46	545.6	22.89	545.6	22.94
	N	4	14	5	14	5	14
S1-S	Average	1218	8.46	546.4	22.91	546.9	22.96
	COV (%)	0.04	1.02	0.05	0.25	0.11	0.50
	Maximum	1218	8.61	546.6	22.99	547.9	23.16
	Median	1218	8.43	546.1	22.94	546.9	22.94
	Minimum	1217	8.31	546.1	22.81	546.4	22.76
	N	4	14	5	14	5	14
S2	Average	1217	8.31	557.3	22.83	556.8	22.76
	COV (%)	0.08	0.60	0.16	0.33	0.26	0.24
	Maximum	1218	8.38	558.3	22.99	558.5	22.83
	Median	1217	8.31	557.0	22.83	556.8	22.76
	Minimum	1216	8.23	556.5	22.73	554.5	22.63
	N	4	14	5	14	5	14
S2-S	Average	1217	8.23	556.3	22.81	556.5	22.81
	COV (%)	0.05	0.51	0.24	0.21	0.21	0.29
	Maximum	1218	8.31	557.5	22.94	558.0	22.91
	Median	1217	8.23	556.8	22.83	556.5	22.83
	Minimum	1217	8.18	554.7	22.68	555.0	22.68
	N	4	14	5	14	5	14

Table 3 Measured and nominal distances from the straight chords between the flange tips closest to the center of curvature at locations 1L and 1R and 2L and 2R and the corresponding flange tips at the mid-length of the girders

Girder	Radial distance from chord between 1L & 1R		Radial distance from chord between 2L & 2R	
	measured (mm)	nominal (mm)	measured (mm)	nominal (mm)
S1				
S1-S				
S2				
S2-S				

Table 4 Maximum initial web out-of-flatness

Girder	Out-of-flatness δ_o (mm)	$\frac{\delta_o}{t_w}$	$\frac{\delta_o}{(d/67)}$
S1	3.00	0.352	0.165
S1-S	3.00	0.339	0.158
S2	5.00	0.602	0.275
S2-S	8.00	0.972	0.440

3.2 MATERIAL PROPERTIES

The material properties of the steel used for fabricating the components were determined from tensile coupon tests conducted in accordance with ASTM E8-00b (ASTM 2000). The four flanges for S1 and S1-S were cut-curved from one 2,896 x 13,260 mm (114 in x 43.5 ft) plate, and the four flanges for S2 and S2-S were cut-curved from another similar plate. Three 305 x 610 mm (12 x 24 in) coupon samples were cut from each of these plates, one at each end at the centerline radius of the four flange cut outs, and one at the centerline of the ordered plate length

on the side toward the center of curvature of the flange cutouts. The long direction of the coupons was oriented tangent to the arc of the flange plates at the ends, and in the long direction of the plate, i.e., in the primary mill rolling direction, at the centerline. The webs of S1 and S1-S were cut from a 1,830 x 24,540 mm (72 in x 80.5 ft) plate, and the webs of S2 and S2-S were cut from another similar plate. Six 305 x 610 mm (12 x 24 in) web coupons were taken from each of these plates, two at each end, and two on the bottom side of the plate at the center of the overall length. At each of these locations, one of the coupons had its long direction aligned with the long direction of the ordered plate, which was the primary mill rolling direction, and one was cut with its long direction at 90^{o} to this orientation.

Three plate-type rectangular tension specimens were prepared from each of the above coupons per ASTM E8-00b (ASTM 2000). The specimens were 38.1 mm (1.5 in) wide and had a 203 mm (8 in) gage length. From these coupons, a total of 12 and 8 tests were conducted for the web and flange plates of girders S1 and S1-S, respectively, and a total of 18 and 9 tests were conducted for the web and flange plates of girders S2 and S2-S, respectively. The coupons were loaded under displacement control at the rate of about 0.02 mm/second up to a strain level slightly higher than that at the onset of strain hardening. The strain rate was then increased to approximately 0.09 mm/second throughout the remaining part of the test. The upper and lower yield strengths were determined by the autographic diagram method defined in ASTM E8-00b. In the majority of the tests, the SSRC Technical Memorandum No. 7 procedure (SSRC 1998) was utilized to determine static yield strengths. In this procedure, the test was interrupted by stopping the cross head motion when the strain reached a value corresponding to approximately 0.2 % offset. This condition was maintained until the load stabilized, and the lowest value of the load and the corresponding strain was recorded. Straining was then resumed at the post-yield

strain rate. The tests were interrupted and static load values were recorded at 0.005 increments of strain until strain hardening began.

Young's Modulus (E) was calculated from the recorded data by a linear regression analysis of the data between a pre-load, selected high enough such that errors at small load could be neglected, and the upper yield strength. Table 5 summarizes the key coupon stress-strain data of the girder tests: the modulus of elasticity E, static yield F_y, strain hardening modulus E_{st} and strain at the onset of strain hardeing e_{st}, the ultimate tensile strength F_u as defined in ASTM E8-00b, and the strain at ultimate e_u. A discussion related to the determination of the strain hardening modulus is presented in Appendix I. No effects of coupon orientation or of small differences in loading rates among the different tests could be discerned statistically from the data. Figure 3 shows typical stress-strain curves for the flange and web plates of girders S2 and S2-S. The static yield strength was not measured in the coupon tests corresponding to the stress-strain curves shown in these figures.

It is well known that Young's modulus E is sensitive to numerous attributes of the test procedures (ASTM 1997; Adams et al. 1964; Galambos and Ravindra 1978). The average E for all of the tension specimens reported in Table 5 is 203 GPa (29,440 ksi) with a coefficient of variation of 2.6 percent. This coefficient of variation is somewhat higher than that reported for each of the separate flange and web plates in the table. Galambos and Ravindra (1978) report average test values for E from various investigations ranging from 202 to 215 GPa (29,360 to 31,200 ksi). It is likely that the differences in elastic moduli for the different plate tests shown in Table 5 are due to measurement error, and therefore one value should be selected for Young's modulus to represent all of the tests. The average value determined from the full set of the tension cou-

pon tests is certainly reasonable, and thus, this value is selected for further analysis of the girder test data.

Table 5 Stress-strain data from tension coupon tests.

Girders	Coupon Location	N		E (GPa)	Avg. Static F_y (MPa)	E_{st} (GPa)	e_{st} (%)	F_u (MPa)	e_u (%)
S1 and S1-S R = 63 630 mm	Web	12	Average	208	410	3.44	1.95	567	14.6
			COV (%)	1.4	3.3	5.9	8.9	1.4	11.1
			Maximum	213	423	3.78	2.13	575	16.0
			Median	209	416	3.43	1.99	569	15.2
			Minimum	203	384	3.07	1.57	548	11.1
	Flanges	8	Average	196	377	3.59	1.59	542	15.6
			COV (%)	1.5	1.4	6.4	17.0	0.4	2.3
			Maximum	200	385	3.97	1.91	545	16.1
			Median	197	376	3.52	1.47	542	15.7
			Minimum	190	372	3.34	1.30	538	15.1
S2 and S2-S R = 36 580 mm	Web	18[1]	Average	202	411	3.36	1.87	564	15.6
			COV (%)	2.3	1.7	7.3	13.7	0.8	4.0
			Maximum	209	419	3.84	2.23	569	16.9
			Median	202	412	3.26	1.82	564	15.6
			Minimum	192	402	3.15	1.60	554	14.6
	Flanges	9[2]	Average	205	397	3.61	1.90	562	15.4
			COV (%)	1.4	0.7	2.9	5.8	0.3	3.8
			Maximum	208	400	3.72	2.00	564	16.3
			Median	206	396	3.63	1.93	562	15.5
			Minimum	200	394	3.47	1.74	559	14.2

[1]Static F_y was measured in six of the 18 tests.

[2]Static F_y was measured in three of the nine tests.

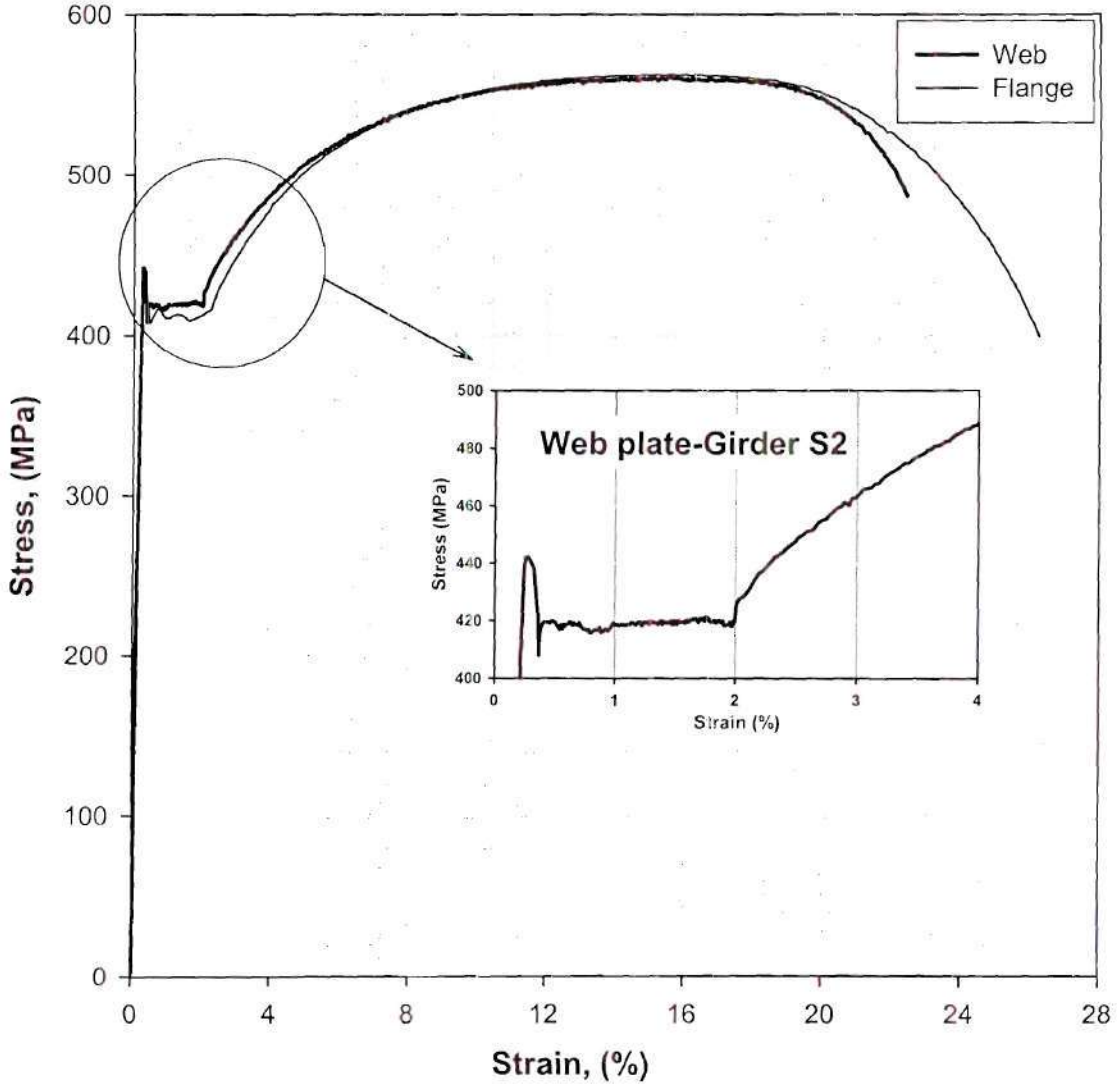

Figure 3 Representative tension stress-strain curves for flange and web plates of girders S2

3.3 TEST SETUP AND INSTRUMENTATION

All the girder tests were conducted in a steel reaction frame in which W920x446 (W36x300) 2,285 mm (7.5 ft) long beams were connected on one side to (20 ft) high W360x216 (W14x145)

columns and on the other side to a 610 mm (2 ft) thick reinforced concrete reaction wall with 3,658 mm (12 ft) buttresses 3,658 mm (12 ft) on center. Figure 4 shows a schematic of the test setup. Figure 5 shows a photograph of the test setup from location 1R. The setup consisted of placing the girder on two steel pedestals located at a distance of 7,315 mm (24 ft) from center to center. The exterior end support was constructed by bolting a 890 kN (200-kip) load cell to the steel pedestal and attaching to the load cell button a 25.4-mm (1-inch) thick steel plate on which a 50.8-mm (2-inch) diameter round steel bar was welded. The round steel bar was aligned in the direction of the end bearing stiffeners as shown in Figure 6. At the interior support, shown in Figure 7, a 3,114- kN (700-kip) load cell having a 120.6-mm (4.75-inch) diameter flat load button was bolted to the interior pedestal and placed directly under the bearing stiffeners, with the center of the load button conciding with the center of the web-flange juncture. A 12.7 x 203.2 x 406.4 mm (1/2 x 8 x 16 in) bearing plate was placed between the load button and the girder, with the 203.2 mm (8 in) dimension oriented along the girder length.

The test girders were braced radially at 3,658-mm (12-ft) intervals by means of two 101-mm (4-inch) diameter steel tubes connected to the bearing stiffeners at locations near the top and bottom flanges, as shown in Figure 8. A detail of the top bracing member attachment is shown in Figure 9 . Double gusset plates were used at the ends of the tube bracing members, and their end attachments were accomplished through a pin that passed through a spherical bearing placed within the bearing stiffener on the girder and within a T-plate attached to the concrete reaction wall. Therefore, the bracing members restrained the girders essentially only along their longitudinal axes. The attachment of the bracing to the girders was placed approximately 50.8 mm (2 in) higher than the attachment to the reaction wall at the beginning of the tests, based on an estimated upper-bound displacement at the load points at maximum load equal to this value, and

an estimated upper-bound required displacement at the load points of 101.6 mm (4 in) at the end of the tests. The lengths between the spherical bearings at the ends of the bracing members ranged from 1,100 to 1,305 mm (43-5/16 to 51-3/8 in), which permitted the bracing members to rotate through the above estimated displacements with negligible lateral bending being induced within the girders. Refined finite element analyses were conducted to verify that this bracing arrangement would have a negligible influence on the test behavior.

Two concentrated loads were applied to the girder, an internal load at the mid-length between the two supports and an external load near the tip of the cantilevered portion (see Figure 4). The internal load was applied by means of a 4,448-kN (1,000-kip) double-acting hydraulic cylinder to which a 3,114 kN (700-kip) load cell was attached. A 12.7 mm (1/2 in) bearing plate was placed between the button of this load cell and the top flange of the girders, similar to the detail in Figure 7. A heavy grease was applied to the contact surface between the load button and the bearing plate at this location, and at the interior support position, to minimize any longitudinal restraint within the tests. The torsional compliance within the reaction beam of the test frame and within the support pedestals was such that the longitudinal forces induced within the system were negligible even if slip did not occur between the button of the load cells and the corresponding bearing plates. The external load was applied by a closed-loop hydraulic actuator having a compressive capacity of 1,460 kN (328 kips). The above loading and vertical support arrangement produced a constant shear force in the web panel between the interior load and the interior support points, with an inflection point at the test girder centerline as illustrated in Figure 4.

Applied loads, reactions, vertical deflections, radial deflections, and strains were recorded during the testing. The vertical deflections were recorded by means of linear variable differen-

tial transformers (LVDTs) positioned under the bottom flange at midspan and at the locations of the applied loads as shown in Figures 10 and 11. Radial deflections were measured by five wire potentiometers attached to the web of the test girders at the mid-depth and 1/4 and 3/4 depth locations and also at 571.5 mm (22.5 in.) above and below the web mid-depth (38.1 mm (1.5 in.) from the inside face of the top flange and 38.1 mm (1.5 in) from the inside face of the bottom flange), as shown in Figure 12.

Each test component was also instrumented with electrical resistance strain gauges to measure strains in the web, flanges, and the bracing members. The web test panels(Panel B) for both components S1 and S2 were instrumented at nine locations with back-to-back three-arm rosettess arranged in the pattern shown in Figure 13. These rosettes are labeled as Rnm where n = 1,2...9, representing the rosette location number, and m takes either the letter i or o to indicate inside (toward the center of curvature) or outside, respectively. For components S1-S and S2-S, one of the two test panels was instrumented with back-to back three-arm strain rosettes at the nine locations shown in Figure 14. Girder S1-S was instrumented in panel B1 and girder S2-S was instrumented in panel B2. In addition, back-to back single-arm straing gauges were mounted on the test panel adjacent to the instrument one.

In addition, the midlength of each tubular bracing member was instrumented with four-single arm gauges placed at 90^{o} intervals around the periphery. These gauges were connected to create four legs of a Wheatstone-bridge configuration. The load output from this arrangement was checked against a calibrated load cell prior to the construction of the bracing members to the test girder.

The strains in the top and bottom flanges were measured at .....

3.4 TEST PROCEDURE

Prior to testing to failure, each test girder was subjected to at least two preliminary cycles of loading and unloading to verify the operation of all testing equipment and ensure proper contacts between the test girder and the loading and support fixtures. The maximum loads applied in these preliminary tests were such that shear force in the test panel was approximately 40 kips, less than 15% of the estimated shear capacity of girders S1 or S2. During the final sequence of loading to failure, the internal and external loads were increased at increments at which the ratios of the interior load to the exterior load was 3. The shear capacity in each test was reached in14 to 20 loading increments. At each load incement, the valves on the hydraulic cylinder (location 2L) and at the actuator (location 1R) were closed until the load readings stabilized. The loading was incremented by setting the actuator to increase the displacemnt at location 1R at a small constant rate while simultaneously pumping oil to the hydraulic cylinder by a manual control. The test girders were then unloaded in a similar fashion. All loads, deflections and strains were recorded by a computer-based data acquisition system.

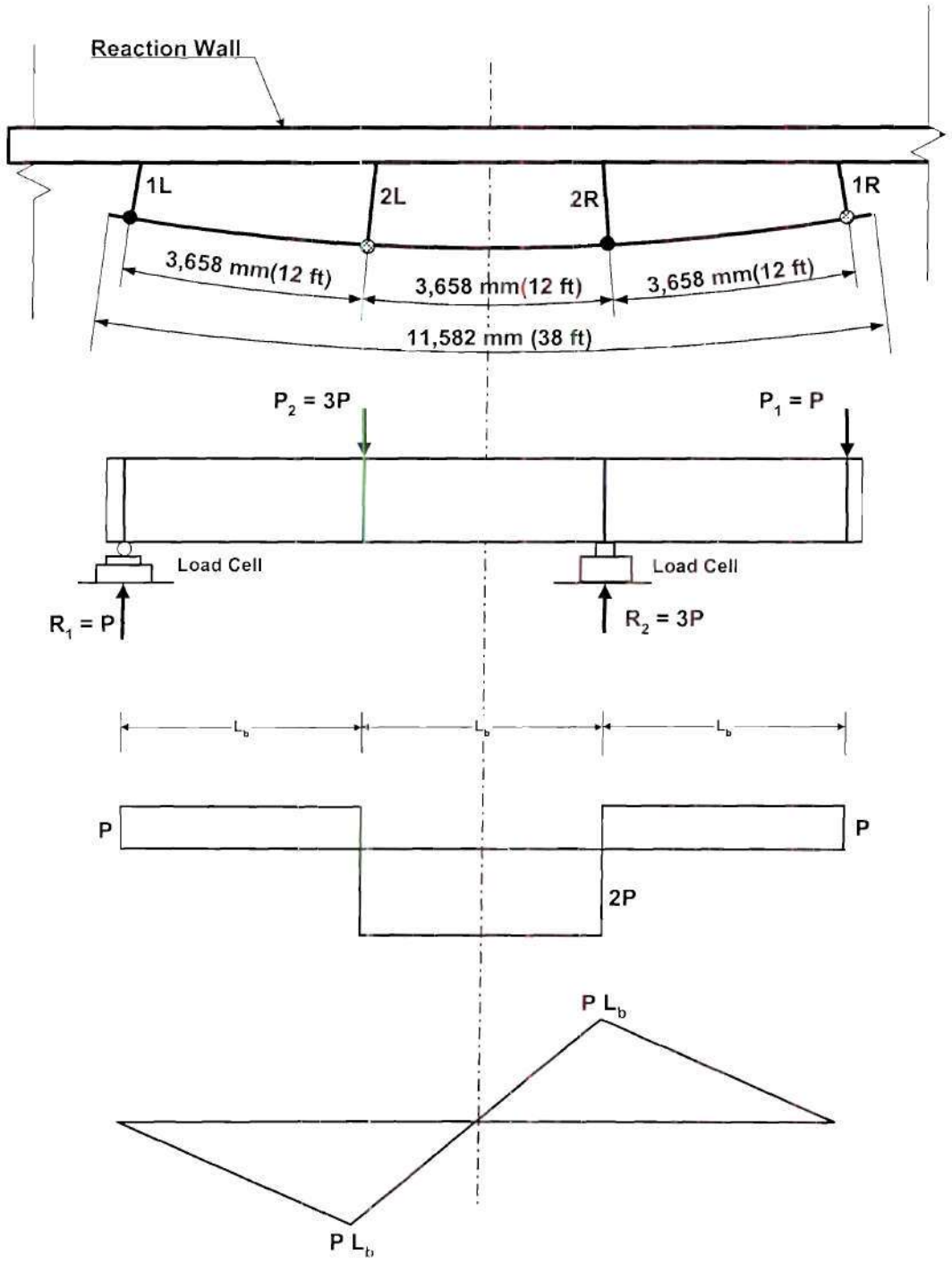

Figure 4 Test setup and shear and approximate moment diagrams.

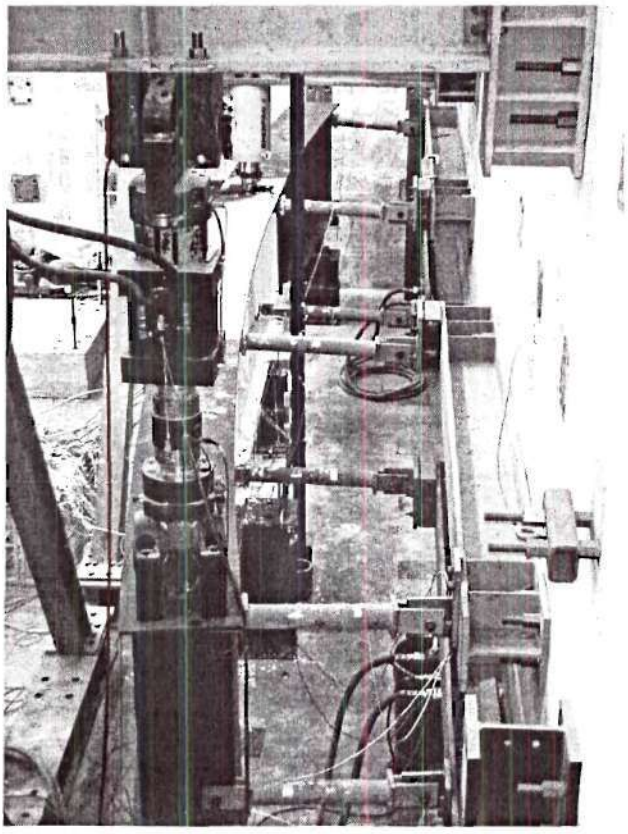

Figure 5 Longitudinal view of test setup from end 1R

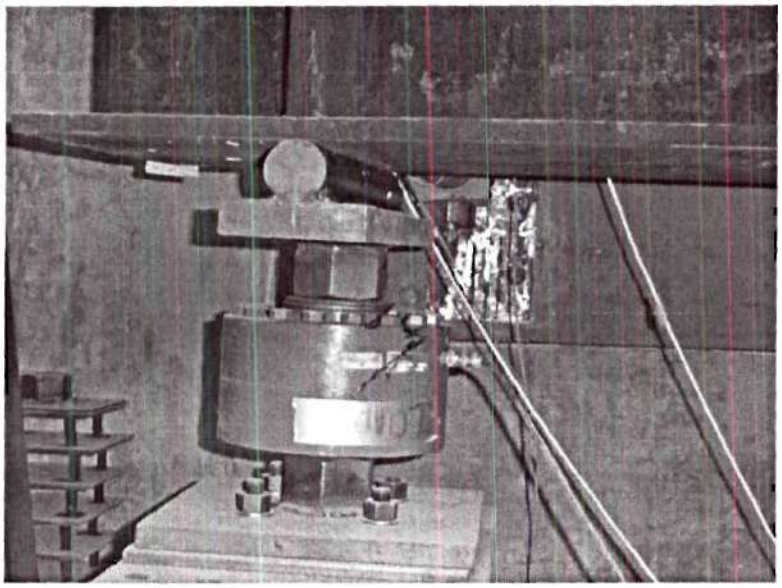

Figure 6 Detail of the exterior end support

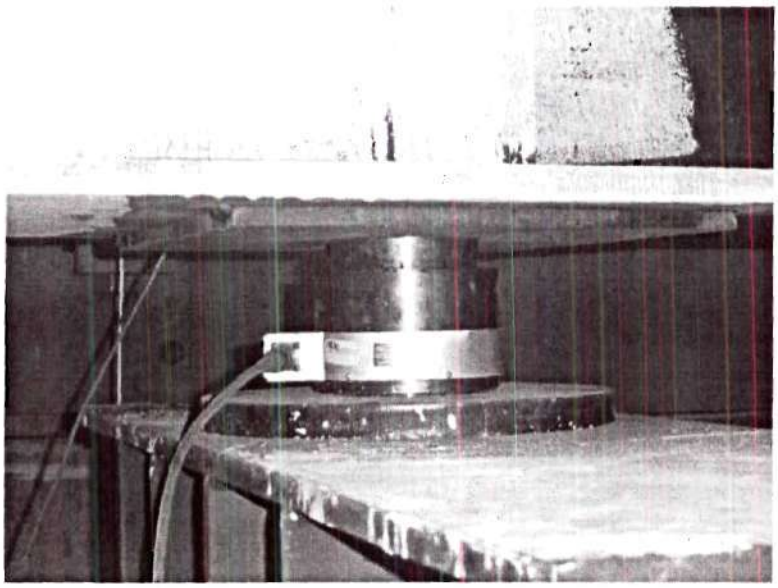

Figure 7 Detail of the interior support

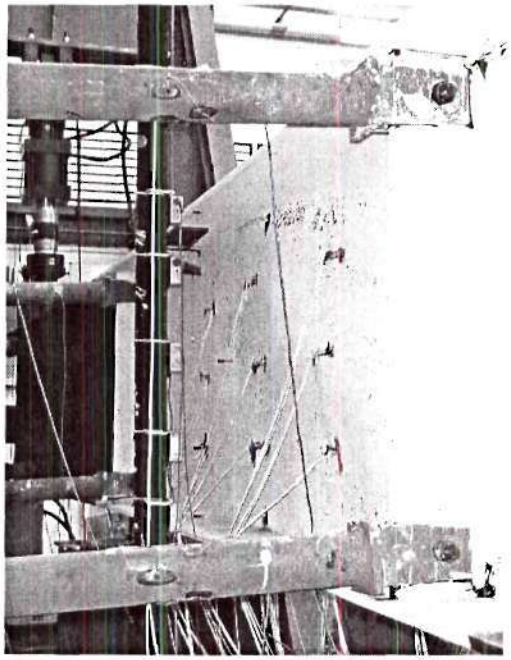

Figure 8 Top and bottom bracing members

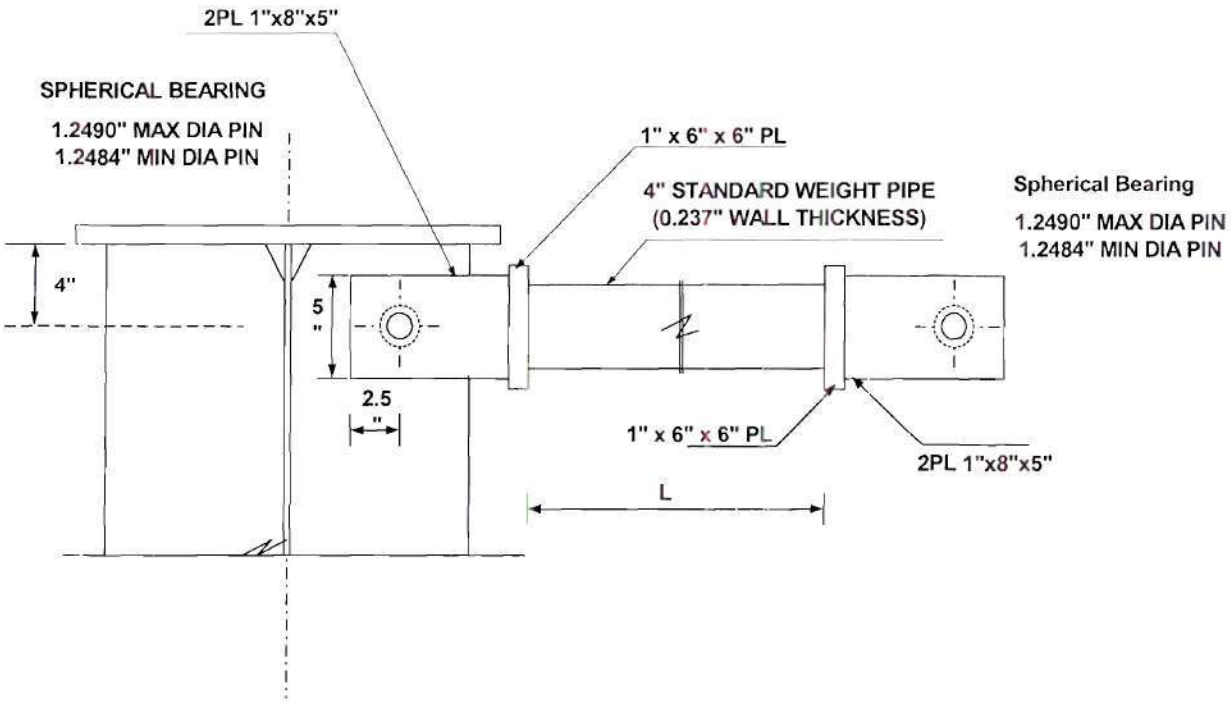

Figure 9 Detail of the top bracing members (bottom similar)

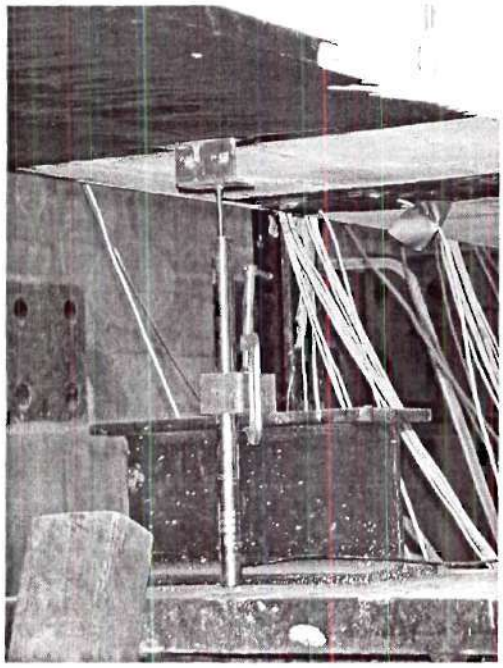

Figure 10 LVDT at location 2L.

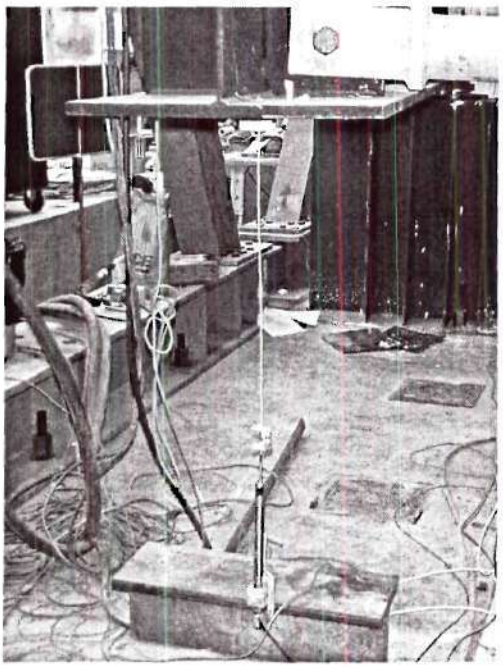

Figure 11 LVDT at location 1R.

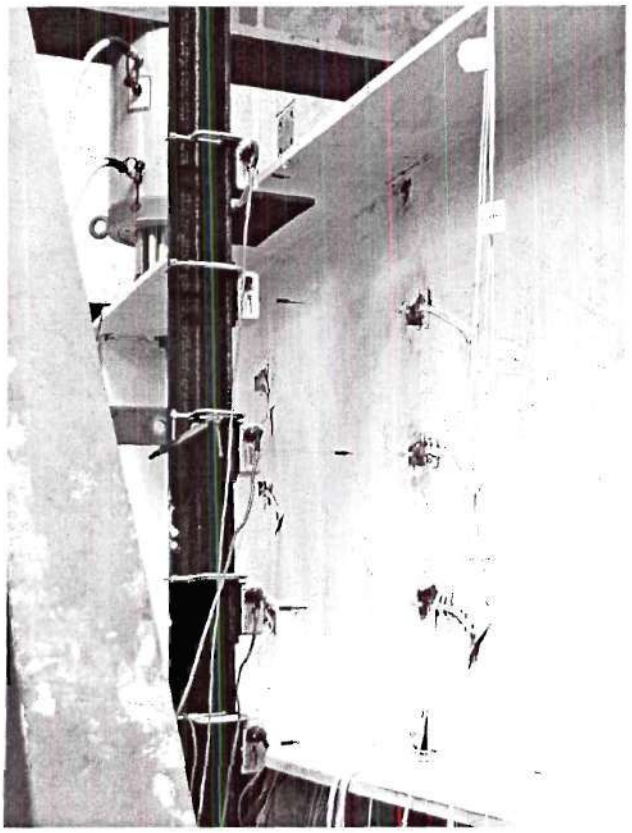

Figure 12 Position of post holding potentiometers

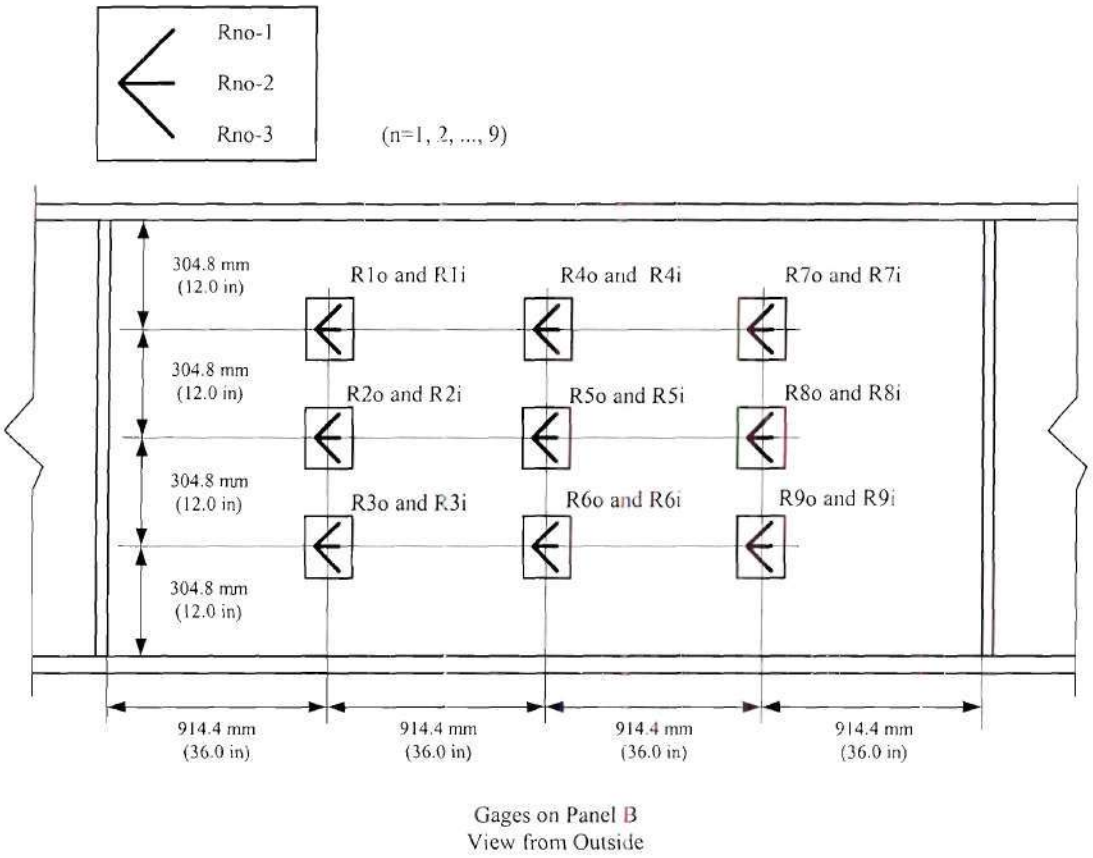

Figure 13 Strain rosettes patterns for components S1 and S2

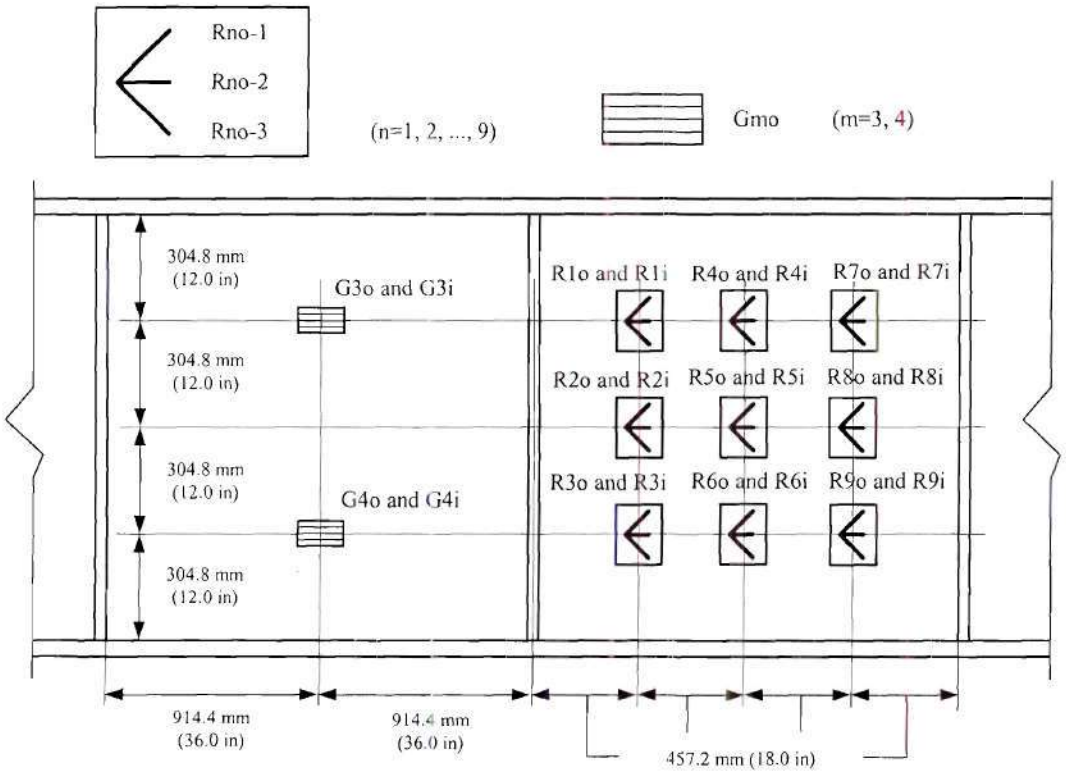

Figure 14 Strain rosette pattern for components S2-S (S1-S similar)

CHAPTER IV - EXPERIMENTAL RESULTS

4.1 PANEL SHEAR FORCE

Theoretically speaking, if the small vertical components of force from the bracing members are neglected, the test panel shear force obtained from the difference ($V_R = R_2 - P_1$) between the interior support reaction and the applied external load on the right-hand side of the test must be the same as that computed from the difference ($V_L = P_2 - R_1$) between the applied internal load and the reaction at the exterior support on the left-hand side (see Figure 4). However, due to unavoidable measurement error, the values of V_R and V_L will be different, even if the vertical components of force from the bracing members are included. Hereafter, the experimentally obtained panel shear force is reported as the average of V_R and V_L. The maximum values of V_R, V_L and $V_{avg} = (V_R + V_L) / 2$ and the ratio of the maximum values of V_R and V_L obtained in the four shear tests are reported in Table 6.

Table 6 Panel shear strengths

	V_R kN (kips)	V_L kN (kips)	V_{avg} kN (kips)	V_R/V_L
S1	1,870 (272)	1,850 (268)	1,860 (270)	1.015
S2	1,780 (258)	1,800 (261)	1,790 (260)	0.989
S1-S	2,190 (317)	2,050 (297)	2,120 (307)	1.067
S2-S	2,170 (315)	2,210 (320)	2,190 (317)	0.984

If the vertical components of force from the bracing members are included in the calculation of the shear forces, the difference between V_R and V_L is reduced in all the cases. However, the largest change in V_{avg} by including the effect of the vertical components of the bracing forces is 0.6 percent (corresponding to test S1).

To examine the measurement error over the full range of loading and unloading, the ratio V_R/V_L versus the loading increment is plotted in Figure 15. The loading increment corresponding to the maximum shear force in the test panel are labeled in the figure. For all the loading increments of all the tests, except in the early stages of the loading, the ratio of V_R/V_L is between 0.9 and 1.1. At the maximum panel shear strength, the difference between V_R and V_L is less than 2% in all the tests except for S1-S, for which the values of V_R and V_L are 317 kips and 297 kips, respectively.

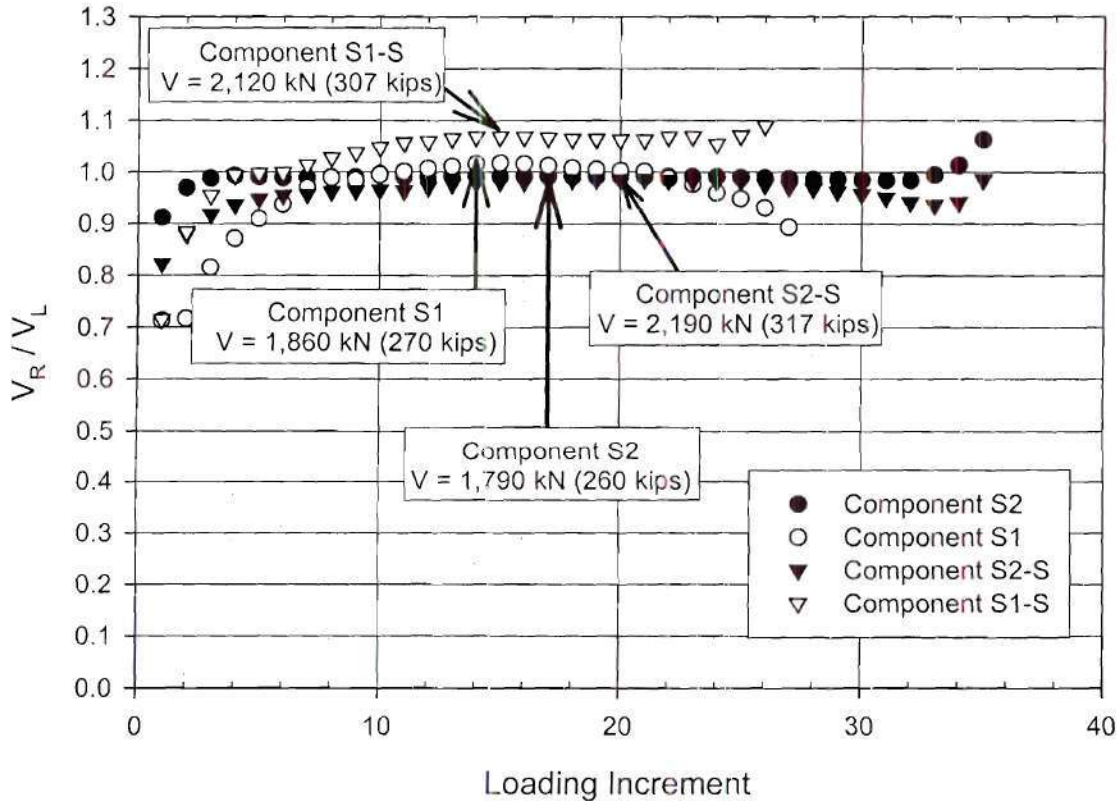

Figure 15 Ratio V_R/V_L versus loading step

4.2 LOAD-DEFLECTION RESPONSE

The vertical deflections at the applied load positions 1 and 2 and at the center of the test panel are plotted versus the panel shear force in Figures 16 through 19. The web radial deflections at the middle of the test segment in girders S1 and S2 and at the center of the instrumented web panel in girders S1-S and S2-S are shown in Figures 21 through 23. The corresponding radial deflections at D/4, D/2 and 3D/4 versus the panel shear force are plotted in Figures 24 through 27.

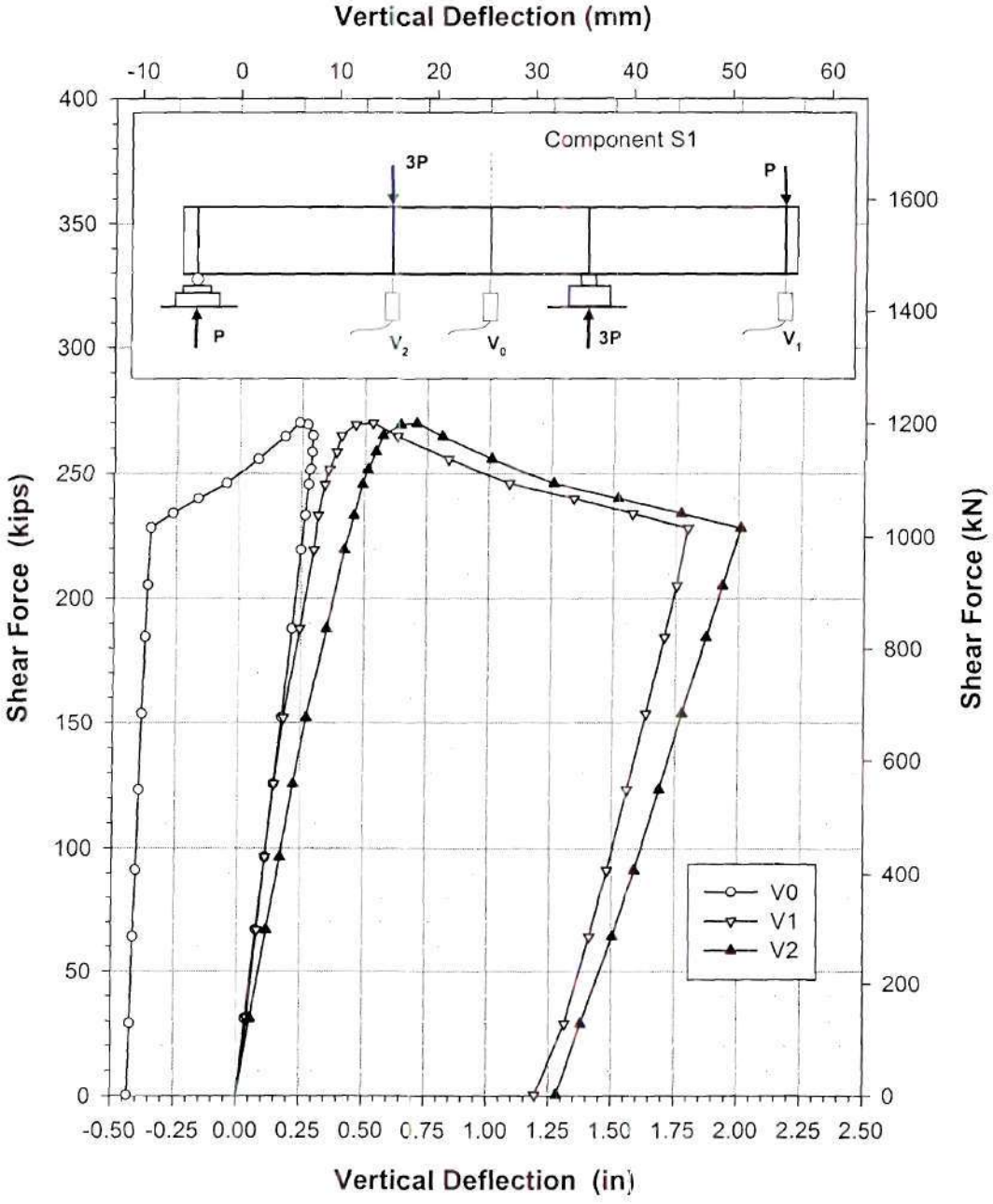

Figure 16 Load-vertical deflection curves of girder S1

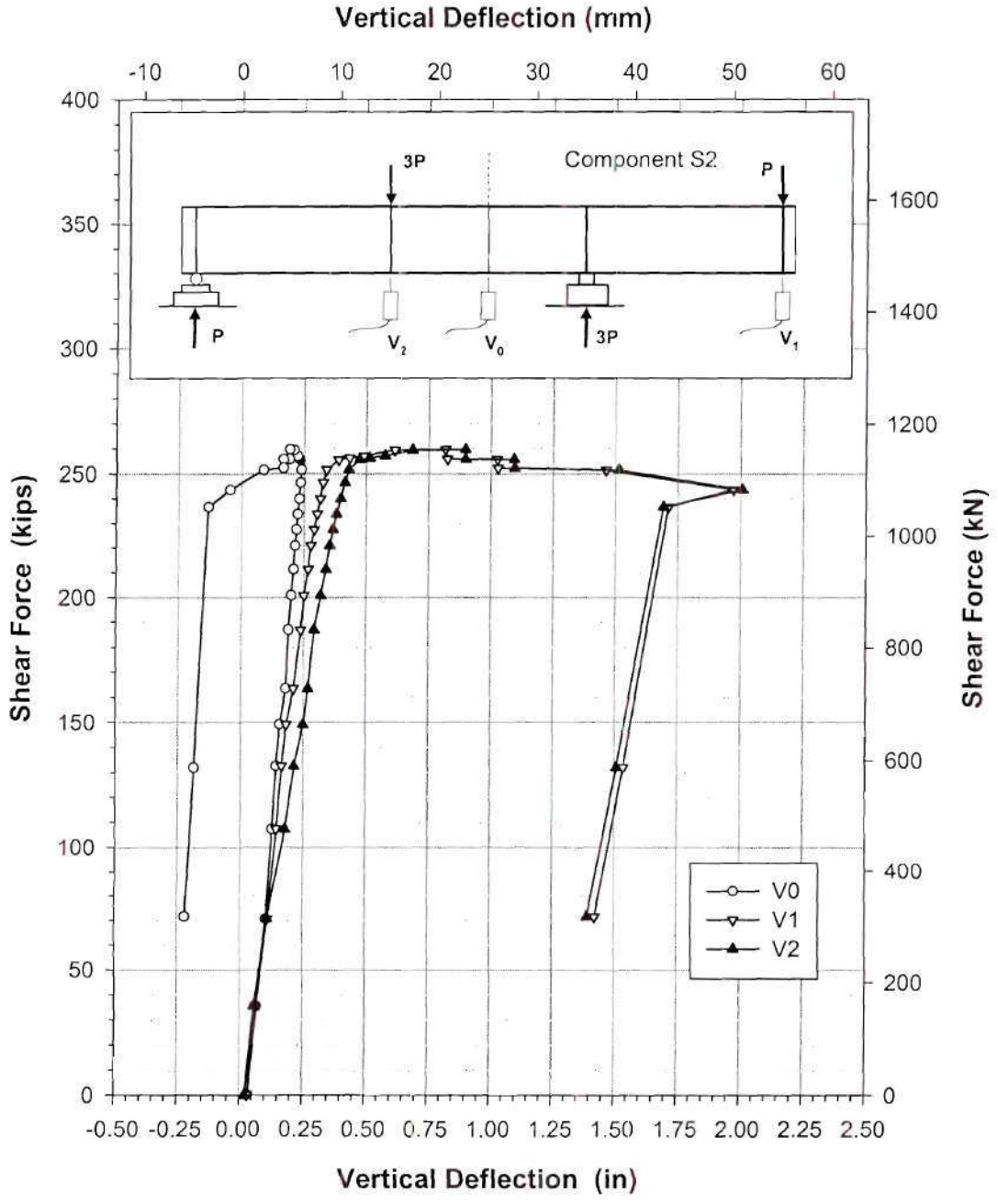

Figure 17 Load-vertical deflection curves for girder S2

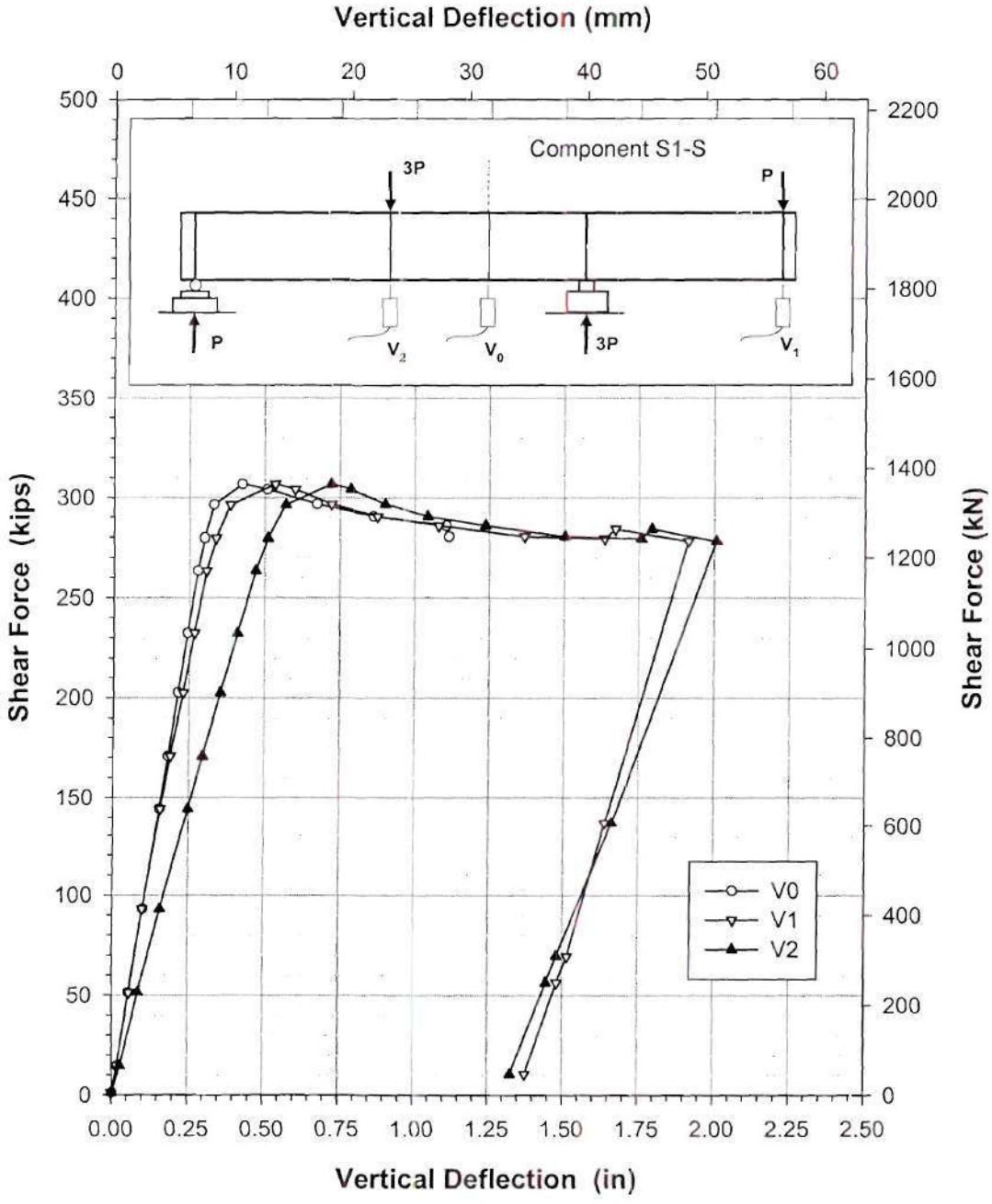

Figure 18 Load-vertical deflection curves for girder S1-S

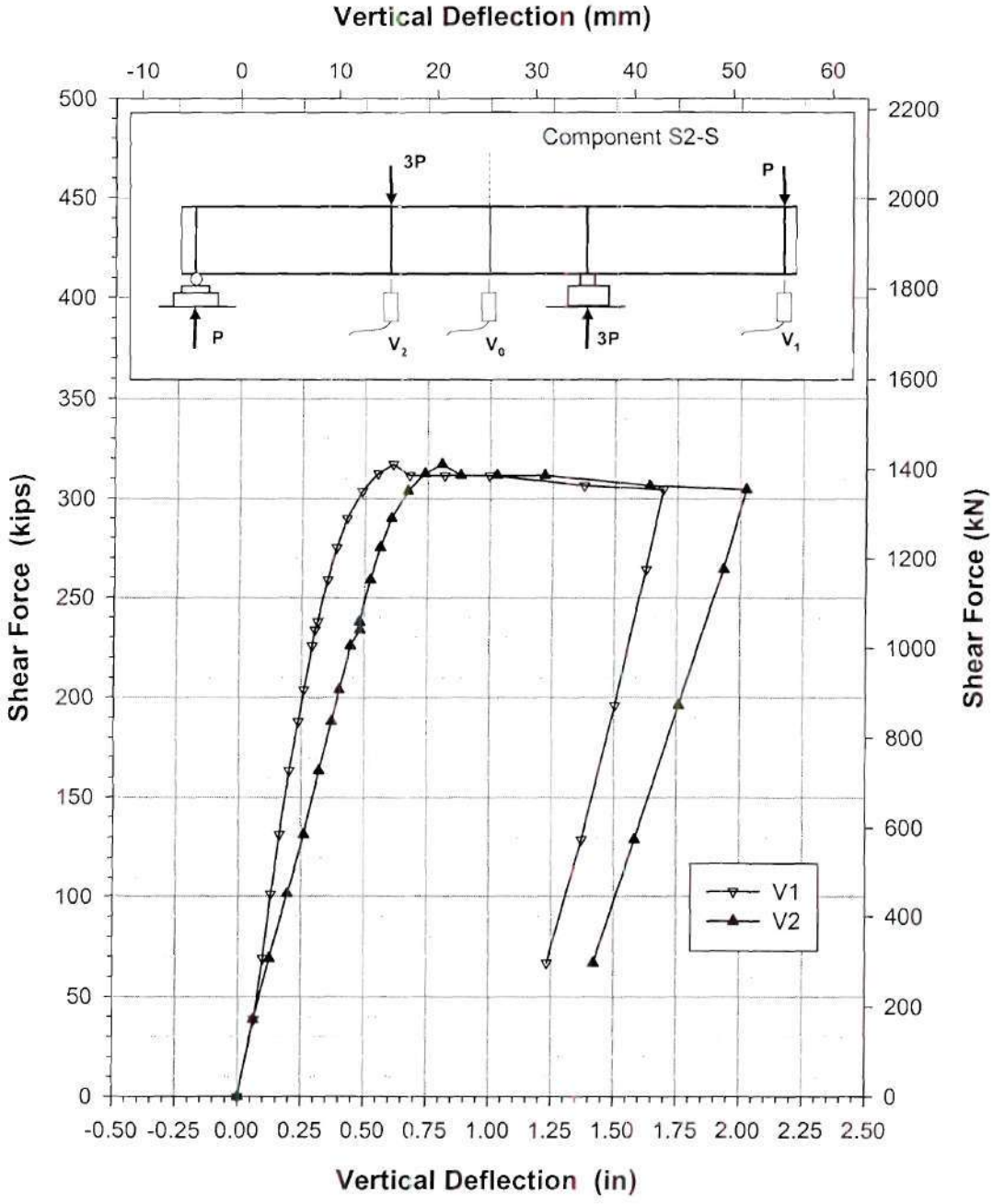

Figure 19 Load-vertical deflection curves for girder S2-S

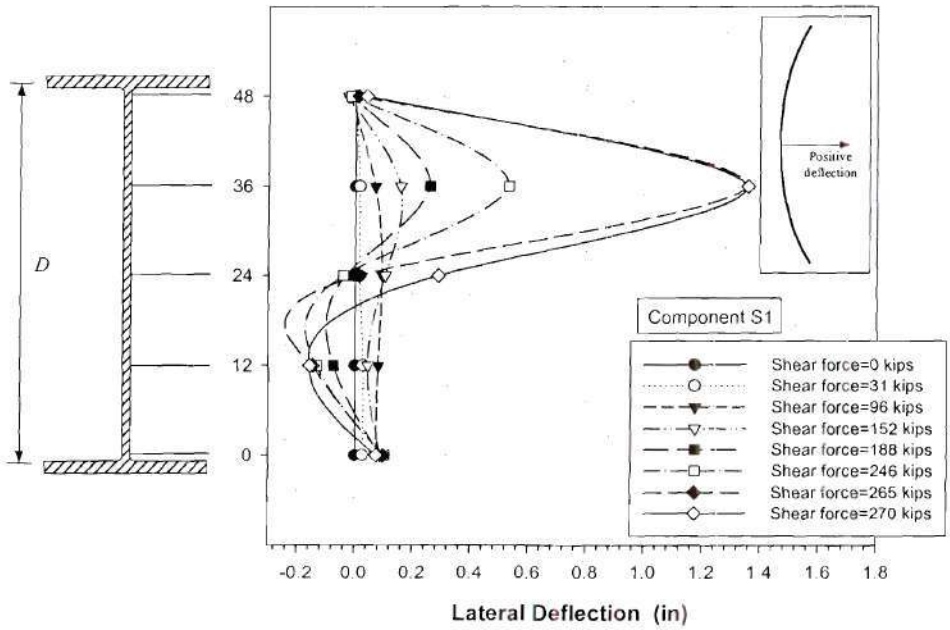

Figure 20 Web radial deflections of girder S1 at the middle of the test segment

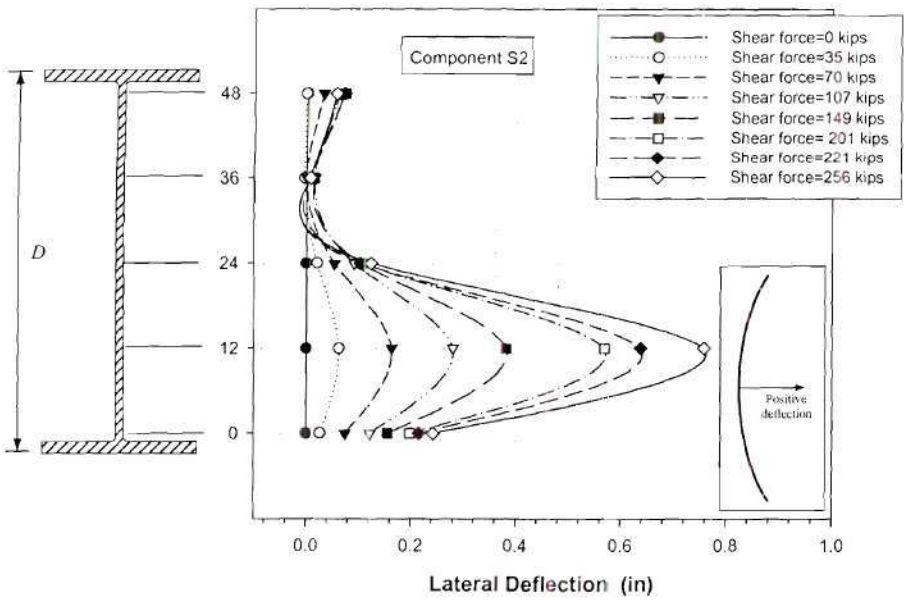

Figure 21 Web radial deflections of girder S2 at the middle of the test segment

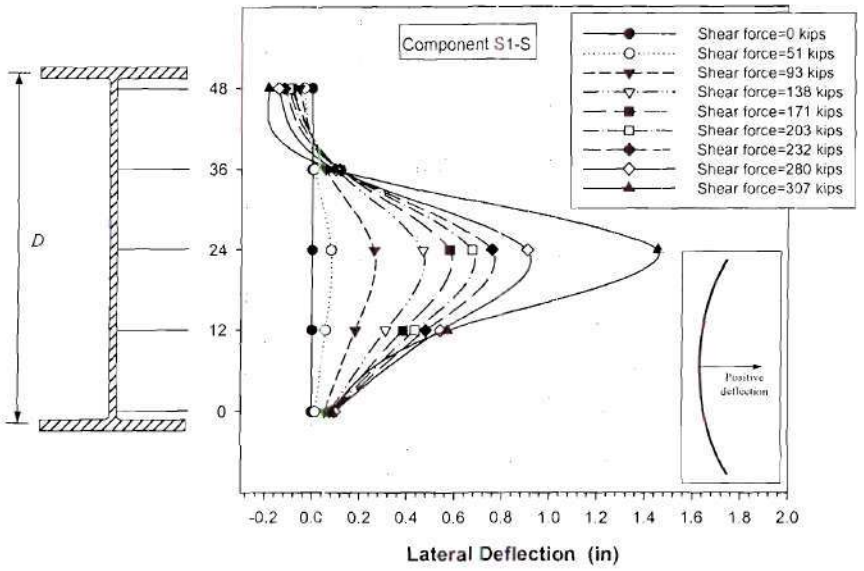

Figure 22 Web radial deflections of girder S1-S at the middle of the left-side test panel.

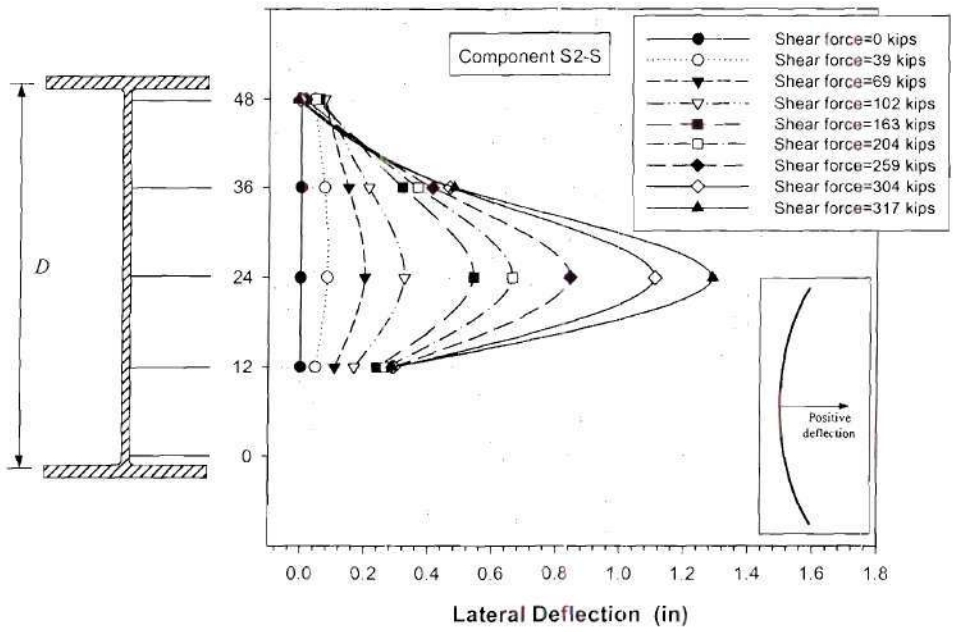

Figure 23 Web radial deflections of girder S2-S at the middle of the right-side test panel

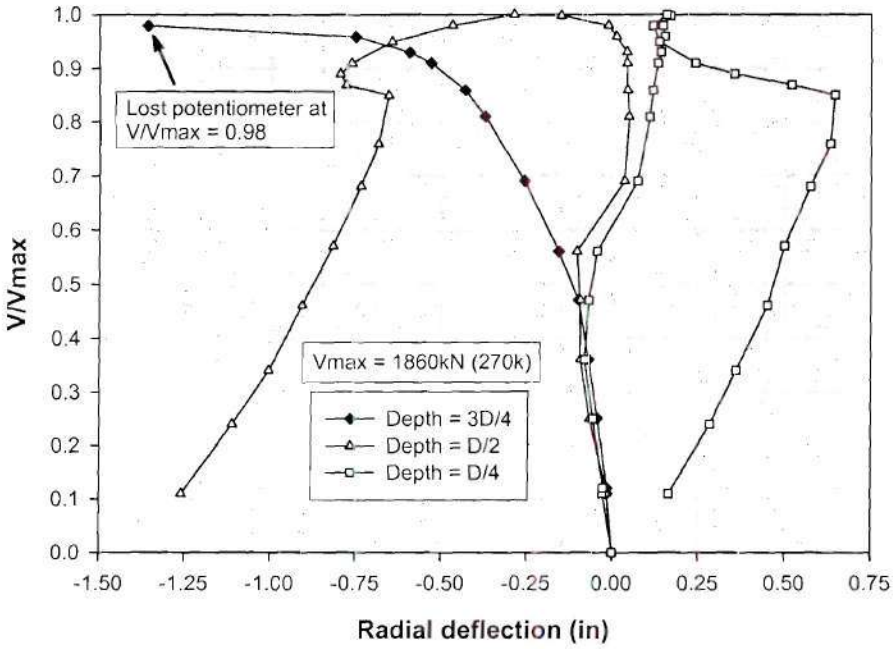

Figure 24 Girder S1- radial displacement at locations D/4, D/2 and 3D/4 versus V/V_{max}

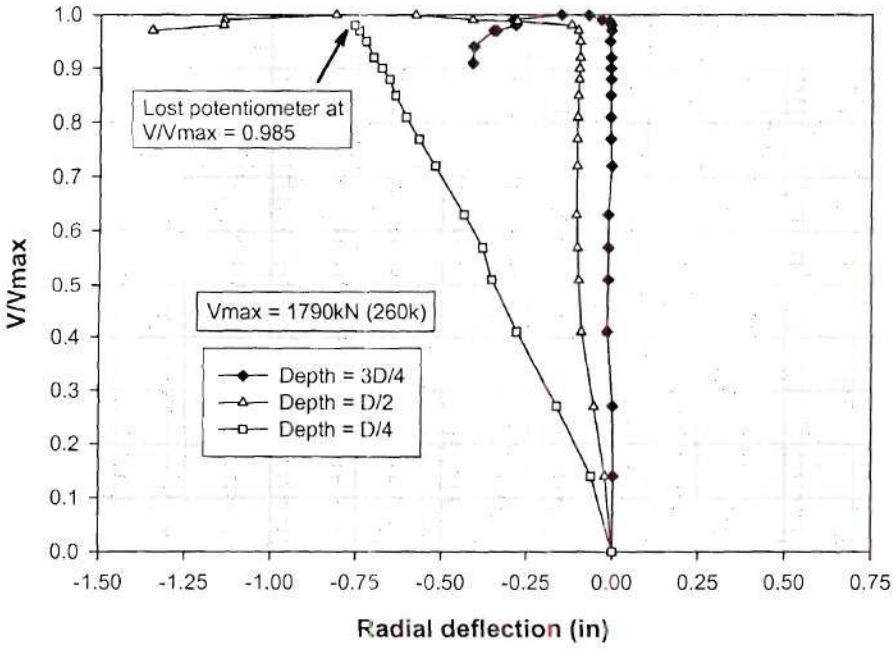

Figure 25 Girder S2 - radial displacement at locations D/4, D/2 and 3D/4 versus V/V_{max}

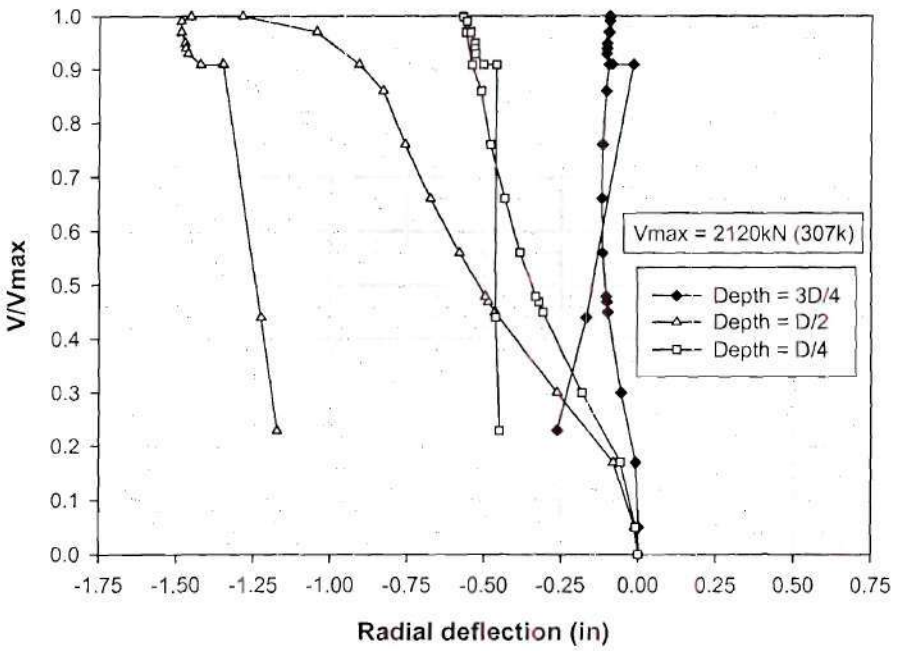

Figure 26 Girder S1-S - radial displacement at locations D/4, D/2 and 3D/4 versus V/V_{max}

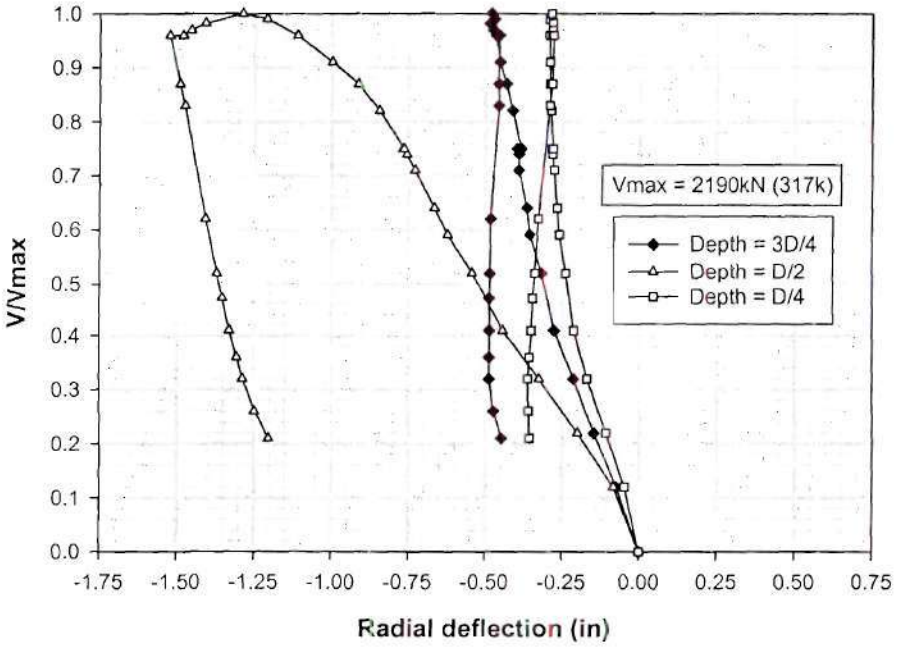

Figure 27 Girder S2-S - radial displacement at locations D/4, D/2 and 3D/4 versus V/V_{max}

One can observe that in all of the tests the load-vertical displacement response was only slightly nonlinear until just before the shear capacity was reached. At 95 percent of the shear capacity, the maximum deviation of the vertical displacements v_1 and v_2 from a secant line taken from the origin through the data point closest to 50 percent of the measured shear capacity was 28 percent (corresponding to the curve for v_2 in girder S2-S, see Figure 19). Furthermore, the loss in shear strength with increasing vertical deflections was small within the post-peak range of the response. The largest reduction in the shear strength in all the tests was approximately 15 percent at the end of the post-peak portion of the tests (corresponding to girder S1, see Figure 16). As noted previously, all of the tests were terminated at approximately $v_2 = 50$ mm (2 in). This deflection ranges from 2.2 to 3.4 times the deflection at the maximum shear strength. The displacement at the middle of the test segment in girders S1 and S2 actually reverses direction, i.e., this point moves upward, after the maximum shear capacity was reached. This behavior was associated with the bottom flange pushing up into the web, and with compressive diagonal strains within the web plate as discussed subsequently.

The radial displacements of the web were predominantly toward the inside direction, i.e., toward the center of curvature of the girders (see Figures 20 through 27). This was due to the initial tendency of the web panel to straighten out along the diagonal tension direction associated with the shear force. However, as the web shear force increases, stability effects associated with the diagonal compression in the web panel result in the gradual development of shear buckling waves. The radial displacements shown in Figures 20 through 23 were maximum at the location through the web depth corresponding to the largest (or dominant) shear buckling wave. The largest measured radial web displacement at the maximum shear capacity was approximately 38 mm (1.5 in) in girder S1-S and 33 mm (1.3 in) in girder S2-S. By extrapolation from

the measured deflections within the bottom of the web in S1 and within the top of the web in S2, and based on approximate measurement of the residual displacements at the completion of the tests, it was apparent that the maximum panel radial displacements in the unstiffened girders was slightly larger than 38 mm (1.5 in) at the maximum load (the maximum residual radial displacements in these girders were XX mm (X.X in) for girder S1 and XX mm (X.X in) for girder S2). These maximum radial displacements were somewhat larger than the initial offset of the web from a straight chord between the positions where the dominant web buckle intersects the flanges. At 95 percent of the shear capacity, the maximum radial displacements range from approximately 18 mm (0.73 in) in girder S1 to approximately 28 mm (1.10 in) in girder S2-S. It is interesting that at 95 percent of the shear capacity, the radial displacements in the two stiffened webs were somewhat larger than those in the two unstiffened webs.

The shear-radial displacement curves shown in Figures 24 through 27 range from essentially linear load-deflection response up to the peak load level (see Figure 25 for girder S2) to a significantly nonlinear pre-peak load deflection response in Figure 24 for girder S1. The load-radial deflection curves for both of the stiffened girders (see Figures 26 and 27) exhibit some nonlinearity, but show a gradual growth in the maximum measured radial displacement throughout the pre-peak portion of the response. The load-radial deflection curves for all the tests indicate the gradual development of shear buckling waves within the web panels with increasing shear force. The web shear-radial deflection behavior in girder S1 was the closest of all the tests to a bifurcation response. In this test (see Figure 24), the slope of the shear-radial deflection curve at 3D/4 (the location of the maximum measured radial displacement) increased noticably at a shear force between 0.46 and 0.56 V_{max}, whereas the corresponding radial deflections at D/4 and D/2 actually decrease and then change sign as the shear increases above this load level (i.e.,

the radial deflections at D/4 and D/2 were initially toward the center of curvature, but the web starts to deflect outward from the center of curvature at these locations as the shear was increased above 0.46 V_{max}. In all of the other tests, the web displacements at locations D/4, D/2 and 3D/4 either increase or remain essentially constant in value as the shear force was increased within the pre-peak range of the response. Due to the presence of initial imperfections in the web panels and the stable nature of the web postbuckling response, there was no clear indication of a web shear buckling load being exceeded (the theoretical web shear buckling loads are discussed in Chapter 5). This behavior was similar to the web response observed by Basler et al. (1960) and others in tests of straight I girders.

4.3 GIRDER DISTORTIONS AT MAXIMUM SHEAR CAPACITY AND IN POST-PEAK

Figures 28 to 31 show photographs of the girder test segments at the maximum shear capacity in each of the experiments. These figures illustrate the fact that the overall girder distortions were relatively small at the maximum shear strength. In each of these photos, one can observe that the white wash started to flake off of the web along a narrow diagonal strip. This strip extended from corner to corner of the left-most panel of the test segement in girders S1-S and S2-S, it extends from the bottom-left corner of the test segment essentially through the rosettes R2 in girder S1, and it extends from the top-right corner of the test segment through the rosettes R6 in girder S2.

Figures 32 through 39 show outside views of the distorted girders at the end of the tests, when the girders were still located within the test frame, and inside views of the distorted test

segments after the girders have been removed from the test frame. Since the girder distortions grow signficantly within the post-peak portion of the tests, these photos are useful in discerning the final failure modes of the girders. The white wash is flaked off of the face of the panels in these photographs primarly due to compressive surface strains associated with the development of the dominant shear buckling wave. As noted by Basler et al. (1960), this flaking of the white-wash reveals surface conditions created by both membrane and bending strains, and therefore, it should not be identified with the width of a tension field. However, these photos show a clear indication of the location and orientation of the dominant shear buckling wave within the web panels.

In girder S1, the dominant shear buckle extends from the bottom-left corner of the test segment (in the outside view) to a location on the top flange approximately $0.40d_o$ to the left of the top right corner of this unstiffened web panel (see Figures 32 and 33). The center of this buckle crossed the radial potentiometer locations at the middle of the test segment at approximately 0.80D, which was just above the rosettes R4. This was evidenced by the large positive (inward) deflection of the web panel at 3D/4 shown in Figures 20 and 24. The center of this buckle also crosses approximately through the rosettes R2. The curvature due to frame action in the top flange was largest at approximately $0.25d_o$ and $0.45d_o$ to the left of the top-right corner; these locations corresponded roughly to the width of the web at the top flange over which a significant amount of whitewash has spalled off (as shown in Figure 33).

The dominant shear buckle in girder S2 was similar to that in S1 except that it extends from the top-right corner to just below the mid-distance between rosettes R7 and R8 (located at $0.25d_o$ from the right-hand end of the panel in the outside view), and through rosettes R6 and radial potentiometer location at D/4 above the bottom of the web at the mid-length of the test segment

(see Figures 34 and 35). This buckle intersected the bottom flange at approximately $0.30d_o$ from the bottom-left of this web panel (again in the outside view). The curvature in the bottom flange due to frame action was largest at approximately $0.19d_o$ and $0.53d_o$ from the left side of this segment.

The dominant web buckle in Girders S1-S and S2-S extended essentially from corner to corner of the right-side web panel in S1-S and the left-side web panel in S2-S (see Figures 36 and 37 for girder S1-S and Figures 38 and 39 for girder S2-S). These panels were the opposite of the instrumented web panels in each of these girders. The behavior of the two web panels within the test segment of these girders was very similar up to the maximum load level. However, after the shear capacity was reached, the girder distortions localized within the panels that did not contain the strain rosettes.

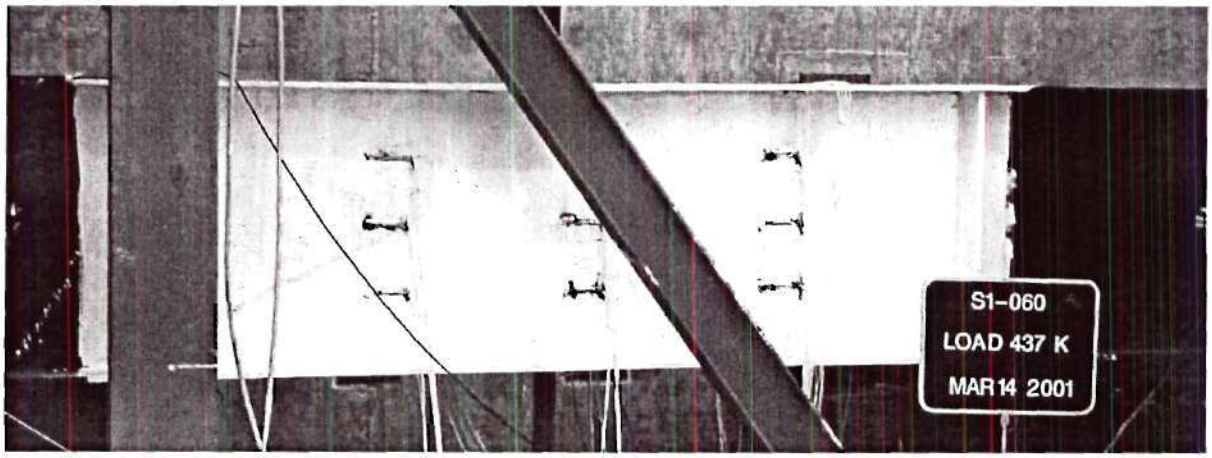

Figure 28 Girder S1 at peak load

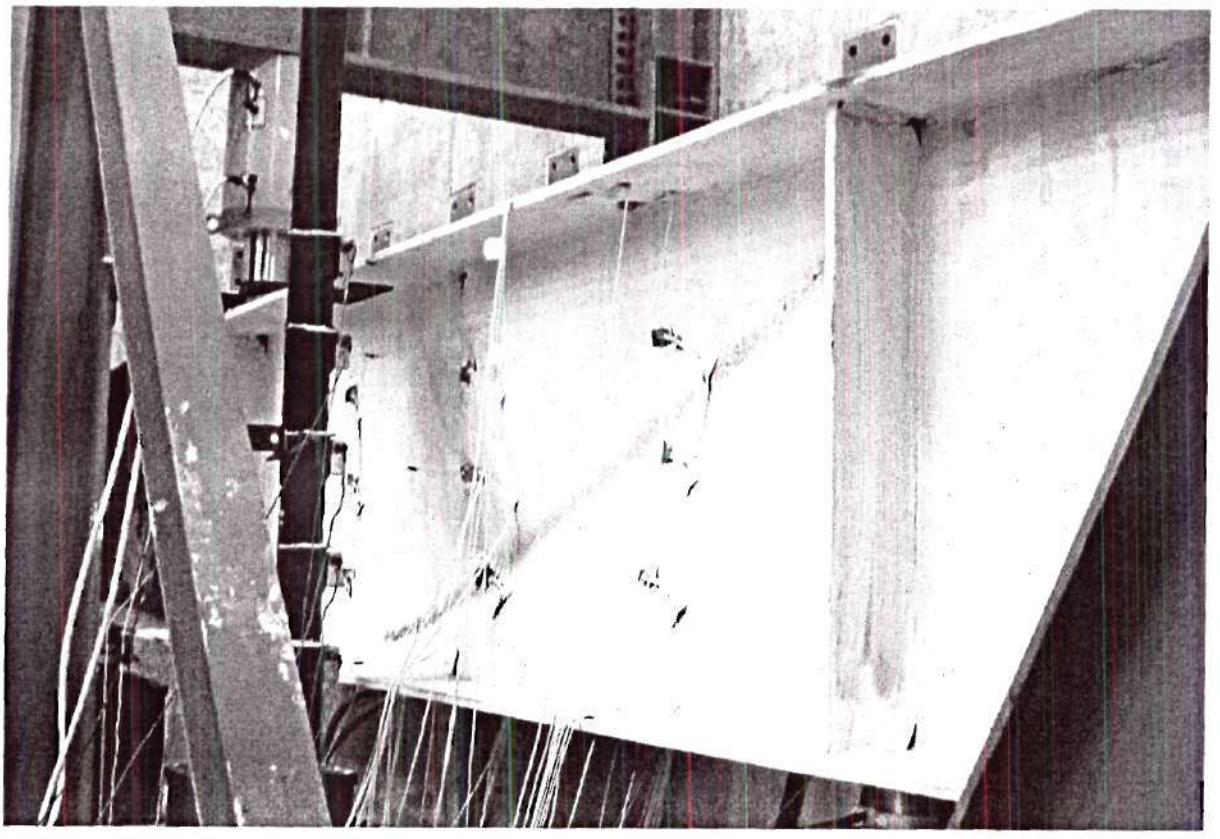

Figure 29 Girder S2 at peak load

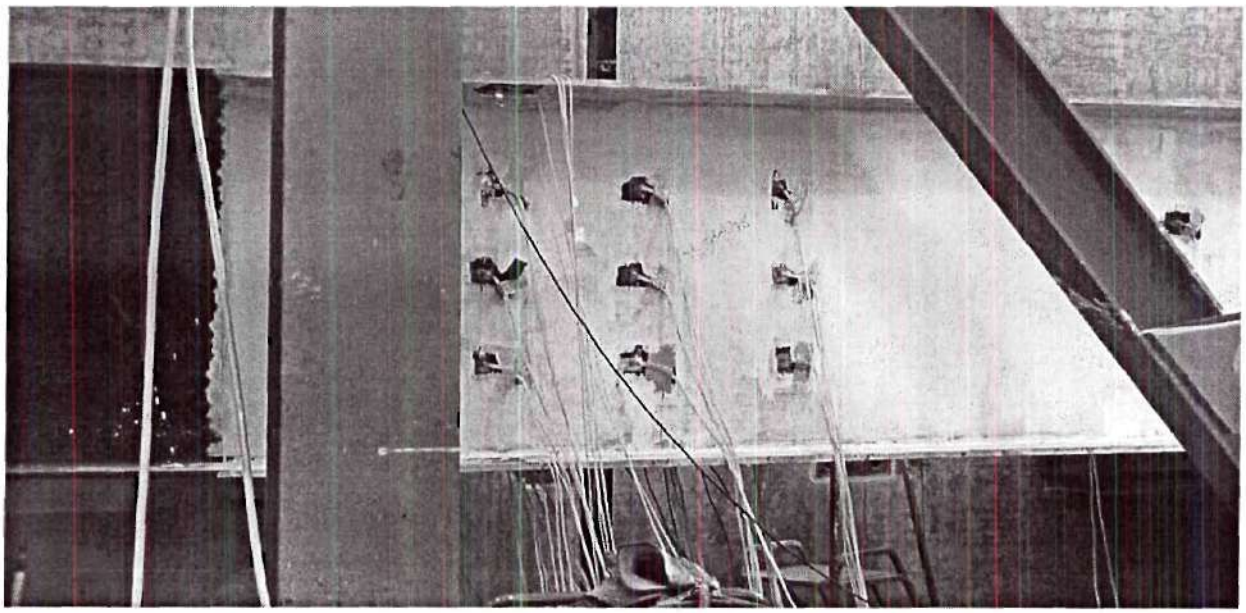

Figure 30 Girder S1-S at peak load

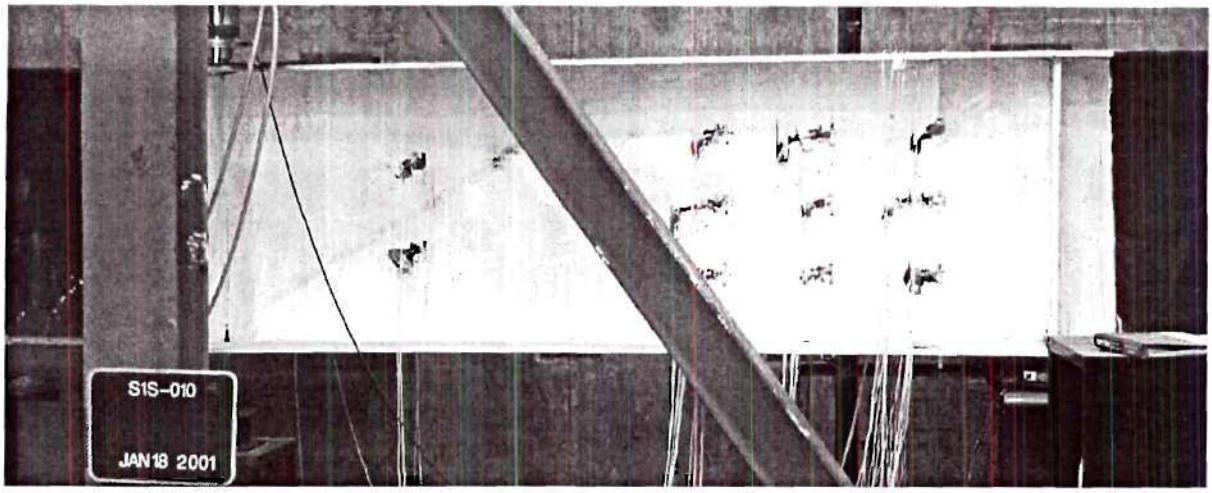

Figure 31 Girder S2-S at peak load

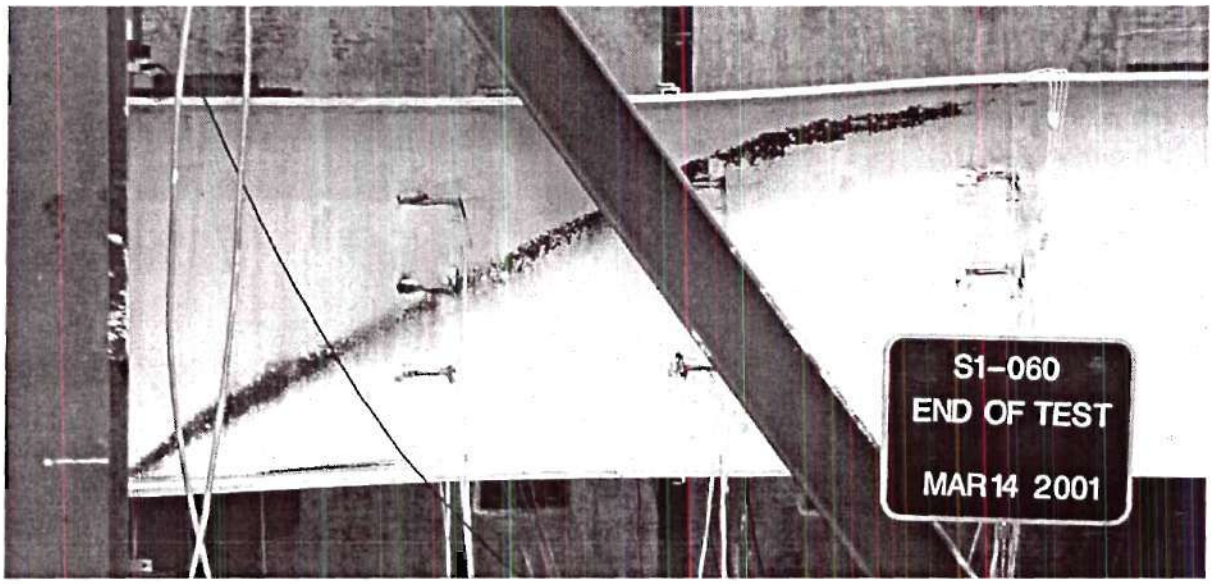

Figure 32 Girder S1, outside view at end of test

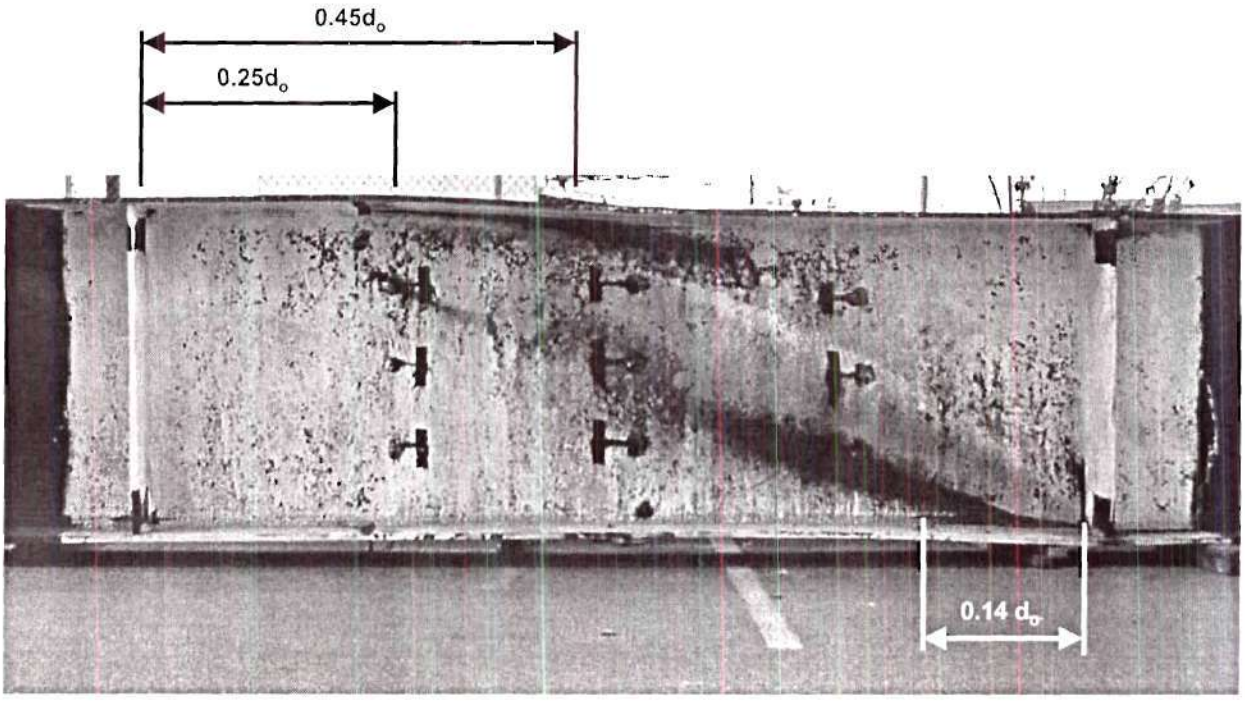

Figure 33 Girder S1, inside view after test

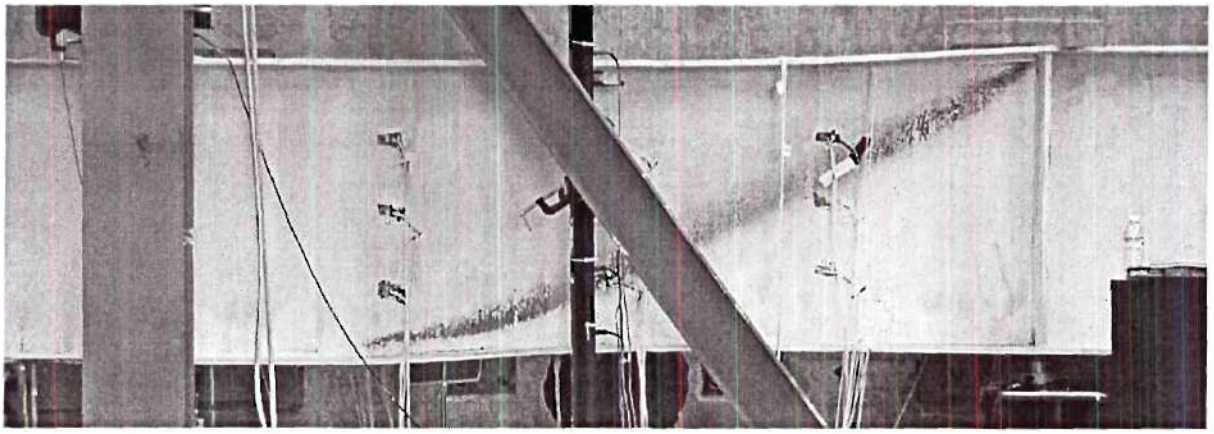

Figure 34 Girder S2, outside view at end of test

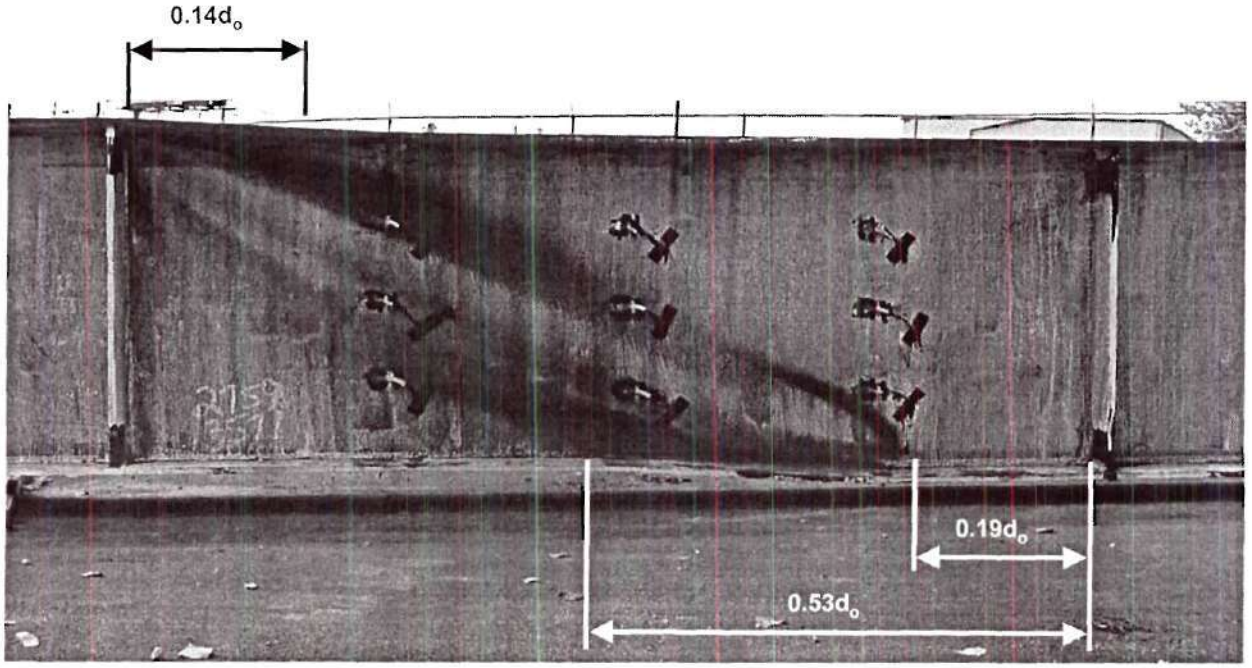

Figure 35 Girder S2, inside view after test

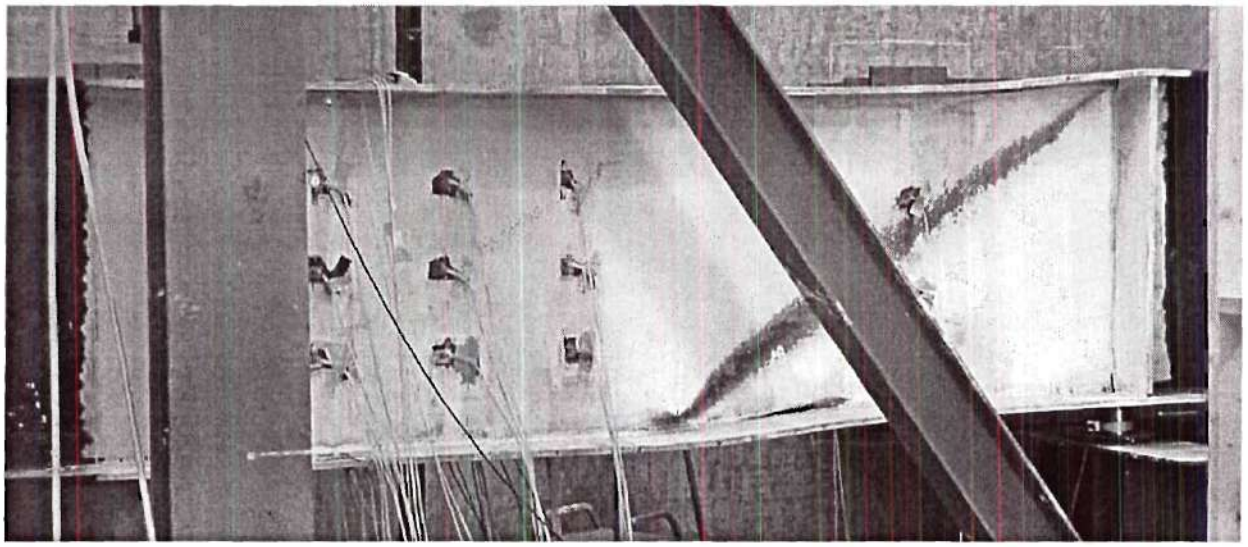

Figure 36 Girder S1-S, outside view at end of test

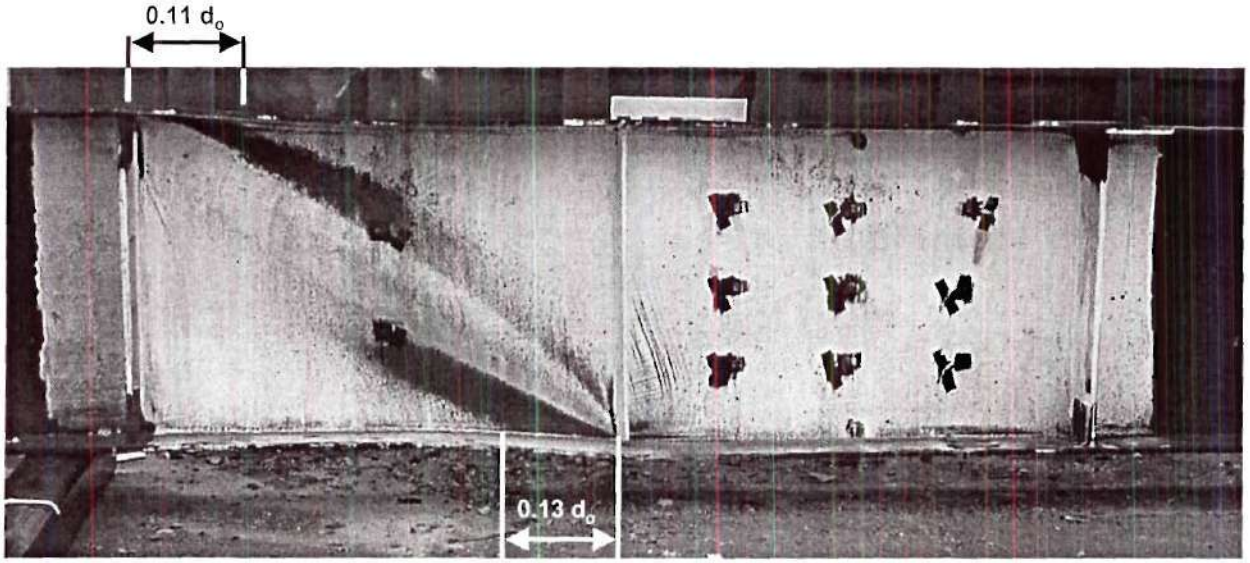

Figure 37 Girder S1-S, inside view after test.

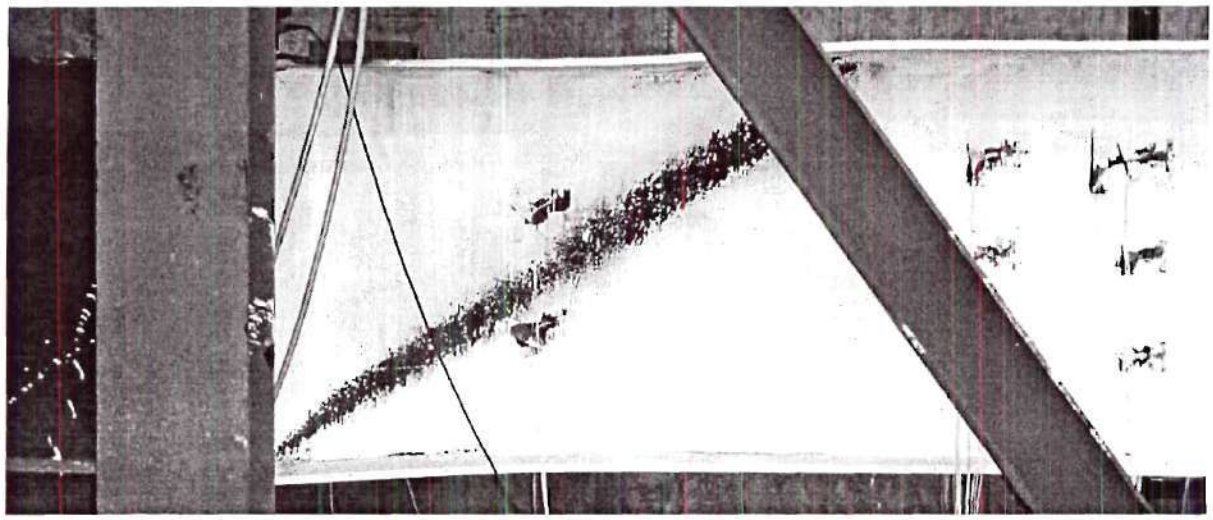

Figure 38 Girder S2-S, outside view at end of test.

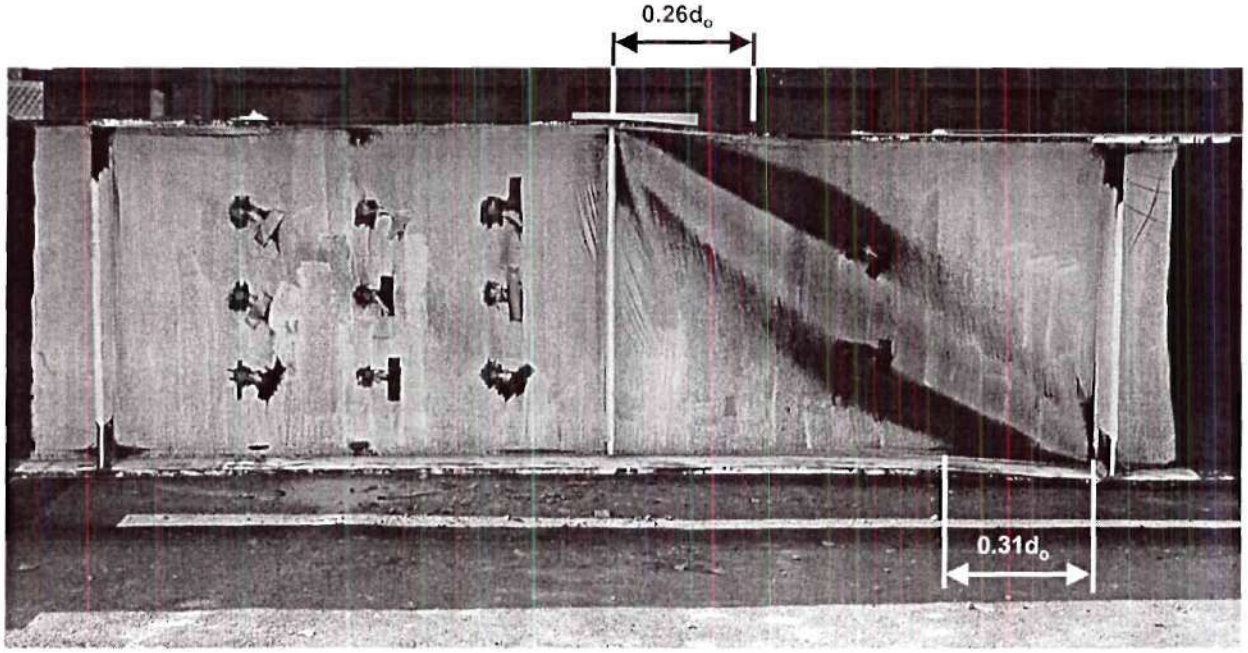

Figure 39 Girder S2-S, inside view after test.

4.4 WEB PRINCIPAL STRAINS AND ELASTIC MISES STRESSES

Figures 40 through 43 and 46 through 49 illustrate the magnitudes and orientations of the principal strains e_1 and e_2 calculated from the average of the surface strains at rosettes R1 through R9, i.e., the web principal membrane strains in each of the tests. These figures show the principal membrane stains at the maximum shear capacity and at the end of the post-peak region of the response, just prior to removal of the loads. The tensile principal strains are indicated by the thin lines in these figures while the compressive principal strains are indicated by the thick lines. The locations at which yielding has occurred at these loading steps (outside surface, inside surface and/or mid-thickness), the level of V/V_{max} at which yielding first occurs at these locations, and the orientation of the principal direction Θ_{p1} with respect to the horizontal are shown next to the gage locations in each of these figures. In the figures illustrating the post-peak responses, the values of V/V_{max} are underlined for the locations at which yielding starts in the post-peak range. The onset of yielding was determined by calculating the elastic Mises stress at each location based on the assumption of an isotropic elastic material and comparing this stress to the average yield strength of the web material. This calculation neglects the influence of any initial residual stresses on the onset of yielding. The lines indicating the principal strain magnitudes are drawn to the same scale in Figures 40, 41, 46 and 47, and are drawn to a scale 3.33 times larger in Figures 42, 43, 48 and 49.

Figures 44 and 45 show the magnitudes and orientations of the outside surface strains in girders S1-S and S2-S at the maximum shear capacity. These figures are included to supplement Figure 43, since the data was not available from several of the rosettes on the inside surface of the web in the test of girder S2-S.

Figures 50 through 57 give the magnitudes of the principal strain differences Δe_1 and Δe_2 and their orientations determined at the rosette locations at the above load stages. The principal strain differences Δe_1 and Δe_2 were determined by first calculating the strains e_x, e_y and γ_{xy} on the inside and outside surfaces at each of the rosette locations, then taking the difference between these strain components at the two surfaces, and finally calculating the prinicpal values of these strain differences. The strain magnitudes in these figures are all drawn to the same scale as those in Figures 40, 41, 46 and 47.

Figures 40 to 43 indicate that at the maximum shear capacity in each of the tests, the web has just yielded through its entire thickness along a diagonal tension band. As would be expected based on the locations at which the whitewash was starting to spall in Figures 28 through 31, this band cuts through gages R2 and R4 in girder S1, through gages R8 and R6 in girder S2, and through gages R3, R5 and R7 in girder S1-S. Although the strains at the inside rosettes at R3 and R5 were lost in girder S2-S, indications from the membrane strains at R7 and from the outside surface strains at R3 and R5 indicate that the web behavior in S1-S was very similar to that in girder S2-S. Both the tensile and compressive membrane strains were relatively large in magnitude at most of the gage locations along the tension band. In girder S1-S (and apparently also in S2-S, based on Figure 45), these tensile and compressive membrane strains were fairly uniform at each of the gage locations along the tension band. However, in girder S1, the membrane strains were highly localized at gage R2. The membrane strains at R3 were also relatively large compared to the other gage locations at the maximum load level, although the web was not yielded through its entire thickness at this location when S1 reaches its maximum shear capacity. In girder S2, the membrane strains were highly localized at R6 at the maximum load level.

The principal membrane tension orientations range from 60 degrees to 16 degrees relative to the horizontal direction in girder S1, with the largest angle of orientation at gages R2 and R3 where the strains were the largest, and from 25 to 37 degrees in girder S2, with the largest angle of orientation located at gage R6 where the strains were the largest. In girders S1-S and S2-S, the principal membrane strains were 35 to 38 degrees for the gages along the tension band. This was approximately the same as diagonal orientation between the corners of the web panel, Θ_d = 34 degrees.

Figures 46 through 49 show the principal membrane strains at the end of the post-peak portion of the tests, just prior to removal of the load from the girders. Generally, in all of the tests, the principal strain orientation Θ_{p1} tended to decrease as the girders were deformed in post-peak. The angle Θ_{p1} ranges from 19 to 48 degrees for the gage locations that experience plastic deformation in girder S1, and from 18 to 26 degrees for these gages in girder S2 at the end of the post-peak region. This angle reduces only slightly to a range of 30 to 35 degrees and 30 to 36 degrees in girders S1-S and S2-S respectively for the rosette locations that experience plastic deformation. At the end of the post-peak region, the web was yielded through its entire thickness at all the rosette locations except R9 in girder S1, and at all the rosette locations except R1 and R2 in girder S2. The top-left region of the web panel experiences much smaller deformations in girder S1, and the bottom-right region of the web panel experiences much smaller strains in girder S2. At the end of the post-peak region, the web was yielded through its entire thickness at gages R3, R5, R7 and R8 in girder S1-S and at gages R4 and R7 (and likely also at gages R3 and R5, although the rosette data was incomplete at these positions).

The compressive principal membrane strain was significant at rosettes R4 in both girder S1 and at rosettes R6 in girder S2 at the end of the post-peak range of the response (see Figures 46

and 47). This was evidenced in Figures 32 and 33 for girder S1 and Figures 34 and 35 for girder S2 by the fact that the distance between the flanges in the vicinity of the middle of the web panel was reduced to less than the original depth of the web.

Figures 50 to 53 indicate significant web plate bending essentially in the transverse direction along the diagonal tension band at the maximum shear capacity in girders S2, S1-S and S2-S. The heavy lines, indicating principal compression strain differences, are associated with compressive strains on the outside surface of the webs due to plate bending. The orientations of the principal strain differences at the maximum shear strength of girder S1 exhibit a more complicated pattern, similar to the orientations of the principal membrane strain in this girder at this load stage (see Figure 40). It is believed that the more complex nature of the web behavior in girder S1, compared to S2, was associated with different states of initial geometric imperfections and/or residual stresses in these two girders.

Figures 54 to 57 show the principal strain differences in the web panels at the end of the post-peak range of the response. One can observe that the orientation and magnitude of the largest strain differences in Figure 54, corresponding to girder S1, were starting to line up with the direction of the maximum principal membrane strains for this girder at this load stage (see Figure 46). For the other girders, the largest principal strain differences were compressive (causing compression on the outside surface due to plate bending) and in orientations approximately orthogonal to the direction of the prinicipal membrane tension in the web panels at the end of the post-peak range of the response.

Detailed plots of the variation of the web principal membrane strains and strain differences and their orientations are presented in Figures 58 through 61 for girder S2. Figure 58 shows the variation in the principal membrane strain orientation Θ_{p1} at gages R1 through R9, Figure 59

shows the variation in the principal membrane strain e1, Figure 60 shows the variation in the prinicpal membrane strain e_2, and Figure 61 shows the variation in the largest of the principal strain differences Δe_1 or Δe_2, all as a function of the normalized applied web shear force. In each of these plots, the load level corresponding to the onset of yielding at the first surface location is indicated by a large grey circle, the load level corresponding to the onset of yielding at both surface locations is indicated by a large grey square, and the load level corresponding to onset of yielding at the mid-surface of the web plate is indicated by a black circle or square. A black circle indicates that yielding was detected at one of the surface gages and at the mid-surface of the plate and a black square indicates the onset of yielding throughout the thickness of the web, i.e., at the two surface gages and at the mid-thickness.

Figure 58 illustrates the tendency of the angle Θ_{p1} to reduce as the web shear increases within the pre-peak portion of the test, and particularly after the maximum shear capacity of the web was reached. Figures 59 and 60 show that the web membrane strains vary in a reasonably linear fashion with the web shear force essentially up to the point that the web shear capacity was reached. Figure 46 shows that the web maximum principal strain differences at rosettes R2, R5, R6 and R8 were actually larger than the maximum web principal membrane strains within the pre-peak range of the response.

It is interesting that at the onset of yielding at one of the surfaces of the web plate, indicated by the large grey circles in Figures 58 through 61, there was generally little change in the slope of the curves. In other words, the apparent onset of yielding does not have any significant impact on the response. This was the case even though the initial yield load level was calculated neglecting potential residual stress effects and even though first yield is defined by the first data

point at which the elastic Mises stress exceeds the average yield strength of the web plate - in some cases the elastic Mises stress for this data point was significantly larger than F_y.

Figures 62 through 64 show the variation of the elastic Mises stresses at locations R1 through R9 in girder S2. These figures help illustrate the progression of yielding within the web panel, which combined with the destablizing effects in the diagonal compression direction, eventually result in the maximum strength of the web being reached. These figures emphasize the fact that a significant portion of the web plate was yielded prior to reaching the maximum shear strength. The maximum strength of the web was reached due to a combination of the effects of progressive yielding and diagonal compression. Figures 41, 51, 59 to 61 and 62 to 64 clearly show that the final failure of the web was associated with large increases in tensile and compressive membrane strains as well as large increases in web plate bending in a direction approximately transverse to the direction of principal membrane tension in the vicinity of the rosettes R6.

Figures 65 through 70 for girder S1-S are organized similarly to Figures 58 through 64 for girder S2. The overall behavior in the strains as a function of the load level was similar to that for girder S1 except that the angles Θ_{p1} in Figure 65 for girder S1-S were generally larger than those in Figure 58 for girder S2, and the web membrane and plate bending strains subsequent to reaching the maximum shear capacity were relatively uniform along the diagonal of the web panel in girder S1-S whereas they were more localized to the region in the vicinity of rosettes R6 in girder S2. The pre-peak maximum principal strains and strain differences were similar in both girders, even though girder S2 has a larger panel aspect ratio and a smaller radius of curvature.

The overall behavior associated with the maximum shear capacity of the web of girder S1 was similar to that in girder S2. However, possibly because of the near bifurcation behavior as

evidenced by the plots in Figures 20 and 24, influenced by potentially different imperfections and residual stresses, the orientations of the web strains were not as simple as in girder S2. Based on the experimental data collected for these girders, it is not possible to identify the specific source of the slightly larger shear capacity in girder S1 compared to girder S2.

The overall behavior in girder S2-S was also very similar to that in S1-S. However, the strains at the outside surface at rosettes R3 and R5 were somewhat larger in girder S1-S compared to girder S2-S at the maximum shear capacity (see Figures 44 and 45). Also, the web radial deflections were somewhat larger at the peak load in girder S1-S (see Figures 26 and 27). These differences are possibly due to different initial imperfections and residual stresses, and it can be inferred that the larger strength of girder S2-S was due to these effects. However, part of the differences between the shear capacities in these tests may be due to the small experimental error exhibited in the measurement of V_{max} in girder S1-S as discussed previously.

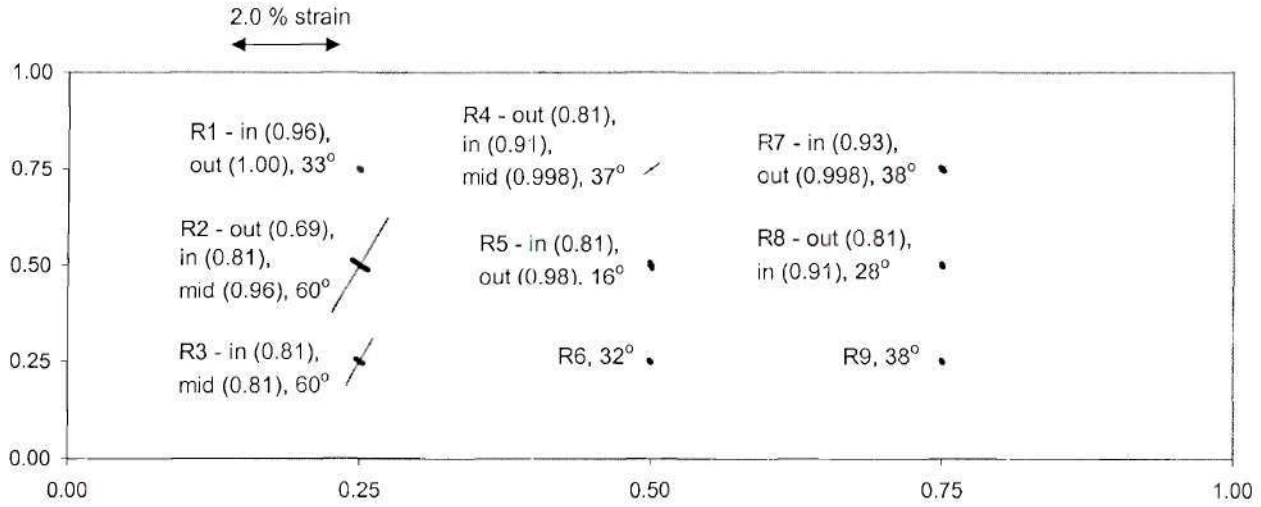

Figure 40 Yield locations and corresponding V/V_{max} values, and web principal membrane strain magnitudes and orientations in girder S1 at the maximum shear capacity

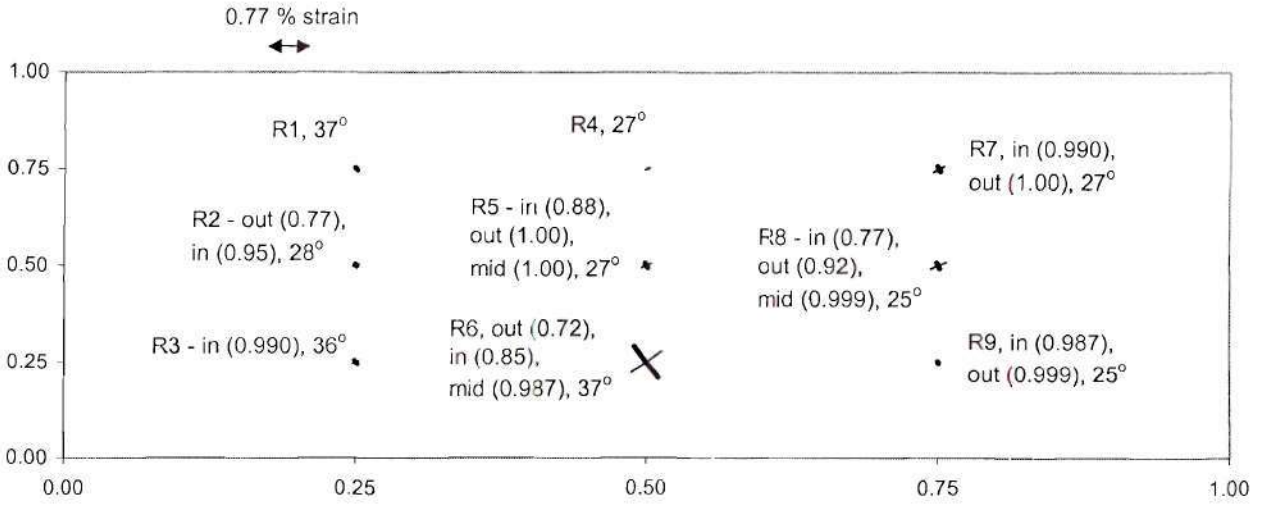

Figure 41 Yield locations and corresponding V/V_{max} values, and web principal membrane strain magnitudes and orientations in girder S2 at the maximum shear capacity

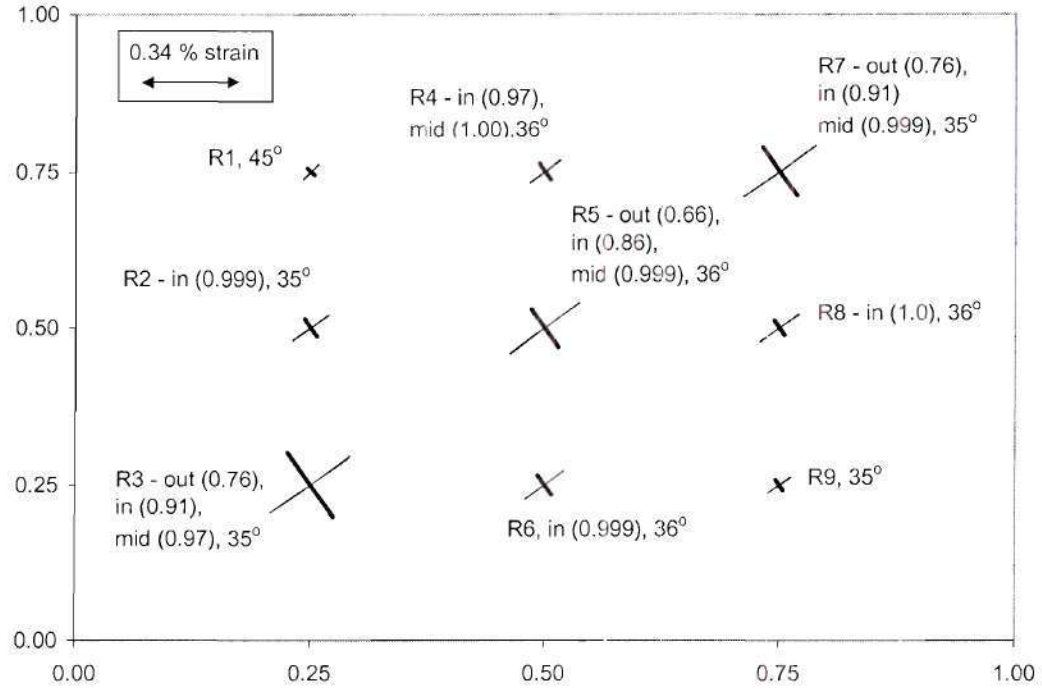

Figure 42 Yield locations and corresponding V/V_{max} values, and web principal membrane strain magnitudes and orientations in girder S1-S at the maximum shear capacity

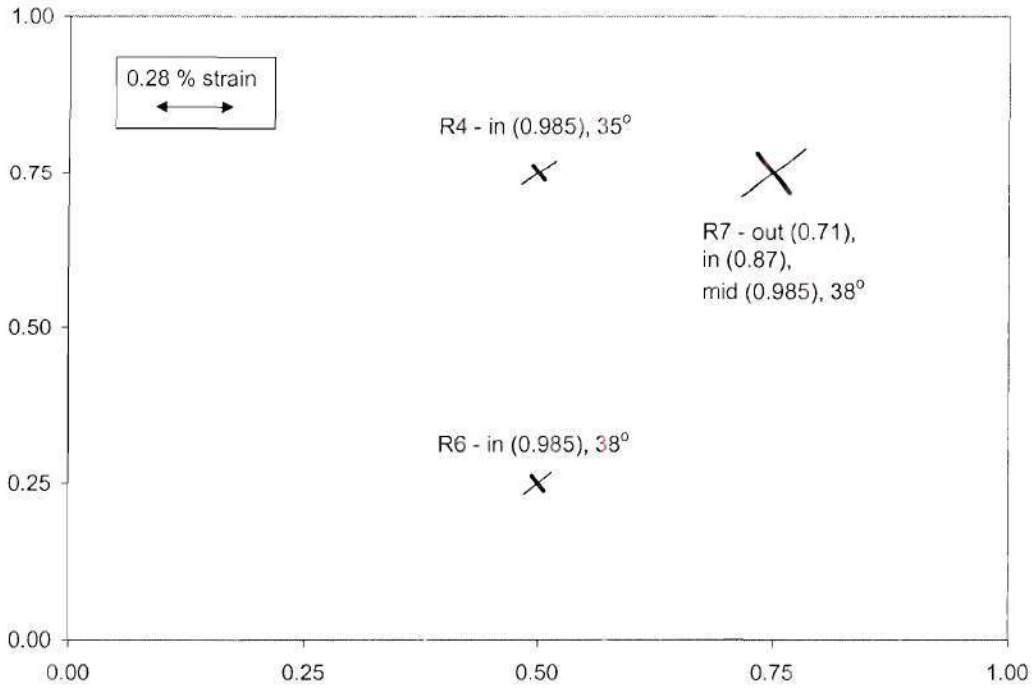

Figure 43 Yield locations and corresponding V/V_{max} values, and web principal membrane strain magnitudes and orientations at rosettes R4, R6 and R7 in girder S2-S at the maximum shear capacity

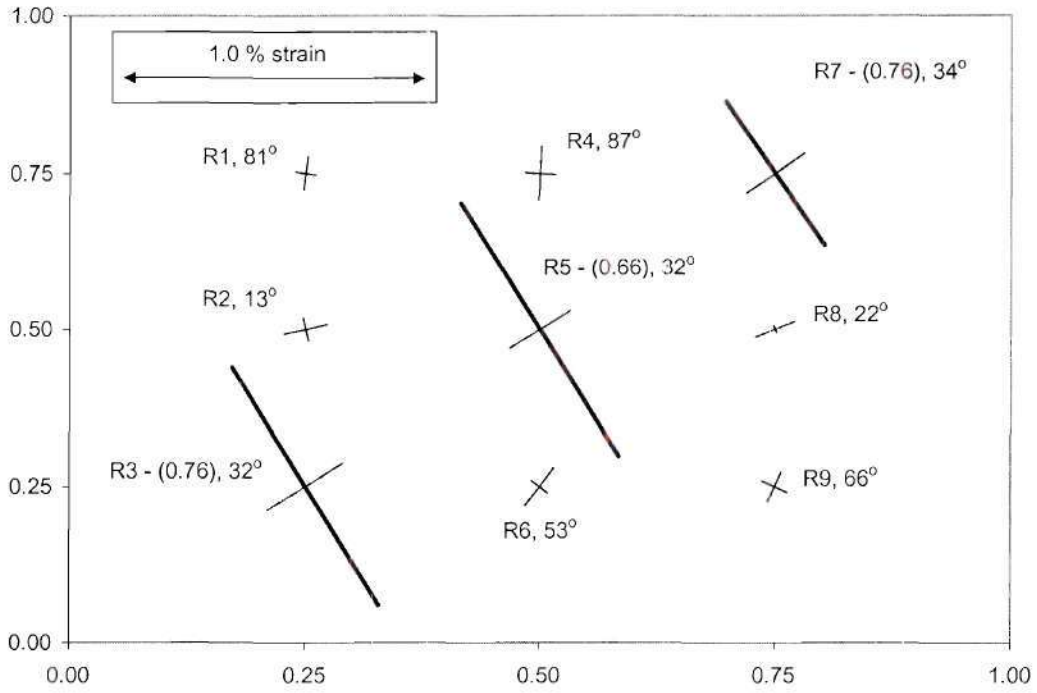

Figure 44 Outside surface yield locations and corresponding V/V_{max} values, and prinicpal strain magnitudes and orientations on the outside surface in girder S1-S at the maximum shear capacity

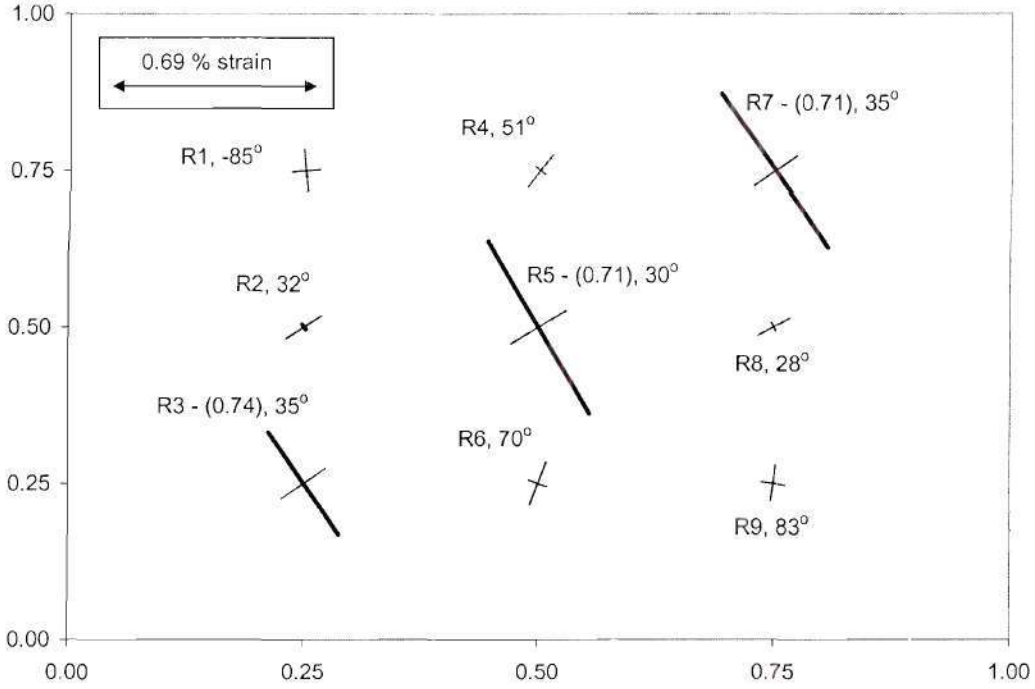

Figure 45 Outside surface yield locations and corresponding V/V_{max} values, and prinicpal strain magnitudes and orientations on the outside surface in girder S2-S at the maximum shear capacity

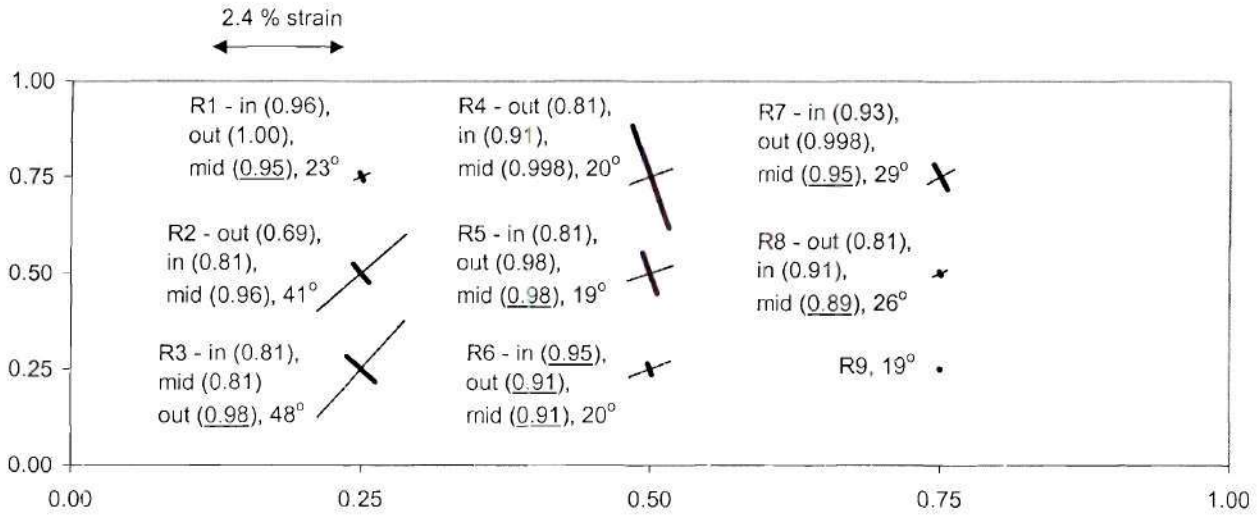

Figure 46 Yield locations and corresponding V/V_{max} values, and web principal membrane strain magnitudes and orientations in girder S1 at the end of the post-peak portion of the test

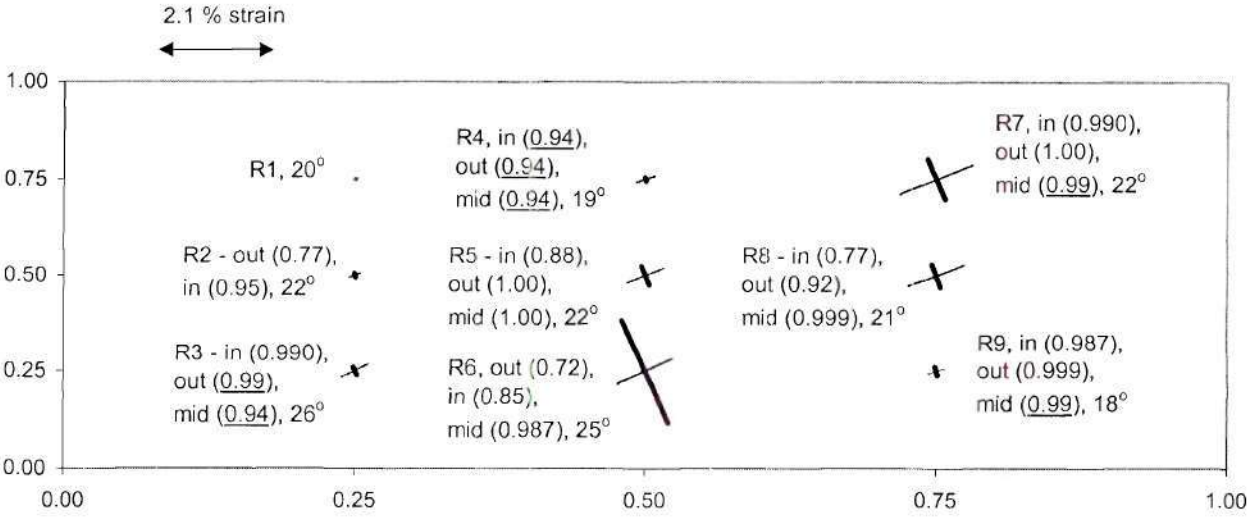

Figure 47 Yield locations and corresponding V/V_{max} values, and web principal membrane strain magnitudes and orientations in girder S2 at the end of the post-peak portion of the test

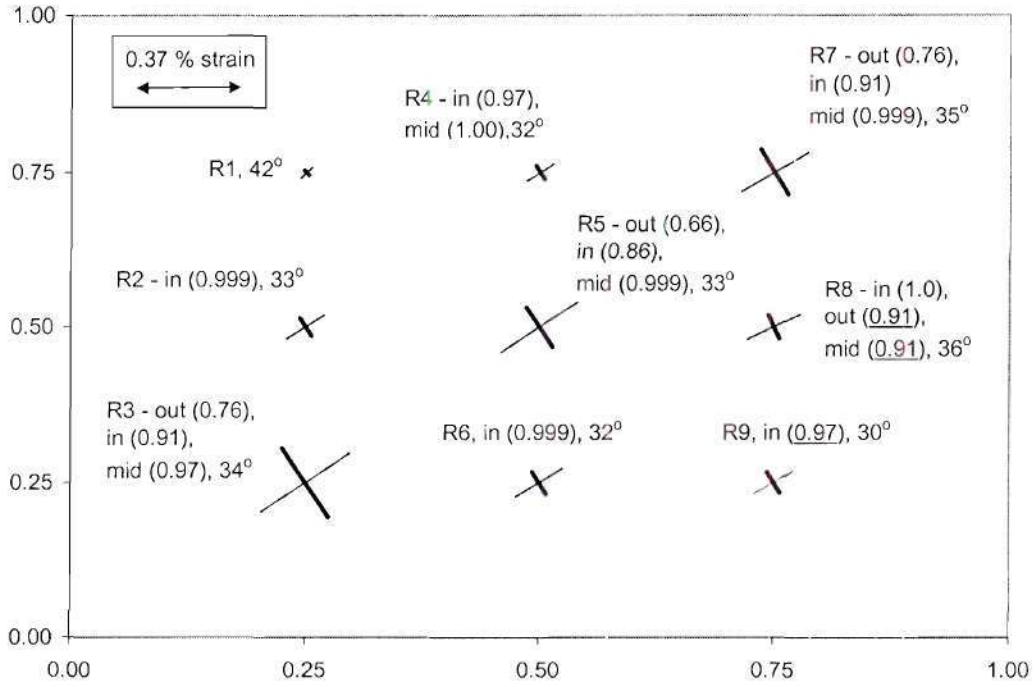

Figure 48 Yield locations and corresponding V/V_{max} values, and web principal membrane strain magnitudes and orientations in girder S1-S at the end of the post-peak portion of the test

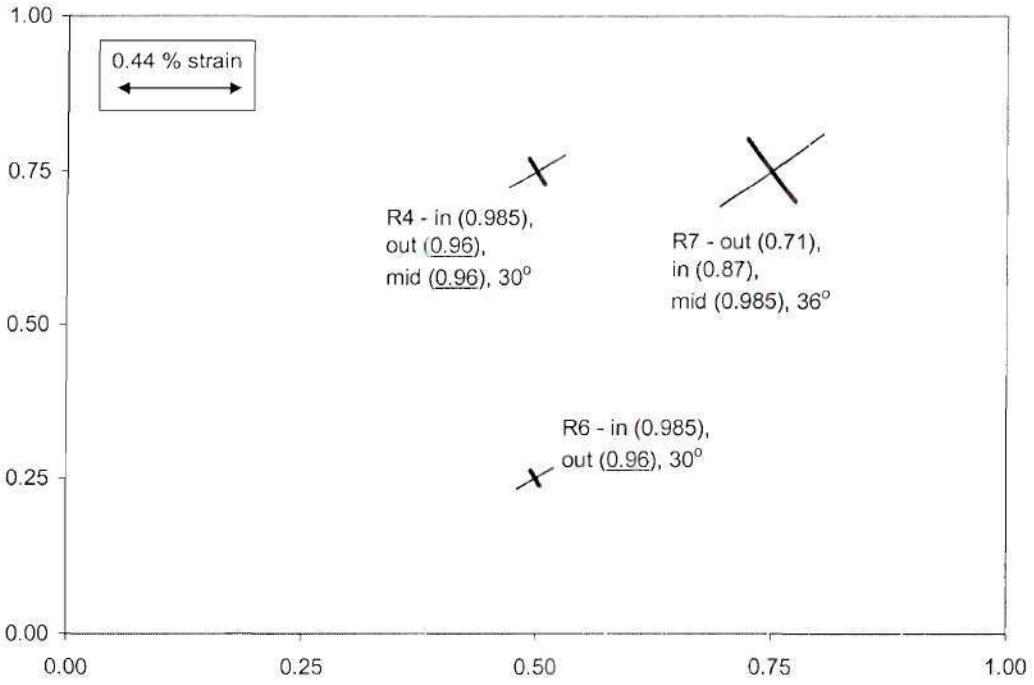

Figure 49 Yield locations and corresponding V/V_{max} values, and web principal membrane strain magnitudes and orientations at rosettes R4, R6 and R7 in girder S2-S at the end of the post-peak portion of the test

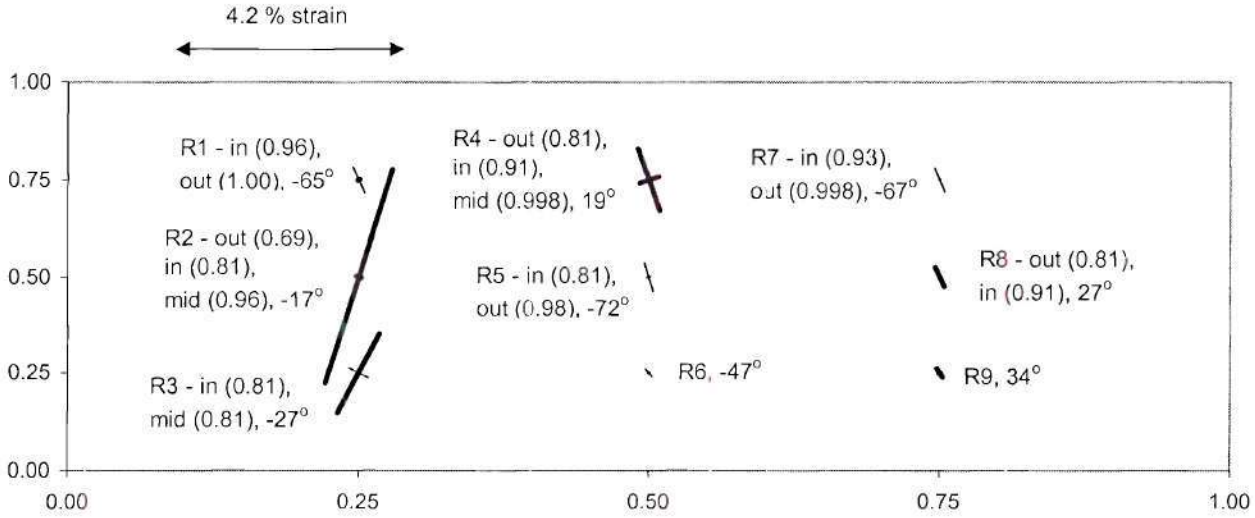

Figure 50 Yield locations and corresponding V/V_{max} values, and web principal strain difference magnitudes and orientations in girder S1 at the maximum shear capacity

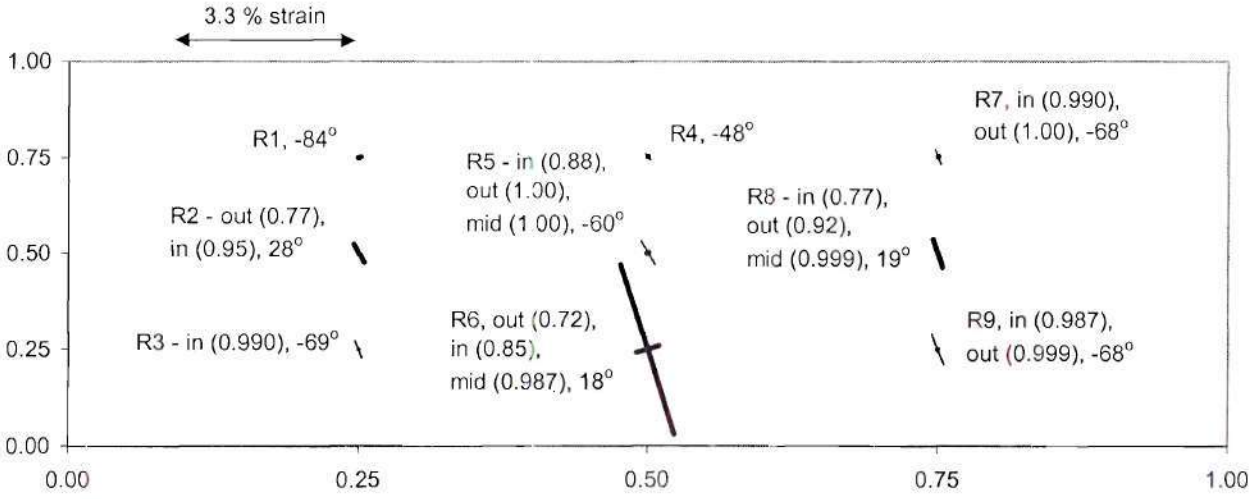

Figure 51 Yield locations and corresponding V/V_{max} values, and web principal strain difference magnitudes and orientations in girder S2 at the maximum shear capacity

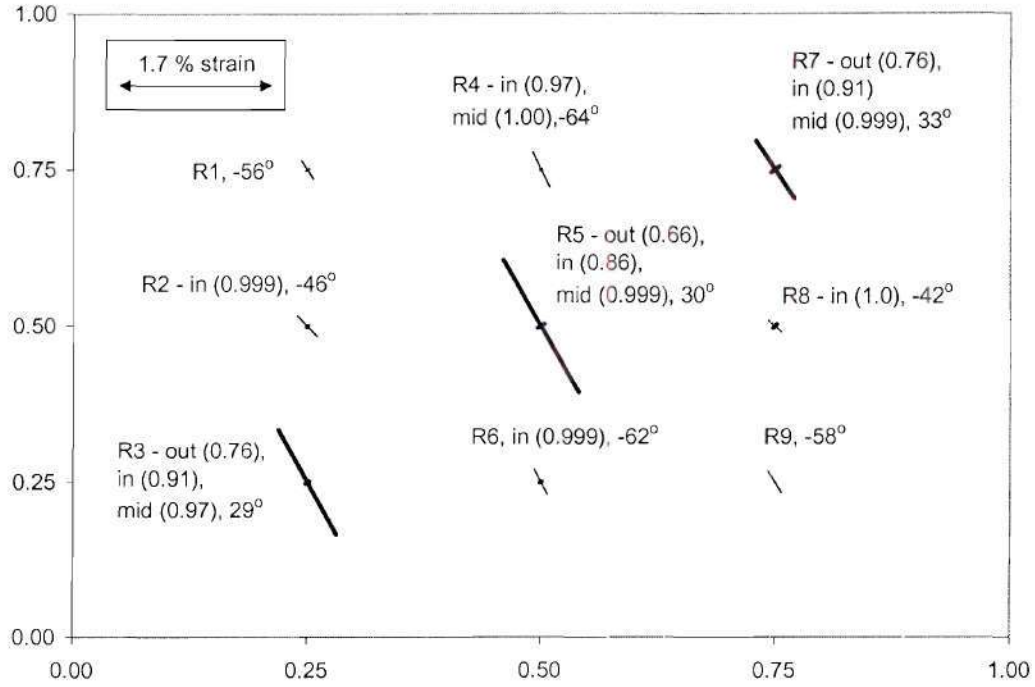

Figure 52 Yield locations and corresponding V/V_{max} values, and web principal strain difference magnitudes and orientations in girder S1-S at the maximum shear capacity

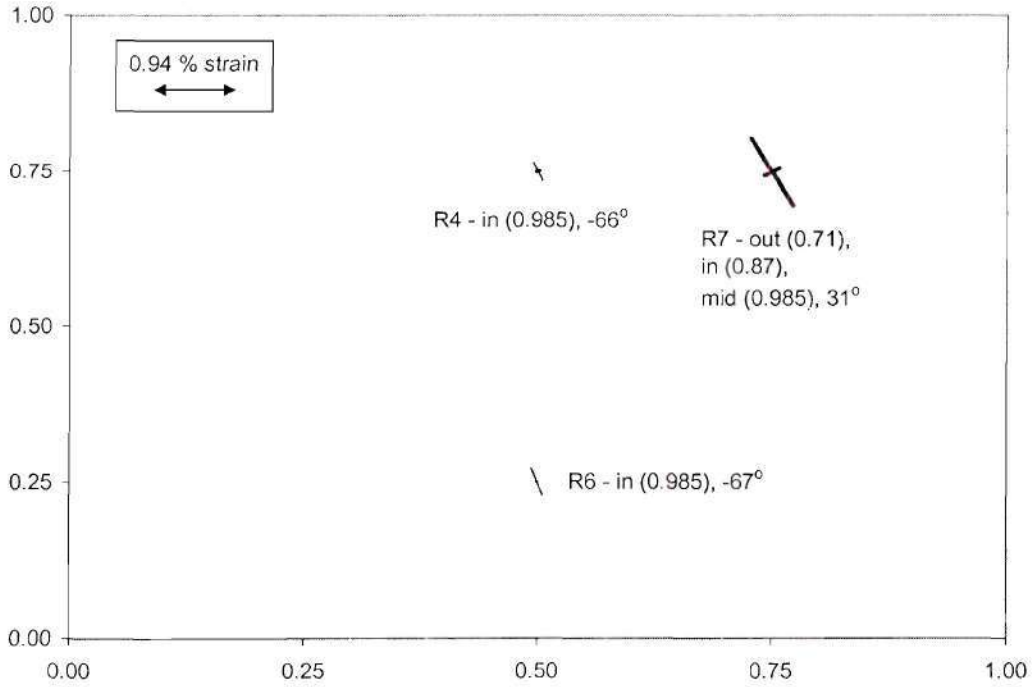

Figure 53 Yield locations and corresponding V/V_{max} values, and web principal strain difference magnitudes and orientations in girder S2-S at the maximum shear capacity

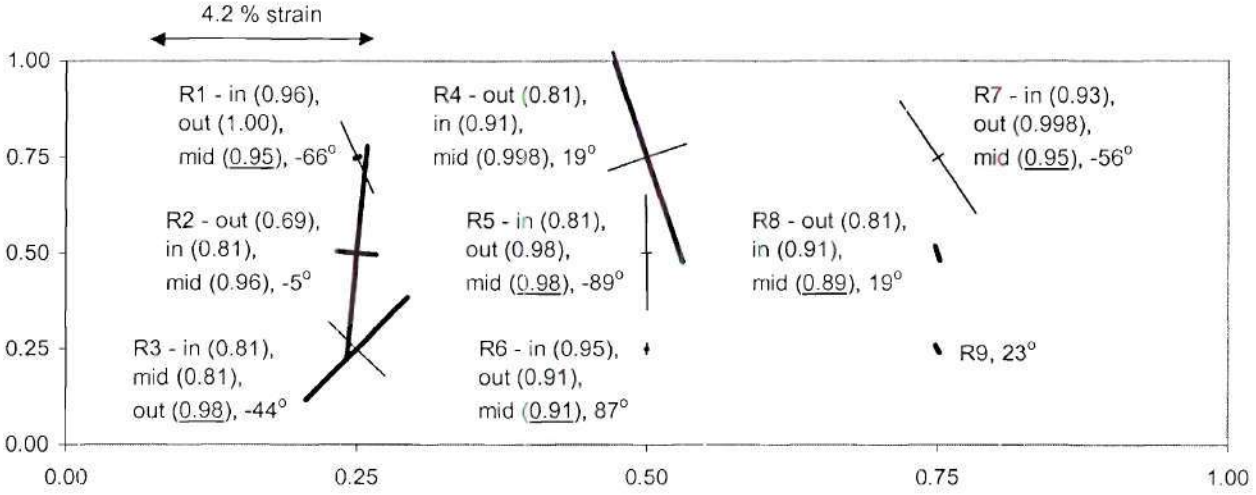

Figure 54 Yield locations and corresponding V/V_{max} values, and web principal strain difference magnitudes and orientations in girder S1 at the end of the post-peak portion of the test

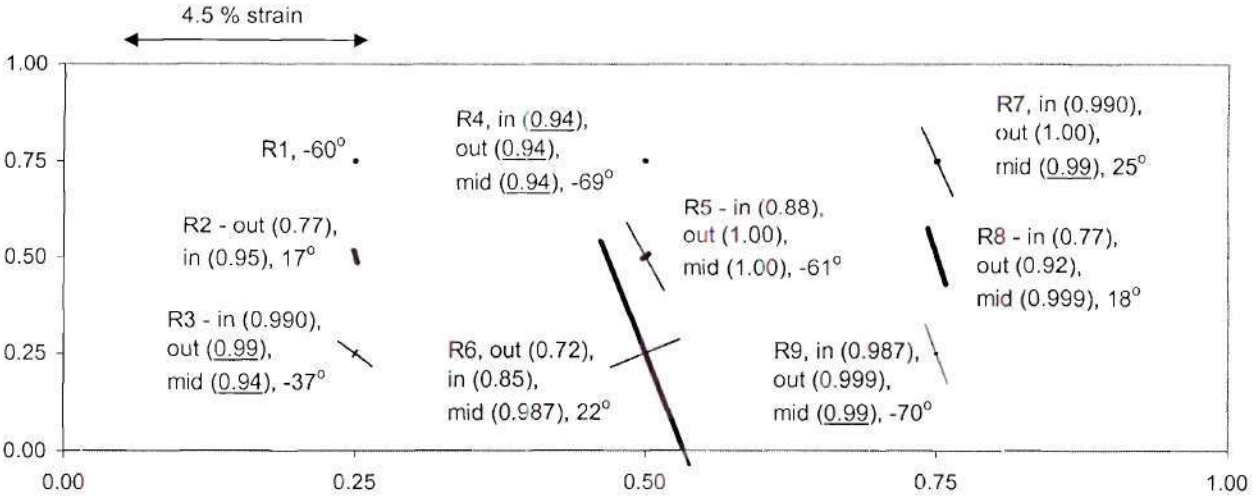

Figure 55 Yield locations and corresponding V/V_{max} values, and web principal strain difference magnitudes and orientations in girder S2 at the end of the post-peak portion of the test

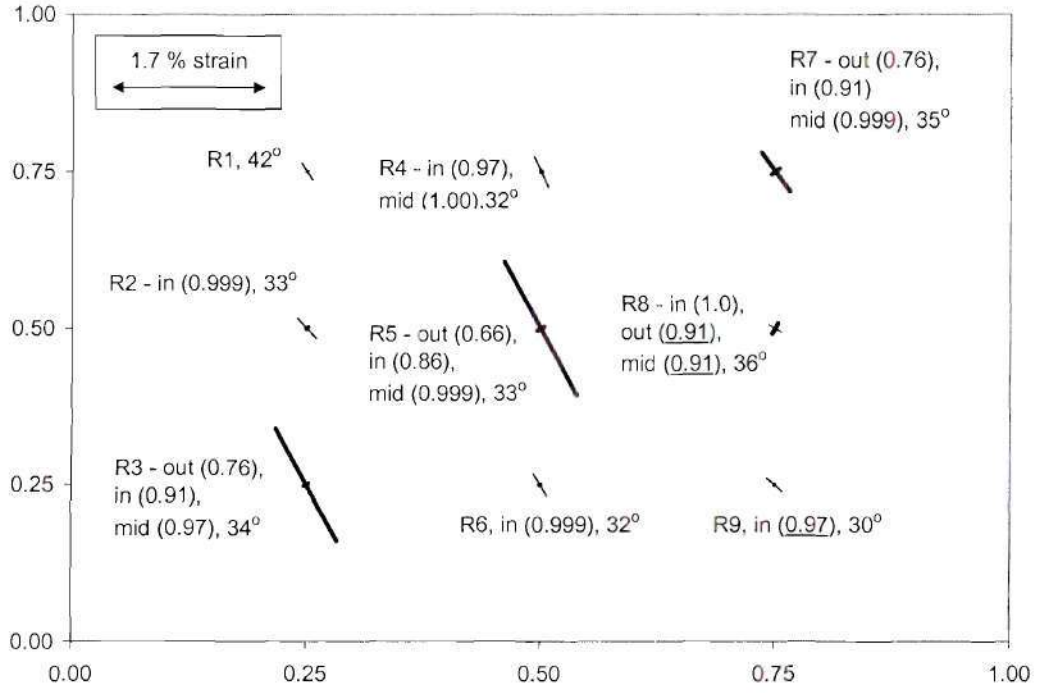

Figure 56 Yield locations and corresponding V/V_{max} values, and web principal strain difference magnitudes and orientations in girder S1-S at the end of the post-peak portion of the test

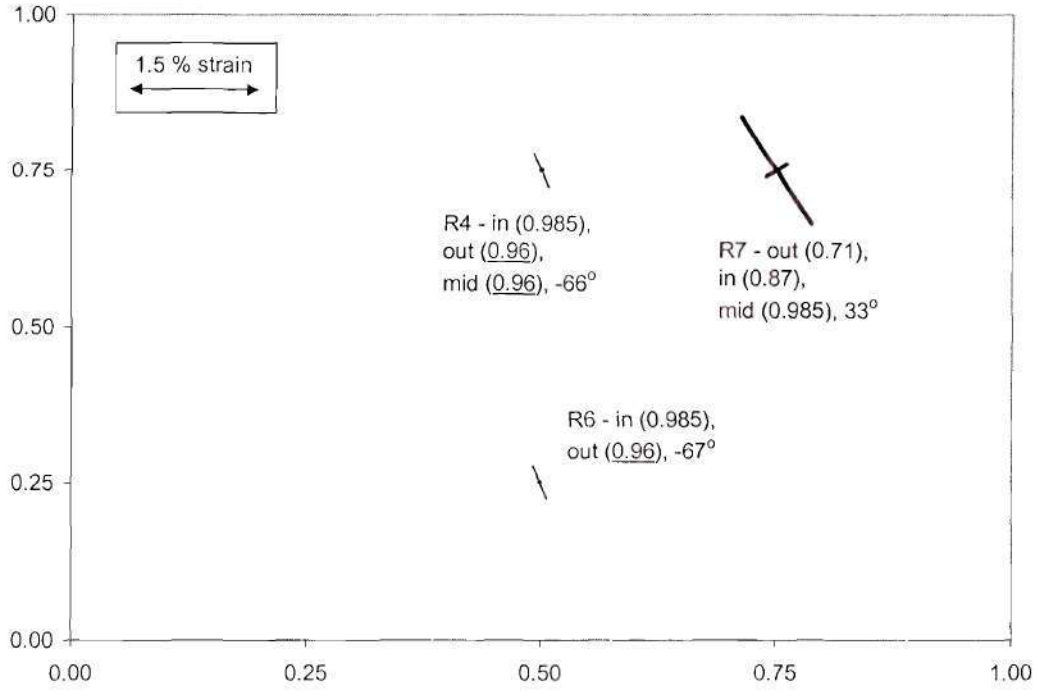

Figure 57 Yield locations and corresponding V/V_{max} values, and web principal strain difference magnitudes and orientations in girder S2-S at the end of the post-peak portion of the test

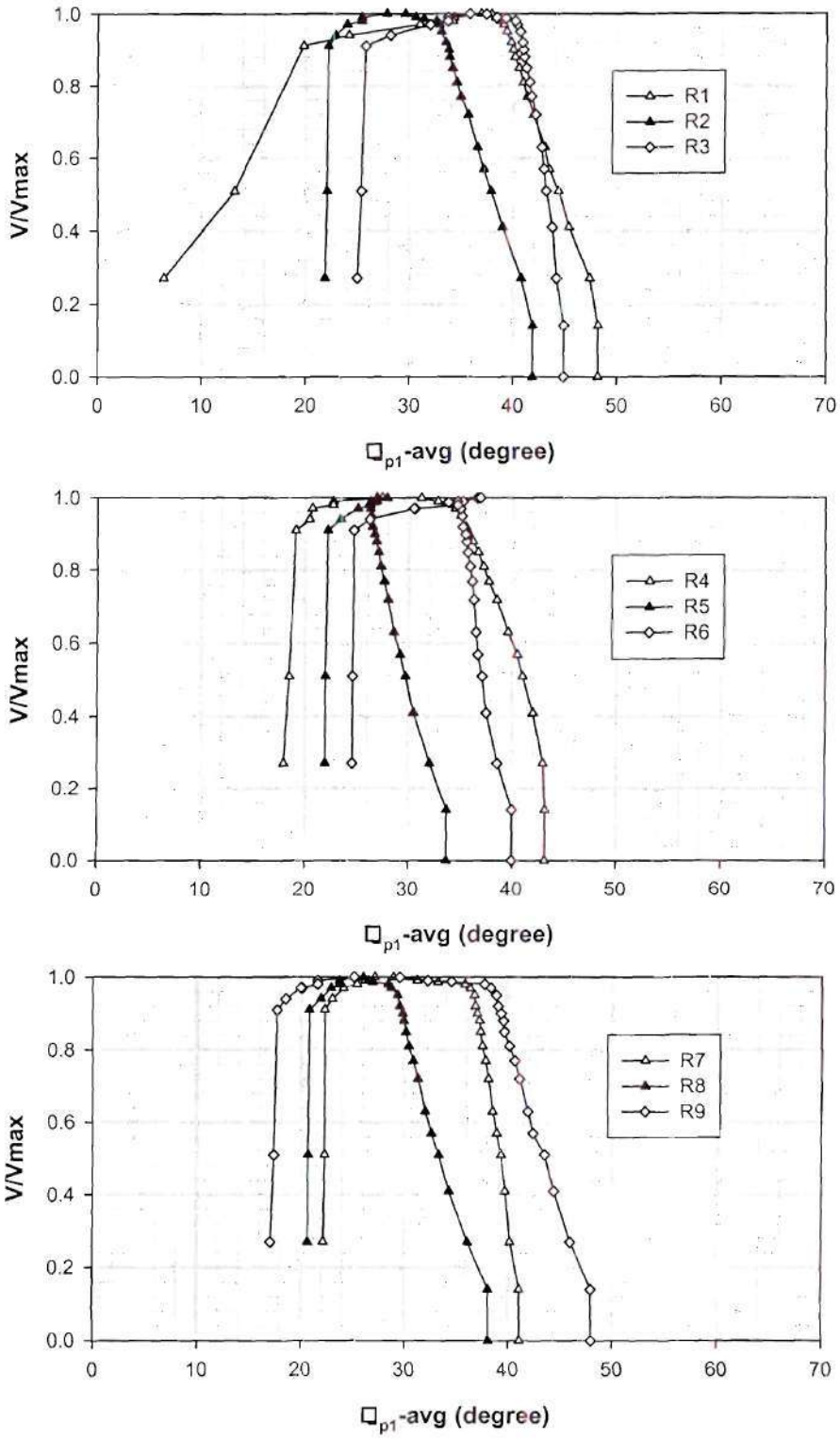

Figure 58 Orientation of maximum principal membrane strains Θ_{p1} versus V/V_{max} in girder S2

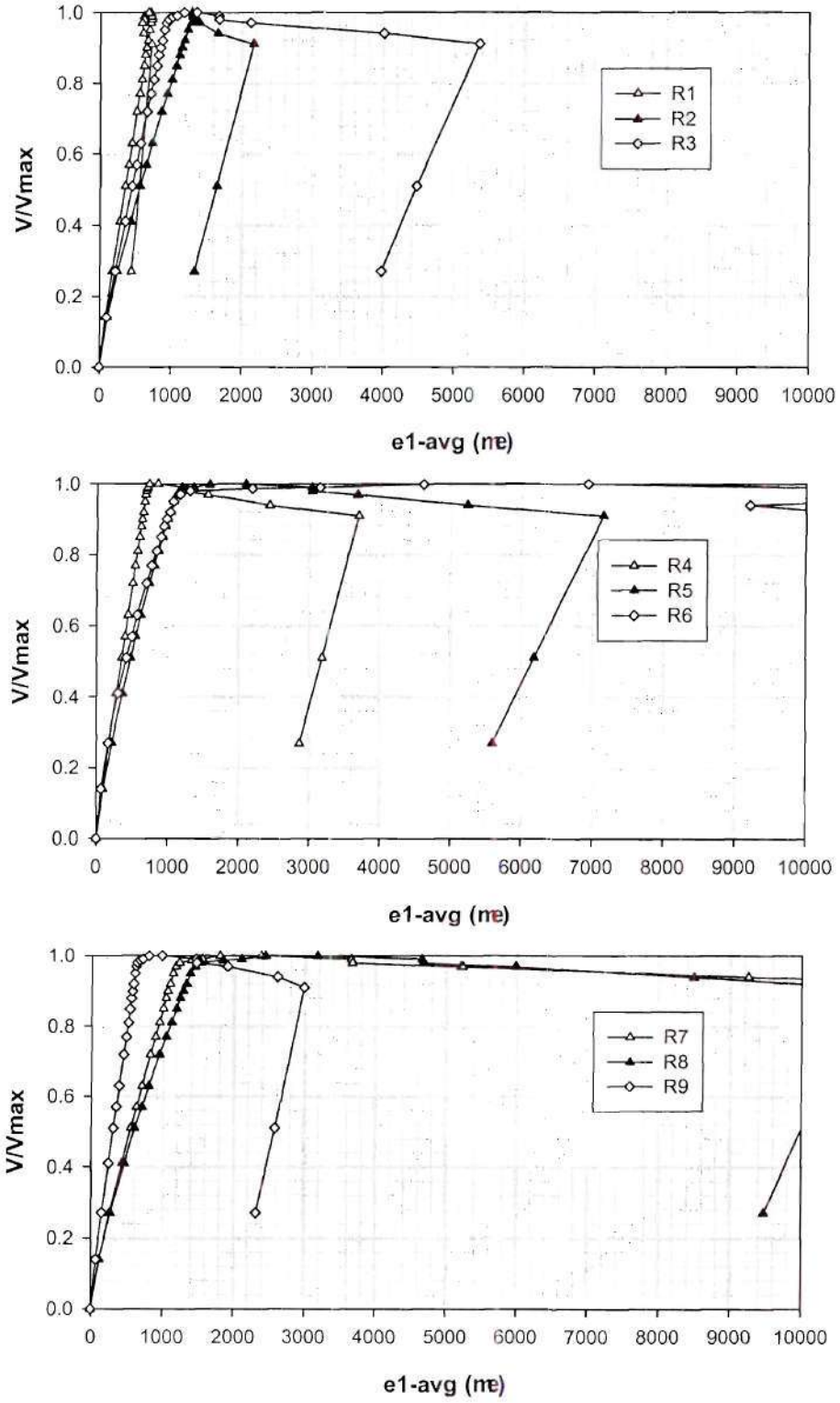

Figure 59 Maximum (tensile) principal membrane strains e_1 versus V/V_{max} in girder S2

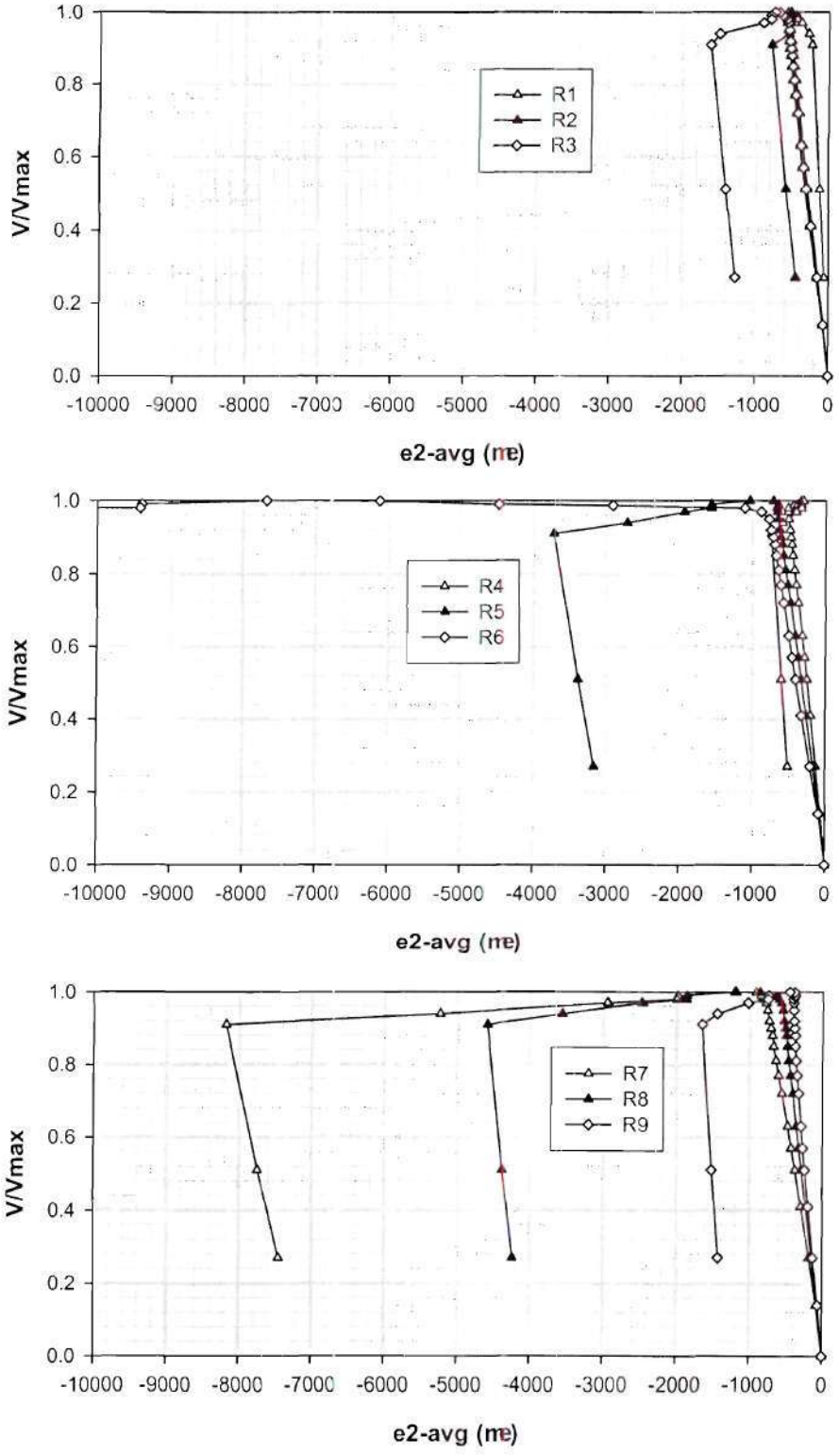

Figure 60 Minimum (compressive) principal membrane strains e_2 versus V/V_{max} in girder S2

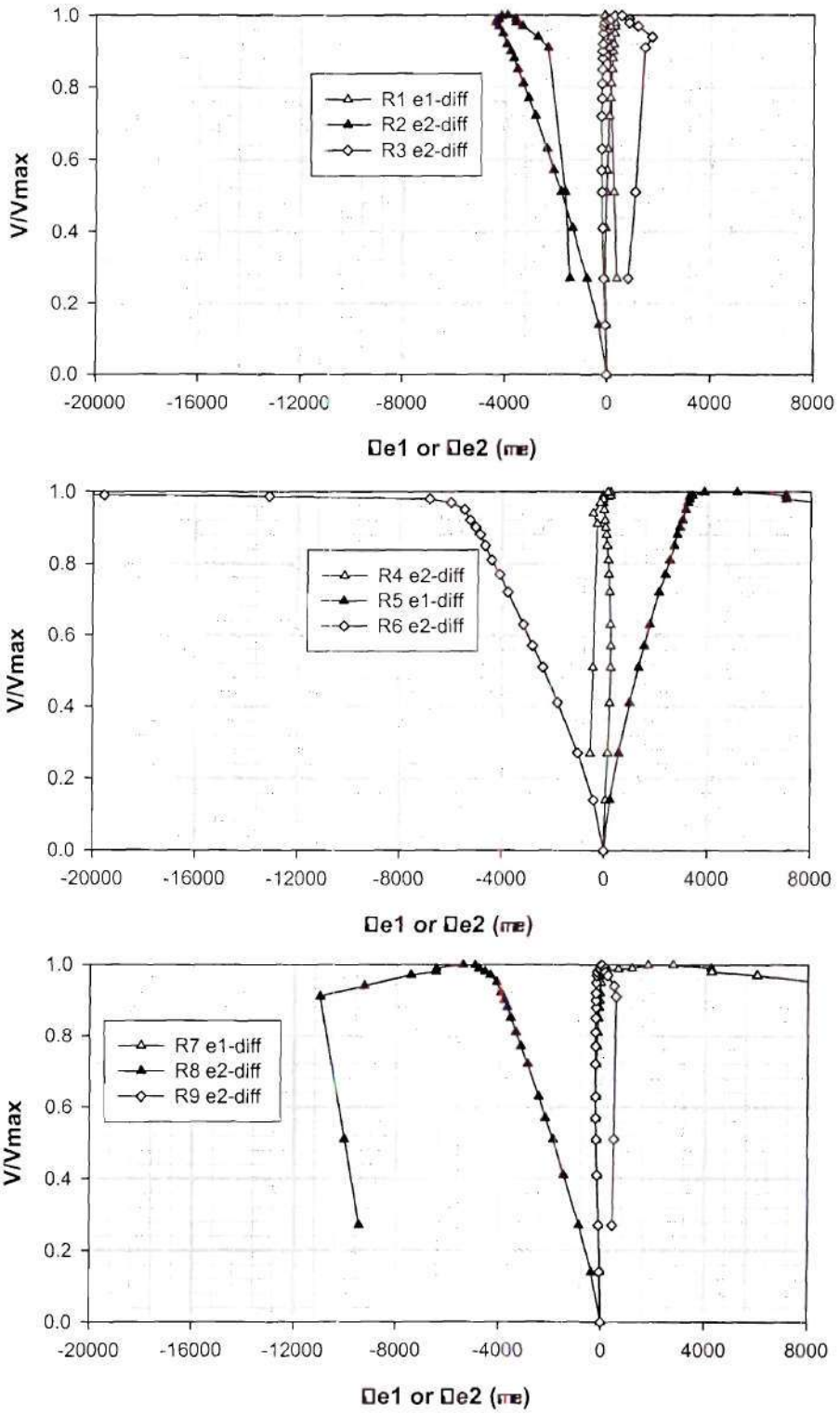

Figure 61 Largest magnitude of the principal strain differences Δe_1 and Δe_2 versus V/V_{max} in girder S2

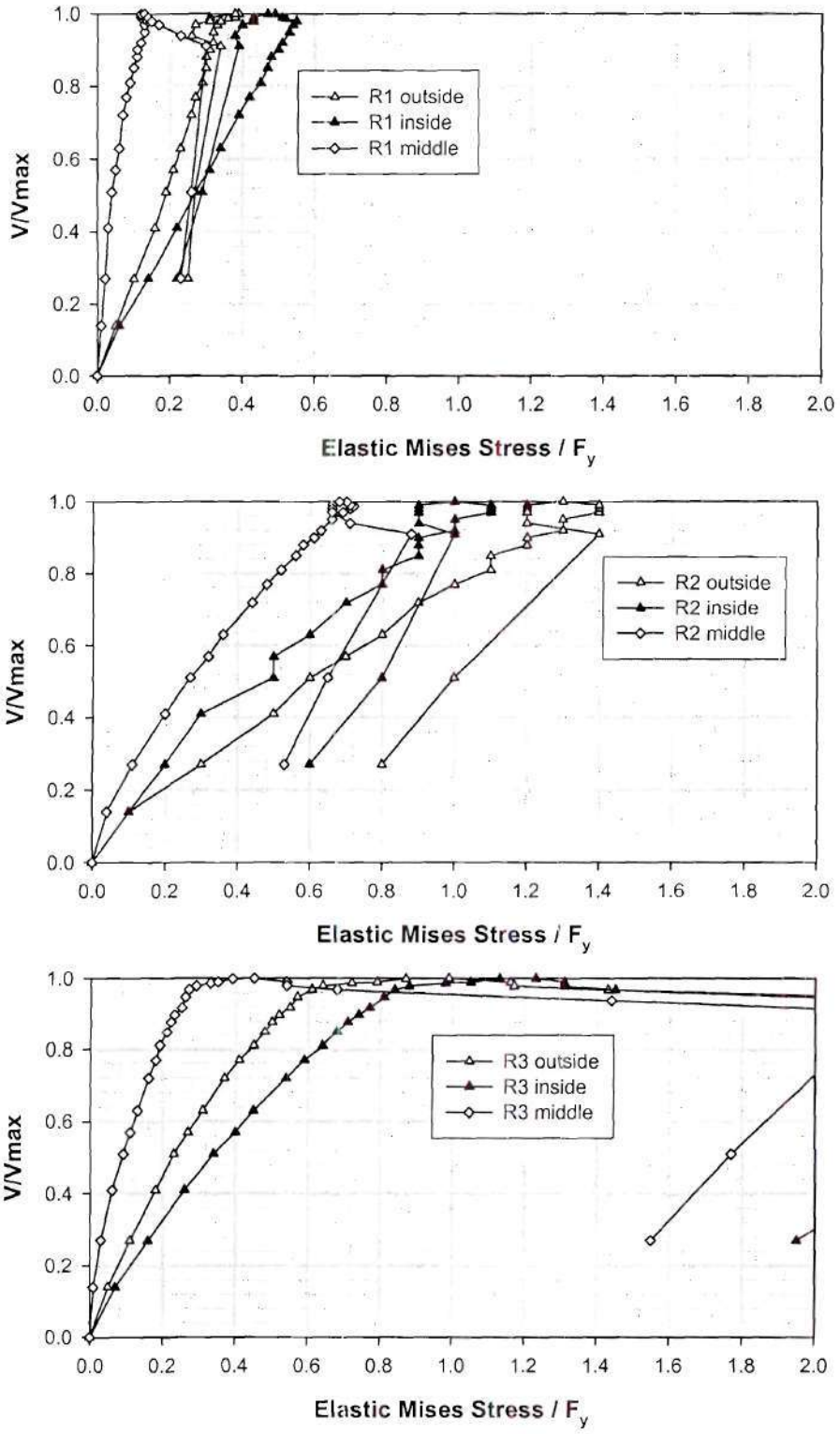

Figure 62 Normalized elastic Mises stresses for gages R1 through R3 versus V/V_{max} in girder S2

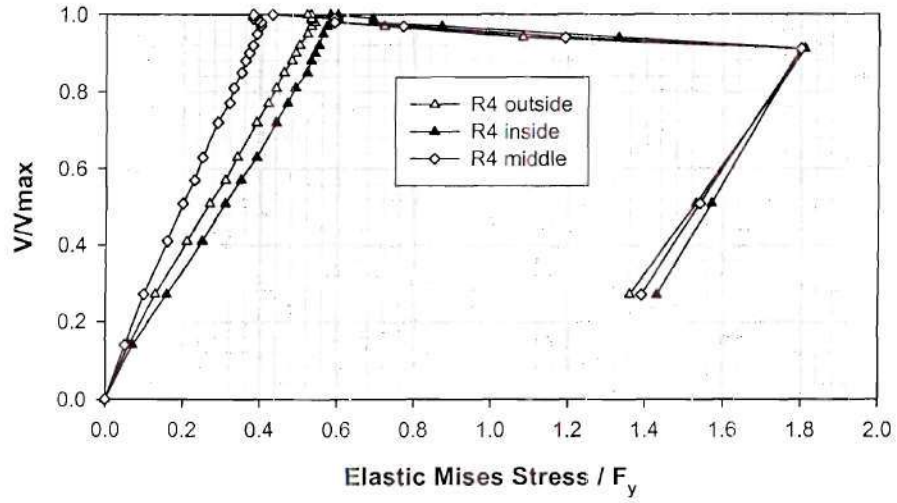

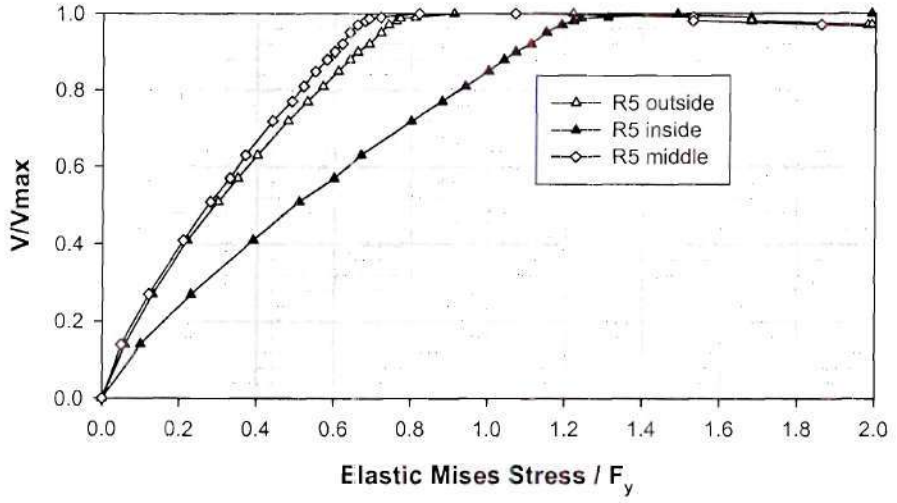

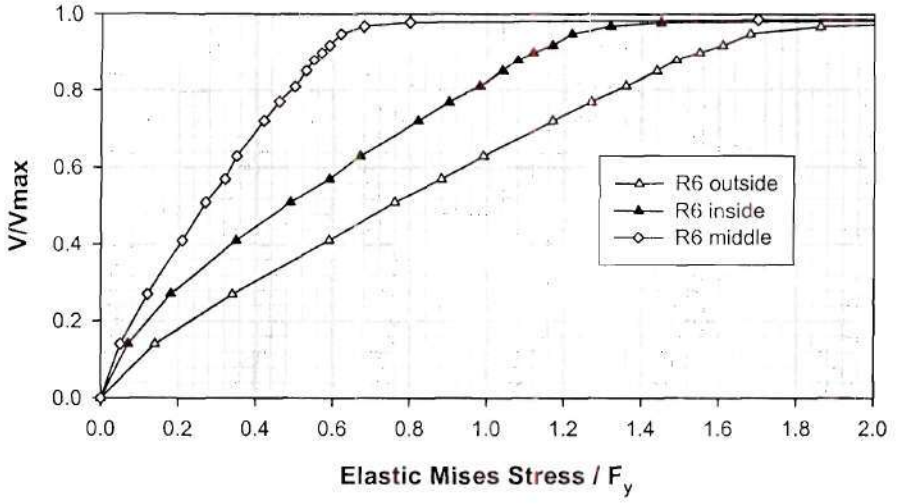

Figure 63 Normalized elastic Mises stresses for gages R4 through R6 versus V/V_{max} in girder S2

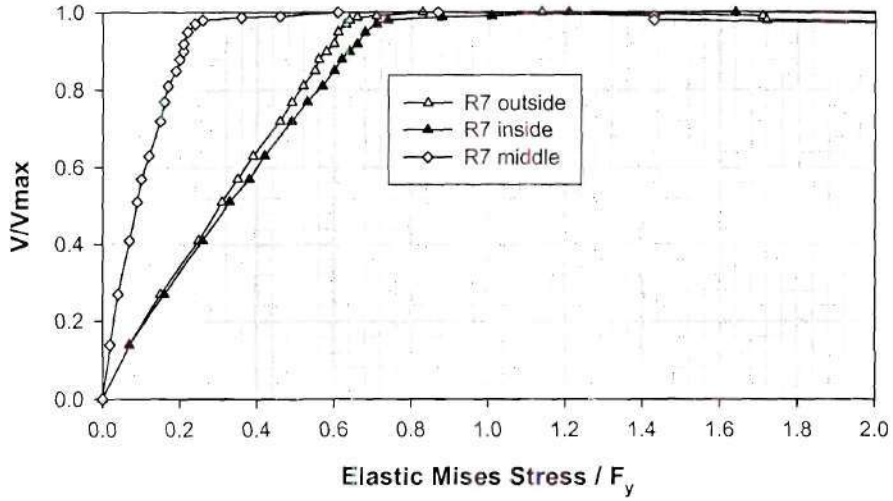

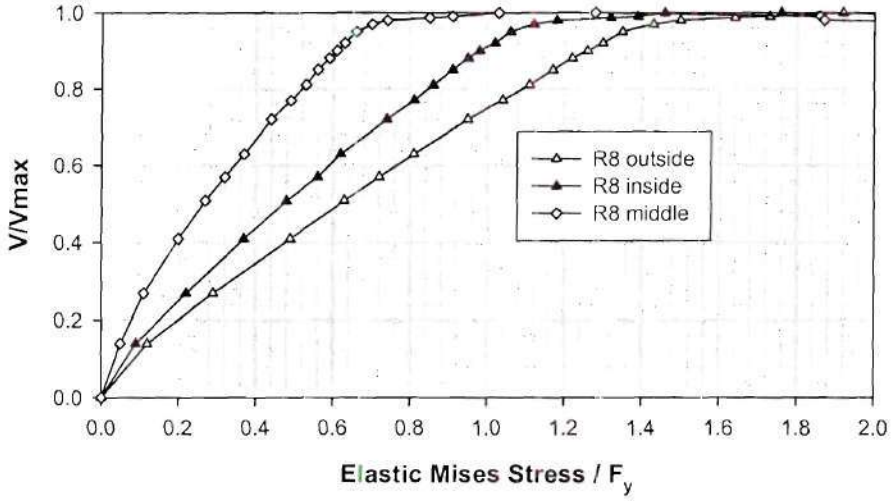

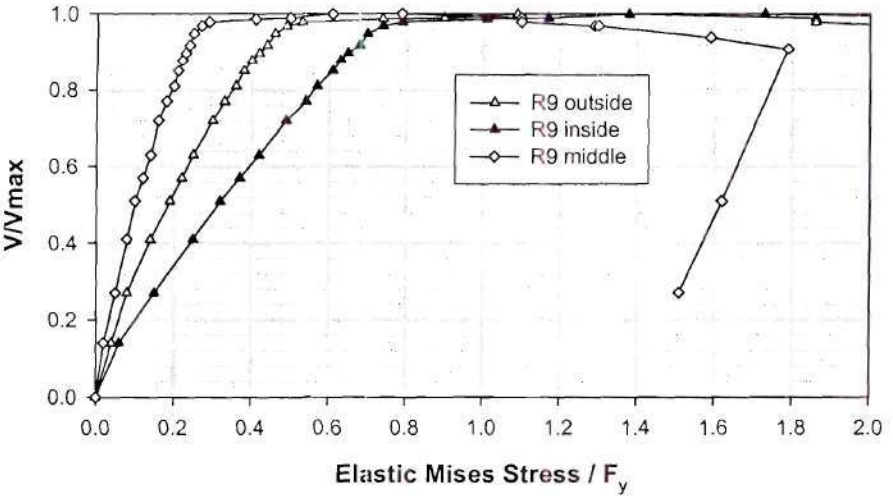

Figure 64 Normalized elastic Mises stresses for gages R7 through R9 versus V/V_{max} in girder S2

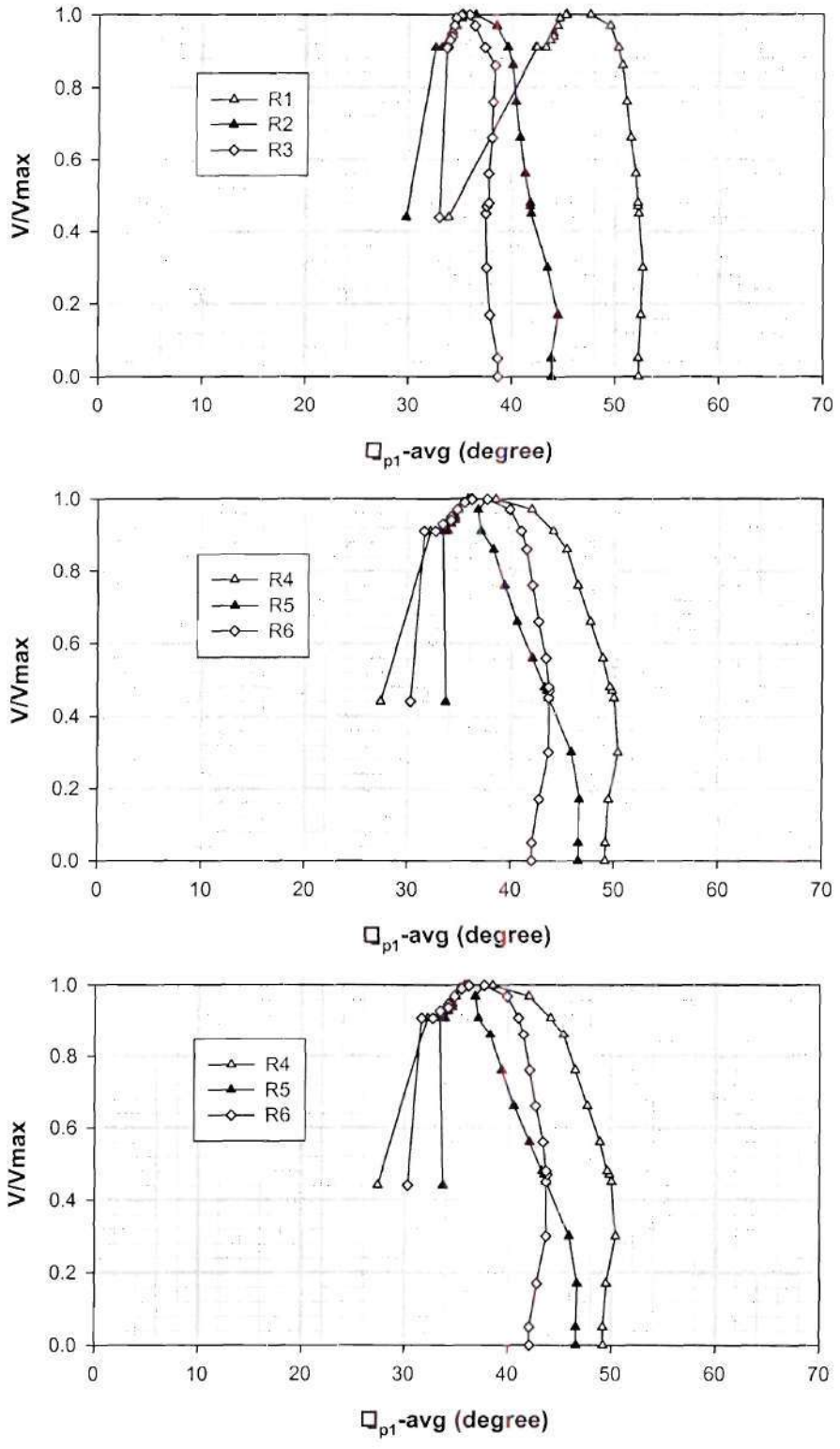

Figure 65 Orientation of maximum principal membrane strains Θ_{p1} versus V/V_{max} in girder S1-S

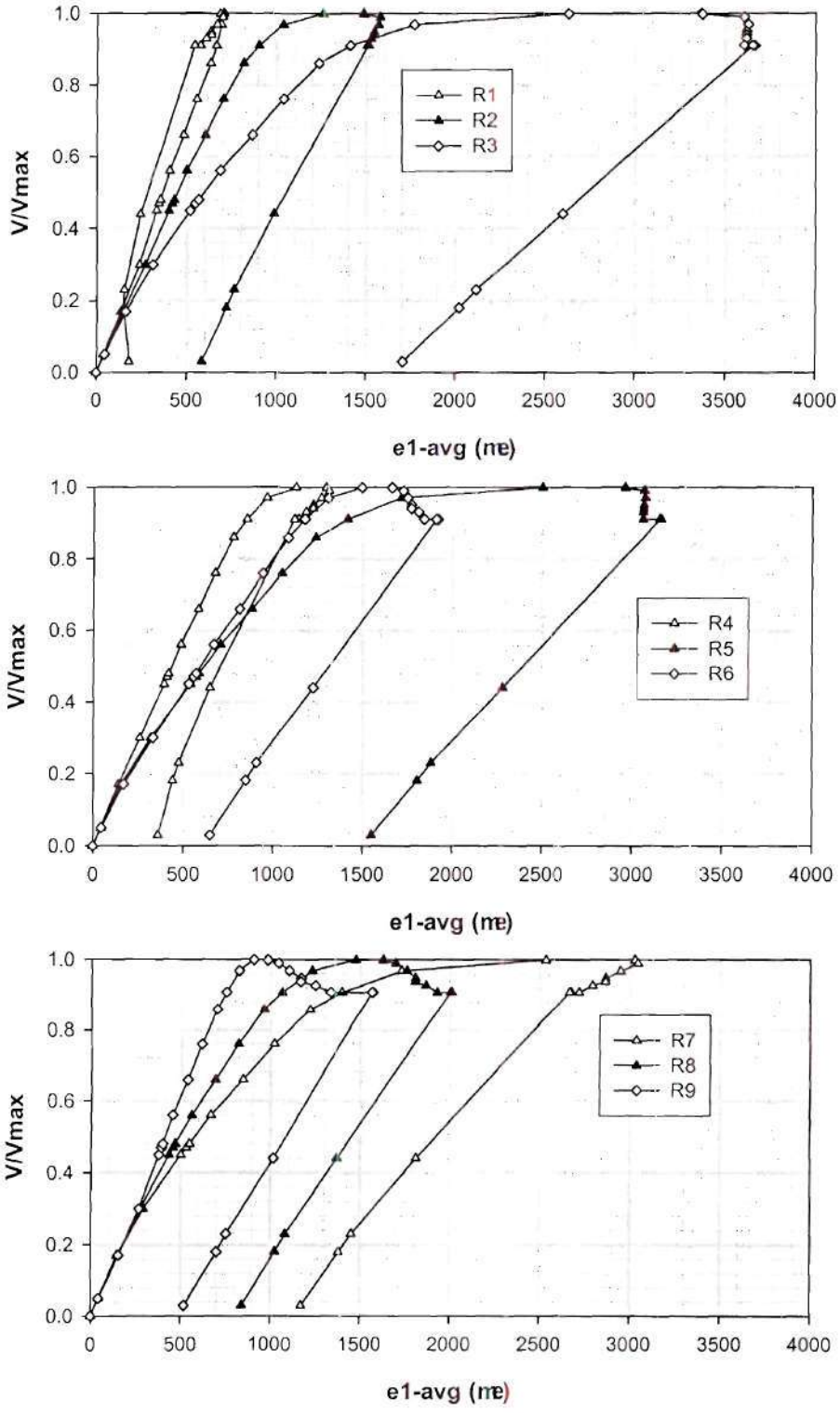

Figure 66 Maximum (tensile) principal membrane strains e_1 versus V/V_{max} in girder S1-S

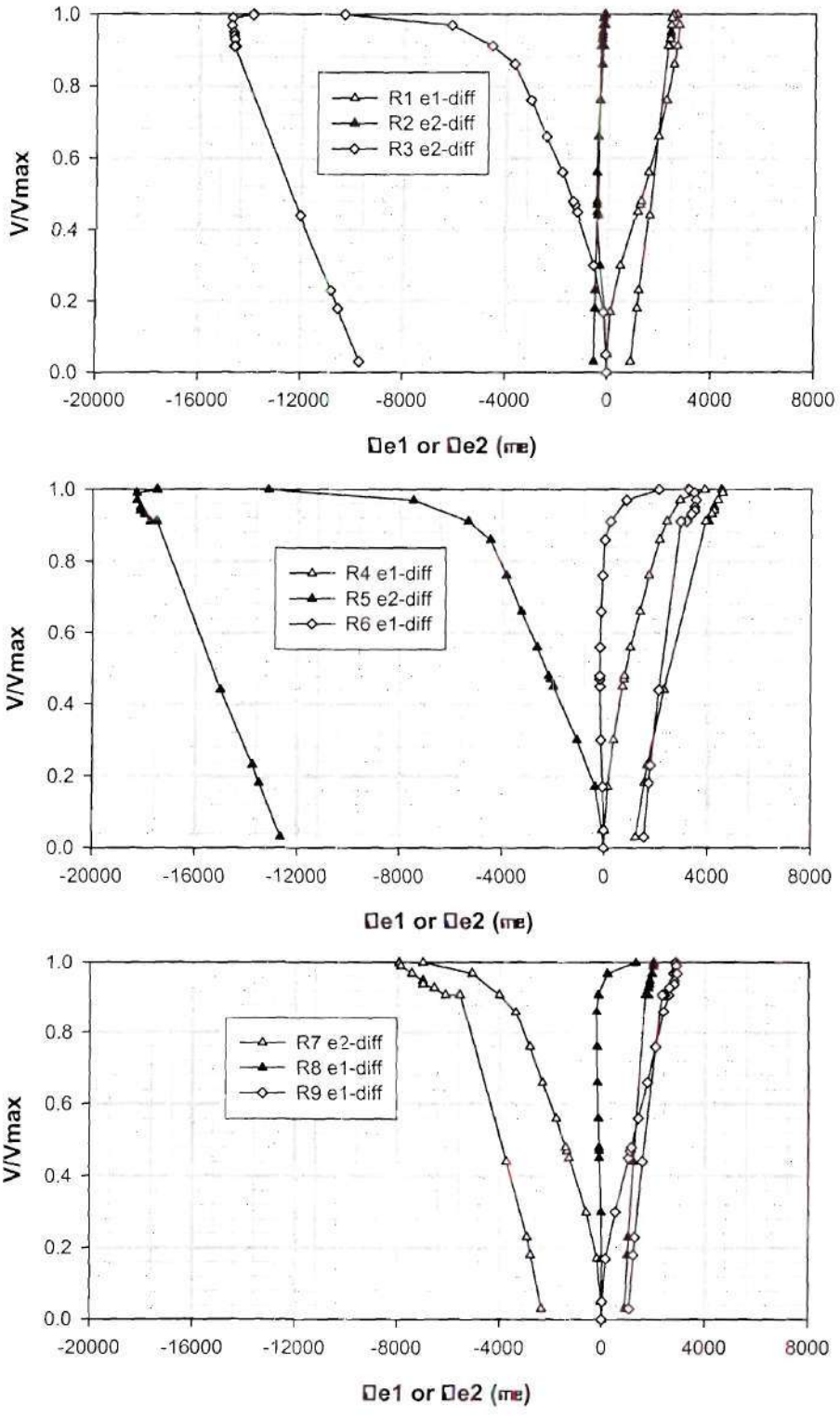

Figure 67 Largest magnitude of the principal strain differences Δe_1 and Δe_2 versus V/V_{max} in girder S1-S

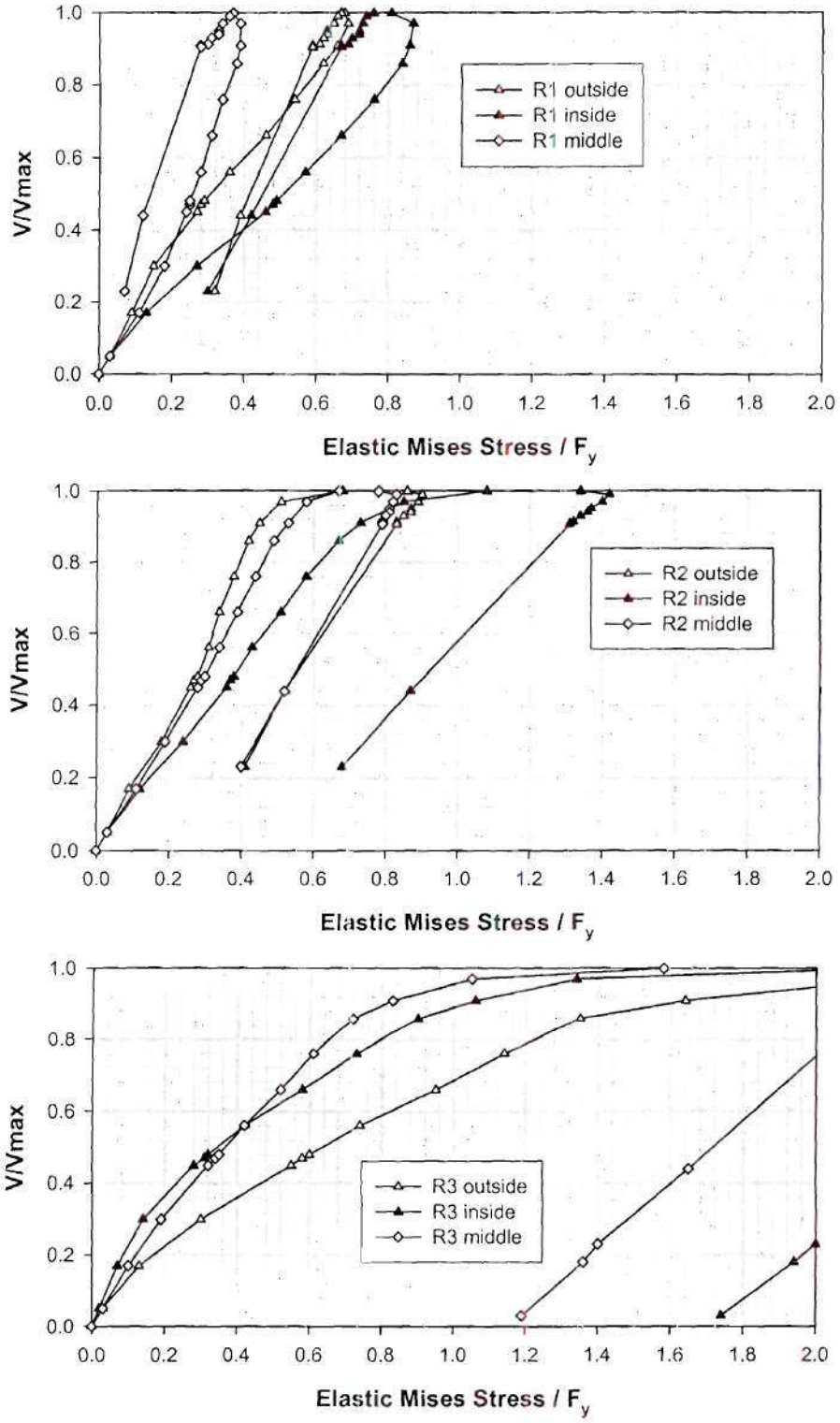

Figure 68 Normalized elastic Mises stresses for gages R1 through R3 versus V/V_{max} in girder S1-S

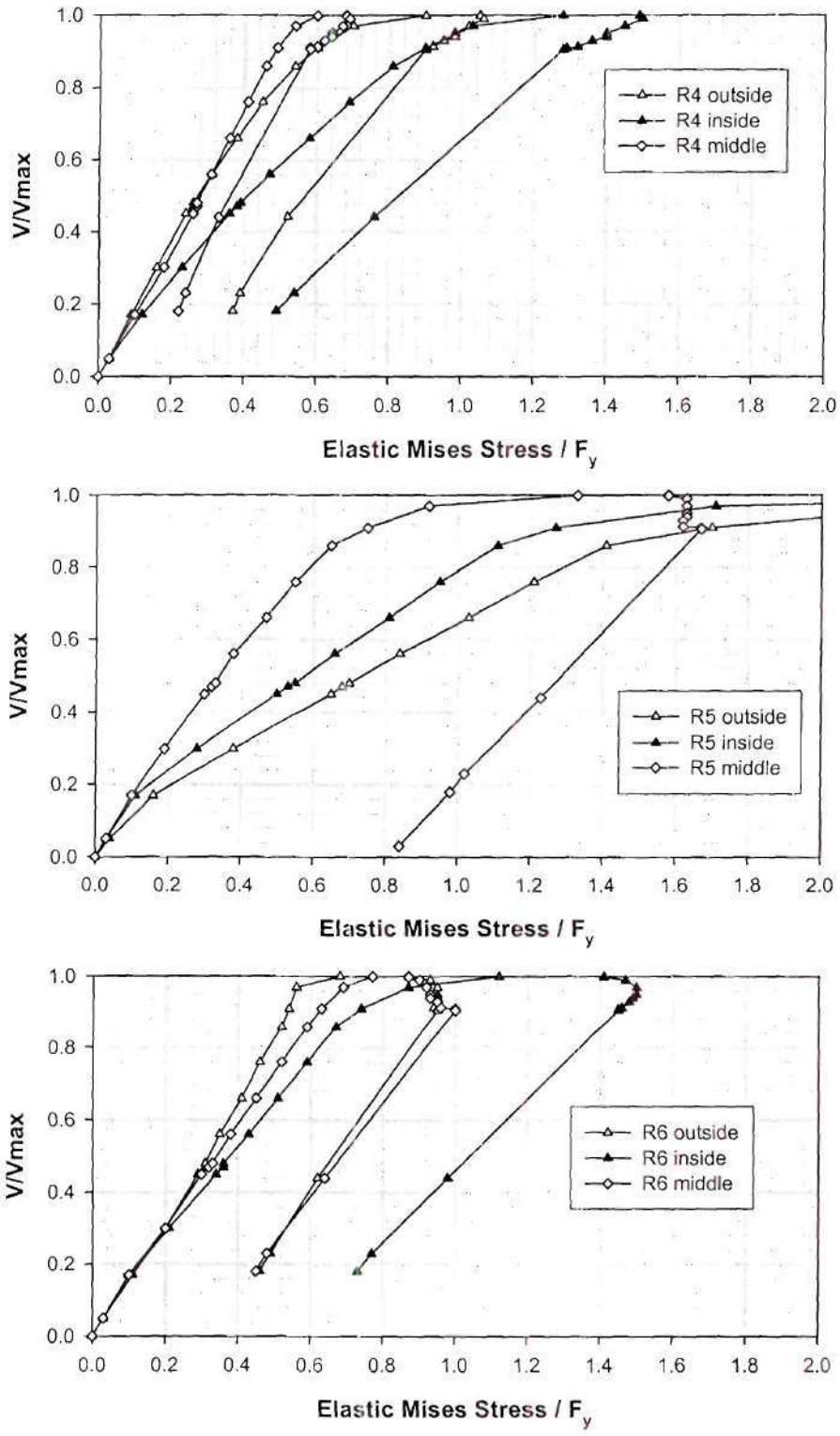

Figure 69 Normalized elastic Mises stresses for gages R4 through R6 versus V/V_{max} in girder S1-S

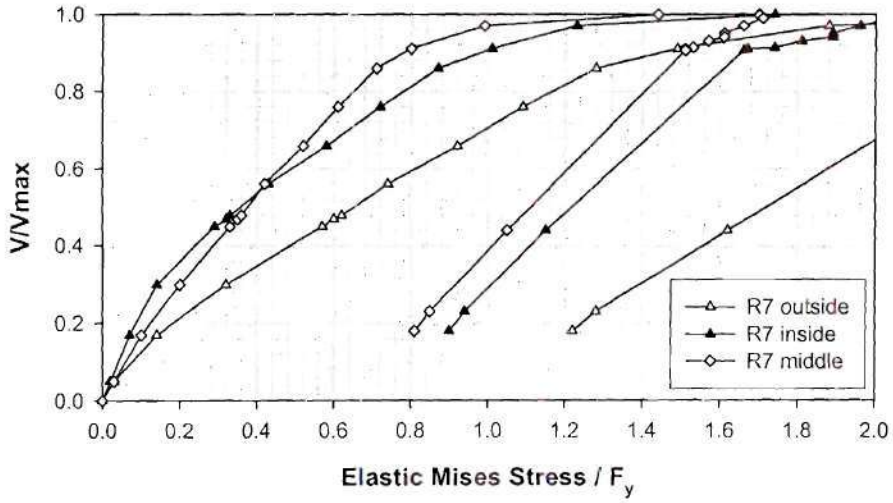
V/Vmax
Elastic Mises Stress / F_y
R7 outside
R7 inside
R7 middle

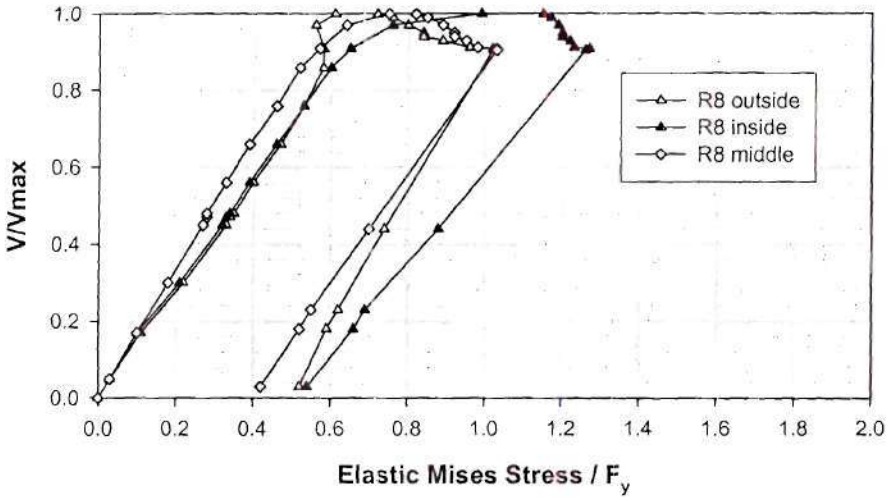
V/Vmax
Elastic Mises Stress / F_y
R8 outside
R8 inside
R8 middle

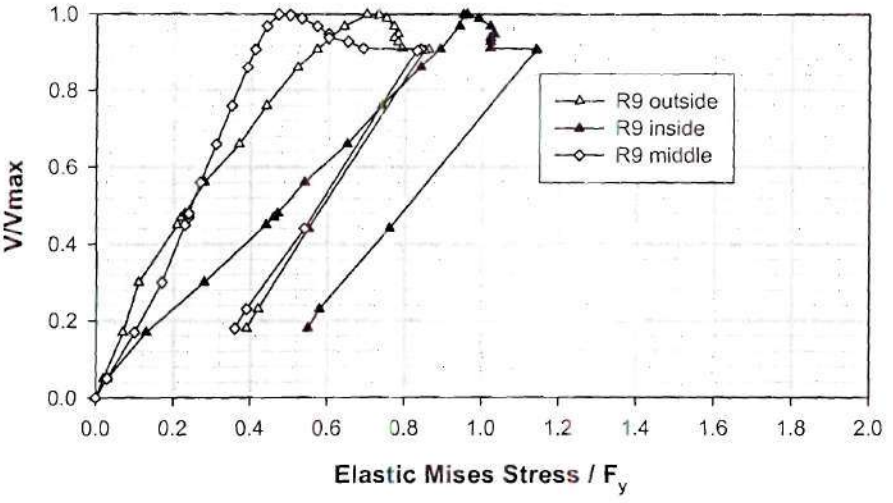
V/Vmax
Elastic Mises Stress / F_y
R9 outside
R9 inside
R9 middle

Figure 70 Normalized elastic Mises stresses for gages R7 through R9 versus V/V_{max} in girder S1-S

4.5 FLANGE STRAINS

4.6 SUMMARY

CHAPTER V - COMPARISON WITH CALCULATED MEMBER STRENGTHS

As noted in an earlier chapter, White et al. (2001) focused on evaluation of the shear strength predictions by the AASHTO (2001b) equations, the equations proposed by Lee and Yoo (1998a, b, 1999b), and the current AASHTO equations modified by use of Lee's shear buckling coefficient formulas. Their rationale for not considering other shear strength predictors was that, although other formulations in the literature tend to provide more accurate characterizations of the shear strength, they generally require the consideration of contributions from the girder flanges (associated with anchorage of a tension field, and with frame action). The calculation of the contributions from the flanges to the shear strength makes the equations more complex, and due to the influence of axial stress in the flanges on their plate bending strength, the resulting equations typically exhibit some interaction between the shear and flexural strengths. White et al. (2001) and White and Aydemir (2002) demonstrated, based on finite element parametric studies, that moment-shear interaction may be neglected if the AASHTO or modified AASHTO shear strength equations are employed, and the maximum panel moment is utilized within the strength check. However, there is significant scatter in the predicted and finite element based shear strengths. White et al. (2002) shows a preliminary assessment of shear strength predictions from more than 100 high-shear low-moment and high-shear high-moment tests of straight steel I girders. The trend in the predictions compared to the expermimental data is very similar to that observed in the above finite element studies.

Based on the above results, the predictions by the AASHTO (2001b) formulas and by a form of the modified AASHTO equations considered by White et al. (2001) are also considered in this chapter. The predictions by the shear strength equations proposed by Lee and Yoo (1998a, b,

1999b) are significantly less accurate compared to the finite element based strengths in White et al. (2001) and White and Aydemir (2002), and compared to the experimental data evaluated in White et al. (2002). Therefore, the Lee and Yoo (1998a, b, 1999b) equations are not considered further in this document. White et al. (2001) discuss a number of reasons for the inaccuracy of these formulas.

For purposes of comparison , the shear capacities predicted by a simple post-critical design method proposed for adoption within Eurocode 3 (CEN 1992) by Davies and Griffith (1999) as well those predicted by the Cardiff model (Davies and Griffith 1999, Porter et al. 1975, Evans et al. 1978 and Evans 19XX) are also considered in this chapter. The Cardiff idealization is one of the more elaborate shear strength models within the literature, and has been shown to provide relatively accurate predictions of I girder shear strengths of transversely-stiffened girders in the above references.

The following section summarizes the four sets of shear strength equations utilized in the current study. Only brief discussions of the theoretical basis for the different equations are provided here. The reader is referred to White et al. (2001) for more extensive discussion of the theoretical basis for the AASHTO (2001b) and modified AASHTO equations, to (Davies and Griffith 1999) for discussion of the theoretical basis of their model, and to (Porter et al. 1975, Evans et al. 1978, and/or Evans 19XX) for discussion of the theoretical basis for the Cardiff model. Section X.X then compares the underlying assumptions and the strengths calculated from the four sets of formulas to the behavior and shear strengths measured within the four curved I girders tested in this work.

5.1 STRENGTH EQUATIONS

Three idealized contributions to the shear strength are considered in some fashion within the development of each of the strength models studied in this chapter:

- the web shear buckling strength
- the web strength due to the development of a tension field, subsequent to buckling of the web
- the strength contribution from the flanges due to frame action.

In general, these three contributions are summed to obtain the total net shear capacity of a web panel, although the contribution from flange frame action is not calculated in two of the models. The flanges also generally contribute to the strength to the extent that they provide rotational restraint against shear buckling along the bottom and top of the web panels, and to the extent that they provide anchorage for the development of a tension field in the postbuckling response of the web. The four models considered here include these contributions to the strength in varying ways. The next three subsections address each of these contributions.

5.1.1 Web Shear Buckling Strength

The calculation of the web shear buckling coefficient is a key variable that is different among the four shear strength models. The shear buckling coefficient utilized by AASHTO (2001b) is

$$k_{AASHTO} = 5 + \frac{5}{\left(\frac{d_o}{D}\right)^2} \qquad (16)$$

for $d_o/D \leq 3$, which is a simplification of the following more precise equations for the shear buckling coefficient summarized in (SSRC 1998):

$$k_{ss} = 4 + \frac{5.34}{\left(\frac{d_o}{D}\right)^2} \qquad \text{for } \frac{d_o}{D} < 1 \tag{17}$$

$$k_{ss} = 5.34 + \frac{4}{\left(\frac{d_o}{D}\right)^2} \qquad \text{for } \frac{d_o}{D} \geq 1 \tag{18}$$

These equations are all based on the assumption of ideally simply-supported boundary conditions at the top and bottom of the web plate. A precise set of equations for the shear buckling coefficient of a panel with fixed rotational restraint at its top and bottom and simply-supported conditions on its sides is (SSRC 1998):

$$k_{sf} = \frac{5.34}{\left(\frac{d_o}{D}\right)^2} + \frac{2.31}{\frac{d_o}{D}} - 3.44 + 8.39\frac{d_o}{D} \qquad \text{for } \frac{d_o}{D} < 1 \tag{19}$$

$$k_{sf} = 8.98 + \frac{5.61}{\left(\frac{d_o}{D}\right)^2} - \frac{1.99}{\left(\frac{d_o}{D}\right)^3} \qquad \text{for } \frac{d_o}{D} \geq 1 \tag{20}$$

Lee et al (1996) studied the degree of restraint at the web-flange juncture for a wide range of representative I girders using elastic finite element models. They found that for $t_f/t_w \geq 2$, the shear buckling load can be predicted reasonably well by assuming a buckling coefficient that is nearly equal to that associated with fully-fixed boundary conditions at the web-flange juncture, i.e.,

$$k_{Lee} = k_{ss} + \frac{4}{5}(k_{sf} - k_{ss}) \qquad \text{for } \frac{t_f}{t_w} \geq 2 \tag{21}$$

and that for girders with thinner flanges, the shear buckling coefficient could be expressed as

$$k_{Lee} = k_{ss} + \frac{4}{5}(k_{sf} - k_{ss})\left[1 - \frac{2}{3}\left(2 - \frac{t_f}{t_w}\right)\right] \qquad \text{for } \frac{1}{2} \leq \frac{t_f}{t_w} < 2 \tag{22}$$

Bradford (1996) also studied the effect of restraint from the flanges on the web elastic shear buckling capacity, and developed charts for the shear buckling coefficient that give values very close to those predicted by Equations (21) and (22). The accuracy of these equations has also been confirmed by White et al. (2001).

Based on the above coefficients, the web shear buckling strengths utilized in the four models evaluated in this research may be written as follows. The elastic shear buckling strength based on the precise coefficient for simply-supported boundary conditions may be expressed as

$$V_{cr(ss)} = \frac{\pi^2 E k_{ss}}{12(1-\upsilon^2)\left(\frac{D}{t_w}\right)^2} Dt_w \tag{23}$$

This is the shear buckling strength assumed within the models by Davies and Griffith (1999) and within the Cardiff model. In AASHTO (2001b), the elastic shear buckling strength is written indirectly as its ratio relative to the plastic shear capacity

$$C_{AASHTO} = \frac{V_{cr(AASHTO)}}{V_{p(AASHTO)}} = \frac{1.52 E k_{AASHTO}}{\left(\frac{D}{t_w}\right)^2 F_{yw}} \quad \text{for } \frac{D}{t_w} > 1.38\sqrt{\frac{E k_{AASHTO}}{F_y}} \tag{24}$$

where

$$V_{p(AASHTO)} = 0.58 F_{yw} D t_w \tag{25}$$

Equation (25) is a simplification of the more precise equation

$$V_p = \frac{F_{yw}}{\sqrt{3}} Dt_w \tag{26}$$

where $F_{yw}/\sqrt{3}$ is the shear yield strength based on the Mises yield criterion. The resulting AASHTO elastic shear buckling strength may be expressed as

$$V_{cr(AASHTO)} = \frac{0.88Ek_{AASHTO}}{\left(\frac{D}{t_w}\right)^2} \tag{27}$$

One can observe that if a Poisson's ratio υ of 0.3 is substituted into Equation (23), Equation (27) is obtained except with a coefficient of 0.90 instead of 0.88. It should be noted that inelastic shear buckling equations are also provided in (AASHTO 2001b) and also within the other references cited above; these equations are not presented here since the theoretical web buckling for the four curved I girders tested in this work is elastic.

White et al. (2001) adopt Lee's (1996) shear buckling coefficient as a modification to the AASHTO shear buckling strength. This leads to improved strength predictions relative to refined finite element predictions and experimental test results (White et al. 2001; White and Aydemir 2001; White et al. 2002). That is,

$$V_{cr(Mod\ AASHTO)} = \frac{0.88Ek_{Lee}}{\left(\frac{D}{t_w}\right)^2} \tag{28}$$

5.1.2 Tension Field Strength

The contribution to the strength from the development of a tension field in the web post-buckling response is taken as

$$V_{t(AASHTO)} = \frac{0.87(1-C)}{\sqrt{1+\left(\frac{d_o}{D}\right)^2}} \tag{29}$$

in (AASHTO 2001b). This equation was derived by Basler (1961b). As discussed in White et al. (2001b), although the flanges are assumed to provide zero anchorage to the tension field in the initial stages of Basler's derivation, such that the tension field extends only over a portion of

the web, the final result expressed by the above equation is actually based on the development of a "complete" tension field in the web. That is, the tension field contribution to the shear strength in Equation (29) is based on the assumption of uniform yielding throughout the web panel with a principal tension along the direction

$$\Theta_{t(Basler)} = \frac{1}{2}\tan^{-1}\left(\frac{D}{d_o}\right) \tag{30}$$

with respect to the horizontal. The orientation of the tension field in Equation (30) is based on Basler's initial assumption that the flanges do not provide any anchorage for the tension field stresses. These attributes of Basler's model have been noted in previous research by Gaylord (1963), Fujii (1968a), Selberg (1973) and others.

As a result of the above anomaly in Basler's (1961b) model, the AASHTO (2001b) shear strength equations implicitly assume that the flanges are sufficient to provide some anchorage to the tension field. Basler (1963) acknowledges these attributes, and illustrates that the flanges are actually not loaded to the extent that would be required by this theory within his tests. Nevetheless, he argues that his theory still provides an acceptable characterization of I girder shear strengths. Gaylord also points out that "The good correlation between predicted values and experimental results cannot be dismissed. For this reason, the author's analysis may be an acceptable prediction of the postbuckling behavior of thin-webbed girders for the practicable range of parameters in civil engineering practice."

White et al. (2001) and White and Aydemir (2002) note that if Lee's (1996) coefficient is utilized in writing the web shear buckling strength, the shear capacity predicted by the sum of the buckling strength and Equation (30) provides a more accurate characterization of the shear capacity of a fairly complete range of straight and curved I girders with D/t_w up to 160 in their

finite element parametric studies. Also, the prediction of the I girder shear strengths of the experimental tests considered in White et al. (2002) is slightly improved. The coefficient of variation of the predicted to the experimental and finite element strengths is reduced by the above improvement in the shear strength equations. However, on average, the experimental and finite element strengths tend to be slightly over-predicted by the design equations when they are configured in this way. Based on assessment of more than 100 expreimental shear strength tests, the mean of the strength ratios can be improved without impacting the coefficient of variation by simply applying an arbitrary constant scale factor of 0.86 to Equation (29). That is, the modified AASHTO shear strength prediction is improved by writing the tension field contribution as

$$V_{t(\text{Mod AASHTO})} = \frac{0.75(1-C)}{\sqrt{1+\left(\frac{d_o}{D}\right)^2}} \tag{31}$$

Davies and Griffith (1999) propose the following equation for the combined buckling and postbuckling shear strength of a web panel for which the buckling resistance is governed by elastic buckling theory:

$$V_{w(\text{Davies})} = \frac{F_{yw}}{\sqrt{3}} \frac{0.9}{\sqrt{V_p / V_{cr(ss)}}} \qquad \text{for } \sqrt{V_p / V_{cr(ss)}} \geq 1.2 \tag{32}$$

This equation is taken from the simple post-critical design procedure incorporated in Eurocode 3 (CEN 1992), and is based on the theory proposed by Hõglund (1971, 1995, 1996). It is applicable to both stiffened and unstiffened girders. The tension field or postbuckling contribution to the shear strength can be factored out of this equation as

$$V_{t(\text{Davies})} = V_{w(\text{Davies})} - V_{cr(ss)} \tag{33}$$

Finally, the tension field contribution to the shear resistance of the Cardiff model can expressed as

$$V_{t(Cardiff)} = F_t^y t_w \sin^2(\Theta_{t(Cardiff)})\left[D\cot(\Theta_{t(Cardiff)}) - \left(d_o + \frac{c_{b(Cardiff)}}{2} + \frac{c_{t(Cardiff)}}{2}\right)\right] \quad (34)$$

where

$$F_t^y = -\frac{3}{2}\tau_{cr}\sin(2\Theta_{t(Cardiff)}) + \sqrt{F_{yw}^2 + \tau_{cr}^2\left[\left(\frac{3}{2}\sin(2\Theta_{t(Cardiff)})\right)^2 - 3\right]} \quad (35)$$

is the tensile principal stress within the tension field and $\Theta_{t(Cardiff)}$ is the inclination of the tension field with respect to the horizontal. The angle $\Theta_{t(Cardiff)}$ must be determined in general by iteration, but it can be approximated as

$$\Theta_{t(Cardiff)approx} = \frac{2}{3}\tan^{-1}\left(\frac{D}{d_o}\right) \quad (36)$$

The "exact" $\Theta_{t(Cardiff)}$ is the one that maximizes the overall shear capacity. The variables $c_{b(Cardff)}$ and $c_{t(Cardff)}$ in Equation (34) are the distances inward from the transverse stiffeners at which plastic hinges form in the top and bottom flanges due to frame action as shown in Figure XX. These distances may be written as

$$c_{b(Cardiff)} = \frac{2}{\sin(\Theta_{t(Cardiff)})}\sqrt{\frac{M_{pfb}}{F_t^y t_w}} \quad (37)$$

and

$$c_{t(Cardiff)} = \frac{2}{\sin(\Theta_{t(Cardiff)})}\sqrt{\frac{M_{pft}}{F_t^y t_w}} \quad (38)$$

where

$$M_{pf} = 0.25F_{yf}b_f t_f^2 \quad (39)$$

is the plastic moment resistance of the flanges, neglecting any reduction due to axial force within the flanges due to flexure and development of the web shear strength (additional subscripts t and b denote the top and bottom flanges respectively). The shear capacity predicted by the Cardiff equations is based on an assumed equilibrium stress field (i.e., tension field) in the girder, which satisfies the theoretical conditions for a lower-bound strength prediction provided that the material possesses sufficient ductility for the tension field to develop. One should note that in general it is possible to reach a maximum strength in a full nonlinear analysis (i.e., an analysis that includes second-order or geometric nonlinear effects) prior to development of a full plastic collapse mechanism.

5.1.3 Contribution of the Flanges to the Shear Strength

Davies and Griffith (1999) find that they can obtain reasonably accurate predictions of the maximum shear capacity of I girders by combining the Eurocode 3 expressions for the combined buckling and postbuckling contribution from the web a contribution from the flanges due to frame action that can be written generally as

$$V_{f(Davies)} = \frac{2M_{pfbr}}{c_{b(Davies)}} + \frac{2M_{pfctr}}{c_{t(Davies)}} \tag{40}$$

where M_{pfbr} and M_{pftr} are evaluated from the equation

$$M_{pfr} = 0.25 F_{yf} b_f t_f^2 \left[1 - \left(\frac{M/S_x}{F_{yf}} \right)^2 \right] \geq 0 \tag{41}$$

(with the subscripts b and t are added to denote the top or bottom flange). The bracketed term in this equation gives the theortical reduction in the plastic flexural strength of a rectangular cross-section due to axial force. Davies and Griffith (1999) are silent about how they calculate this

axial force within the flange elements. In this chapter, the flange axial stress is determined simply as M/S_x, similar to the procedure proposed by Hõglund (1971, 1995, 1996). The moment M in Equation (41) is taken as the average moment between the two plastic hinge locations in the applicable flange (see Figure XX), based on the procedure proposed by Evans (19XX).

Davies and Griffith (1999) propose that the variables $c_{b(Davies)}$ and $c_{t(Davies)}$ in Equation (40) may be expressed as

$$c_{b(Davies)} = d_o\left(0.25 + \frac{1.6 b_{fb} t_{fb}^2 F_{yfb}}{t_w D^2 F_{yw}}\right) \tag{42}$$

and

$$c_{t(Davies)} = d_o\left(0.25 + \frac{1.6 b_{ft} t_{ft}^2 F_{yft}}{t_w D^2 F_{yw}}\right) \tag{43}$$

These equations are also based on Hõglund's theory.

In the Cardiff model, the contribution of the flanges to the shear strength due to frame action may be written as

$$V_{f(Cardiff)} = \frac{2M_{pfc}}{c_{c(Cardiff)}} + \frac{2M_{pfct}}{c_{t(Cardiff)}} \tag{44}$$

if the reduction in the flange plastic bending resistance due to the axial stresses in the flanges is neglected. Porter et al. (1975), Evans (19XX), Evans et al. (1979), and Davies and Griffith (1999) suggest various approaches to account for interaction between shear and flexural strengths in the context of the Cardiff model (including a reduction in the flange plastic resistances in Equation (44) due to flange axial stresses as well as other theoretical interaction effects). The approach discussed by Davies and Griffith (1999) is the simplest, and is the one adopted in this chapter. In this approach, the shear strength contributions are calulated as

described above, and zero reduction is taken in this shear strength due to flexure as long as the maximum moment within the web panel is less than 50 percent of the girder flexural capacity associated only with the yield strength of the flanges, taken here as

$$M_f = \min(b_{fb}t_{fb}F_{yfb}, b_{ft}t_{ft}F_{yft})\left(D + \frac{t_{fc} + t_{ft}}{2}\right) \tag{45}$$

Davies and Griffith (1999) propose a linear reduction in V_f from the value given by Equation (44) to zero as the maximum moment within the web panel increases from $0.5M_f$ to M_f. For the four curved I girders considered in this research, M is always less than $0.5M_f$, and thus no moment-shear interaction is considered.

5.1.4 Ultimate Shear Strength

As noted at the beginning of this section, the maximum shear strength is calculated in each of the four methods studied in this chapter by summing separate contributions. In the AASHTO (2001b) and modified AASHTO equations, the web shear buckling and the postbuckling tension field strengths from Basler's theory are summed to estimate the shear capacity, i.e.,

$$V_{n(AASHTO)} = V_{cr(AASHTO)} + V_{t(AASHTO)} \tag{46}$$

and

$$V_{n(Mod\ AASHTO)} = V_{cr(Mod\ AASHTO)} + V_{t(Mod\ AASHTO)} \tag{47}$$

No direct contribution of the flanges is considered, although as noted previously, an implicit contribution of the flanges associated with anchorage of the tension field is included. Davies and Griffith (1999) do not distinguish directly between web buckling and postbuckling contributions in their proposed shear strength equation, but they include an explict contribution from frame action of the flanges, i.e.,

$$V_{n(Davies)} = V_{w(Davies)} + V_{f(Davies)} \quad (48)$$

Finally, the Cardiff model includes an explicit calculated contribution from each of the above theoretical categories. That is,

$$V_{n(Cardiff)} = V_{cr(Cardiff)} + V_{t(Cardiff)} + V_{f(Cardiff)} \quad (49)$$

5.2 SHEAR STRENGTH PREDICTIONS FOR THE TEST GIRDERS

Table 7 Shear buckling coefficients

Girder	d_o/D	k_{AASHTO}	k_{ss}	k_{sf}	k_{Lee}
S1	3	5.56	5.78	9.53	8.78
S2	3	5.56	5.78	9.53	8.78
S1-S	1.5	7.22	7.12	10.88	10.13
S2-S	1.5	7.22	7.12	10.88	10.13

Table 8 Shear buckling loads

Girder	D/t_w	$V_{cr(AASHTO)}$ kN (kips)	$V_{cr(ss)}$ kN (kips)	$V_{cr(Mod\ AASHTO)}$ kN (kips)
S1	143	498 (112)	534 (120)	792 (178)
S2	146	463 (104)	494 (111)	729 (164)
S1-S	144	632 (142)	641 (144)	885 (199)
S2-S	148	583 (131)	587 (132)	818 (184)

Table 9 Contributions from theoretical tension field action

Girder	F_y MPa (ksi)	$V_{t(AASHTO)}$ kN (kips)	$V_{t(Mod\ AASHTO)}$ kN (kips)	$V_{t(Davies)}$ kN (kips)	$V_{t(Cardiff)}$ kN (kips)
S1	410 (59.5)	543 (122)	396 (89)	498 (112)	409 (92)
S2	411 (59.6)	534 (120)	400 (90)	485 (109)	405 (91)
S1-S	410 (59.5)	876 (197)	649 (146)	485 (109)	698 (157)
S2-S	411 (59.6)	872 (196)	654 (147)	476 (107)	694 (156)

Table 10 Theoretical angles of tension field versus the range of maximum (tensile) prinicipal strains at rosette locations that experience yielding

Girder	$\Theta_{t(Basler)}$ degrees	$\Theta_{t(Cardiff)}$ degrees	$\Theta_{p1(exp)}$ degrees
S1	9.2	11.6	19 to 48
S2	9.2	11.8	18 to 26
S1-S	12.3	20.6	30 to 35
S2-S	12.3	20.7	30 to 36

Table 11 Flange plastic hinge locations and contributions to shear strength from flange frame action

Girder	$\frac{c_{b(Davies)}}{d_o}$	$\frac{c_{t(Davies)}}{d_o}$	$\frac{c_{b(Cardiff)}}{d_o}$	$\frac{c_{t(Cardiff)}}{d_o}$	$V_{f(Davies)}$ kN (kips)	$V_{f(Cardiff)}$ kN (kips)
S1	0.283	0.283	0.252	0.252	99 (22)	118 (27)
S2	0.285	0.286	0.256	0.258	105 (24)	122 (27)
S1-S	0.283	0.283	0.303	0.301	197 (44)	196 (44)
S2-S	0.286	0.286	0.311	0.311	208 (47)	201 (45)

Table 12 Predicted shear capacties

Girder	$V_{n(AASHTO)}$ kN (kips)	$V_{n(Mod\ AASHTO)}$ kN (kips)	$V_{n(Davies)}$ kN (kips)	$V_{n(Cardiff)}$ kN (kips)
S1	1041 (234)	1188 (267)	1130 (254)	1063 (239)
S2	996 (224)	1125 (253)	1080 (243)	1019 (229)
S1-S	1508 (339)	1535 (345)	1321 (297)	1530 (344)
S2-S	1454 (327)	1472 (331)	1272 (286)	1485 (334)

Table 13 Ratio of predicted shear capacities to measured experimental shear strengths

Girder	$\frac{V_{n(AASHTO)}}{V_{n(Exp)}}$	$\frac{V_{n(Mod\ AASHTO)}}{V_{n(Exp)}}$	$\frac{V_{n(Davies)}}{V_{n(Exp)}}$	$\frac{V_{n(Cardiff)}}{V_{n(Exp)}}$
S1	0.87	0.99	0.94	0.88
S2	0.86	0.98	0.94	0.88
S1-S	1.10	1.12	0.97	1.12
S2-S	1.03	1.04	0.90	1.05

APPENDIX VI. STRAIN HARDENING

The strain hardening modulus and strain hardening strain, E_{st} and e_{st}, were calculated using the method labeled as E_{st2} and suggested as a standard in (ASCE 1971). This method first requires that the point at the apparent onset of strain hardening be identified, but (ASCE 1971) does not provide a precise definition for this point. Therefore, the data point associated with the definition of the yield point elongation per ASTM E8-00b was used for this purpose. This point is established as the intersection between (1) a horizontal line drawn tangent to the curve at the last zero slope and (2) a line drawn tangent to the strain hardening portion of the stress-strain curve at the point of inflection at or after the onset of strain-hardening. For purposes of discussion, this point is referred to here as (e_{ype}, f_{ype}). Given this point, the (ASCE 1971) suggested procedure requires that the points on the stress-strain curve corresponding to strains of $e_1 = e_{ype} + 0.003$ and $e_2 = e_{ype} + 0.01$ be identified. These points are referred to here as (e_1, f_1) and (e_2, f_2). The strain hardening modulus E_{st} is then calculated as the slope of the line between the above two points, i.e.,

$$E_{st} = \frac{(f_2 - f_1)}{(e_2 - e_1)} = \frac{(f_2 - f_1)}{0.007} \tag{50}$$

Finally, the strain hardening strain e_{st} is defined by the intersection of the line through (e_1, f_1) and (e_2, f_2) with a horizontal line at the ordinate $f = f_{ype}$. This procedure is somewhat involved, and Alpsten (1972) suggests an alternate simpler procedure. However, the value of E_{st} determined by the above procedure exhibits the least scatter of experimental values, and it defines the average slope of the part of the stress-strain curve into which most steel members are strain hard-

enened (ASCE 1971). Although the procedure is involved, the method can be programmed if the point (e_{ype}, f_{ype}) is used as the definition of the onset of strain hardening.

Table 5 summarizes the key coupon stress-strain data required for analysis of the girder tests: the modulus of elasticity E, static yield F_y, strain hardening modulus E_{st} and strain at the onset of strain hardeing e_{st} as defined above, the ultimate tensile strength F_u as defined in ASTM E8-00b, and the strain at ultimate e_u. No effects of coupon orientation or of differences in test speeds could be discerned statistically from the data. Figure 2 shows typical stress-strain curves for the flange and web plates of girders S2 and S2-S. Figures 3 and 4 show an enlarged view of these curves within the yield plateau and initial strain-hardening regions, and illustrate the calculation of E_{st} and e_{st} as explained above. The static yield strength was not measured in the coupon tests corresponding to the stress-strain curves shown in these figures.

Table 14 Stress-strain data from tension coupon tests.

Girders	Coupon Location	N		E (GPa)	Avg. Static F_y (MPa)	E_{st} (GPa)	e_{st} (%)	F_u (MPa)	e_u (%)
S1 and S1-S R = 63 630 mm	Web	12	Average	208	410	3.44	1.95	567	14.6
			COV (%)	1.4	3.3	5.9	8.9	1.4	11.1
			Maximum	213	423	3.78	2.13	575	16.0
			Median	209	416	3.43	1.99	569	15.2
			Minimum	203	384	3.07	1.57	548	11.1
	Flanges	8	Average	196	377	3.59	1.59	542	15.6
			COV (%)	1.5	1.4	6.4	17.0	0.4	2.3
			Maximum	200	385	3.97	1.91	545	16.1
			Median	197	376	3.52	1.47	542	15.7
			Minimum	190	372	3.34	1.30	538	15.1

Table 14 Stress-strain data from tension coupon tests.

Girders	Coupon Location	N		E (GPa)	Avg. Static F_y (MPa)	E_{st} (GPa)	e_{st} (%)	F_u (MPa)	e_u (%)
S2 and S2-S R = 36 580 mm	Web	18[1]	Average	202	411	3.36	1.87	564	15.6
			COV (%)	2.3	1.7	7.3	13.7	0.8	4.0
			Maximum	209	419	3.84	2.23	569	16.9
			Median	202	412	3.26	1.82	564	15.6
			Minimum	192	402	3.15	1.60	554	14.6
	Flanges	9[2]	Average	205	397	3.61	1.90	562	15.4
			COV (%)	1.4	0.7	2.9	5.8	0.3	3.8
			Maximum	208	400	3.72	2.00	564	16.3
			Median	206	396	3.63	1.93	562	15.5
			Minimum	200	394	3.47	1.74	559	14.2

[1]Static F_y was measured in six of the 18 tests.

[2]Static F_y was measured in three of the nine tests.

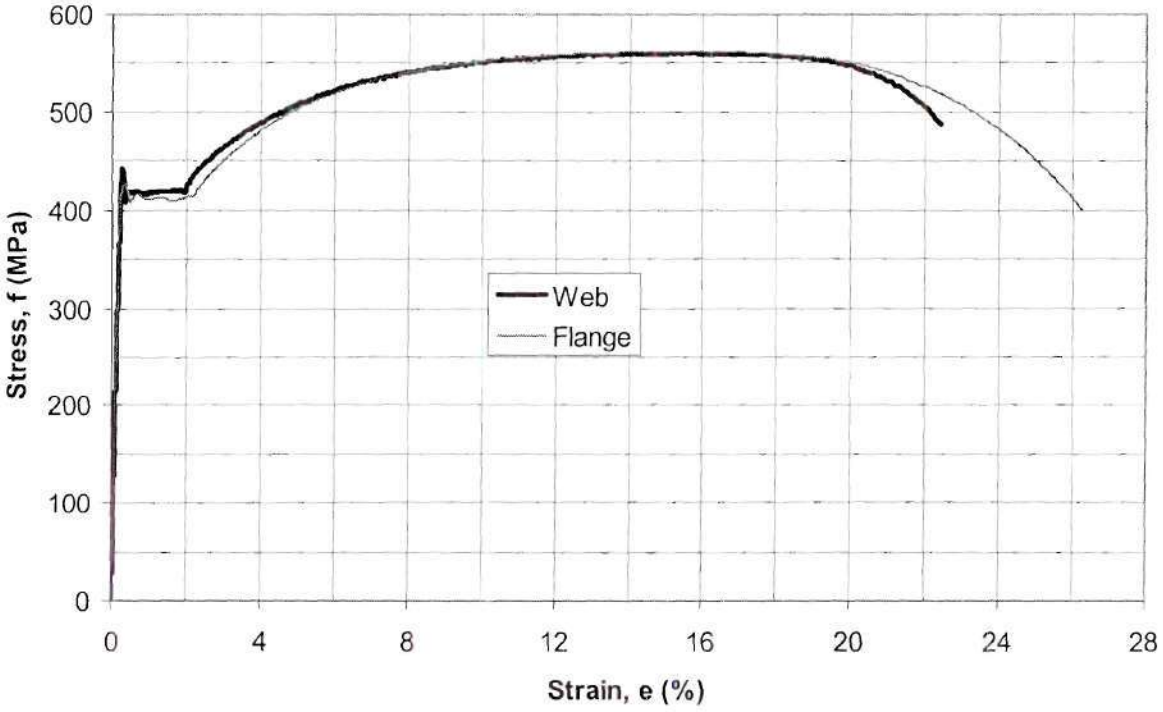

Figure 71 Representative stress-strain curves from tension coupon tests for flange and web plates of girders S2 and S2-S.

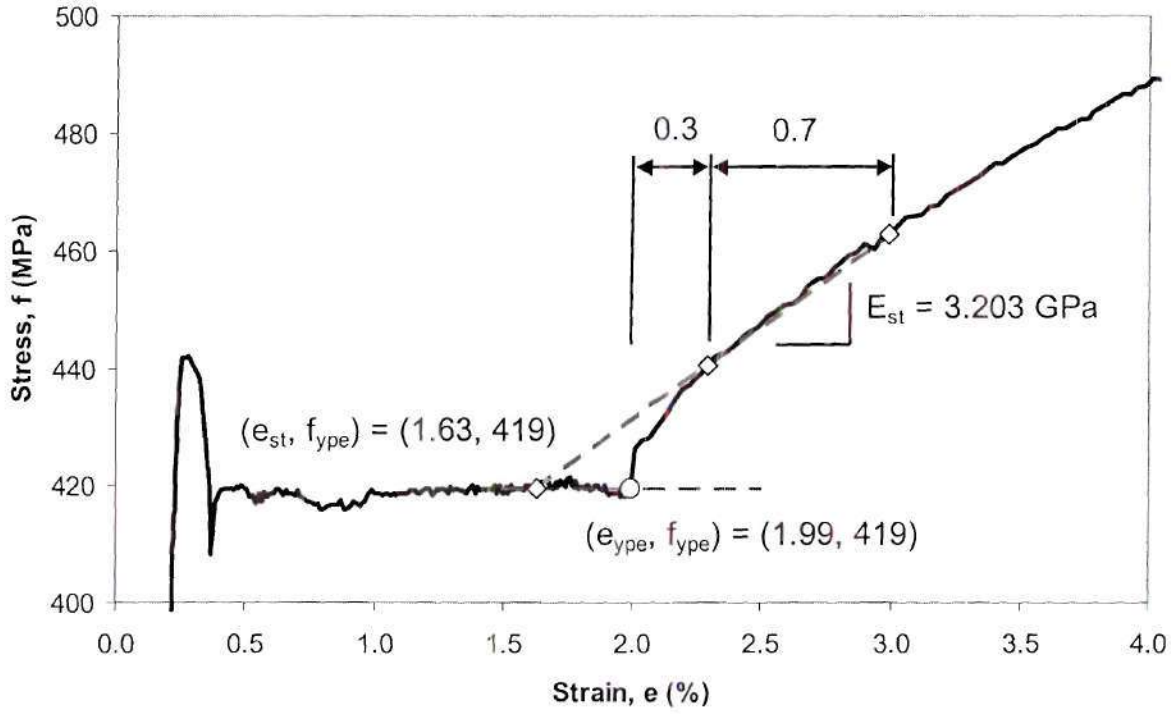

Figure 72 Enlarged view of a typical stress-strain curve for the web plates of Girders S2 and S2-S illustrating the calculation of e_{st} and E_{st}.

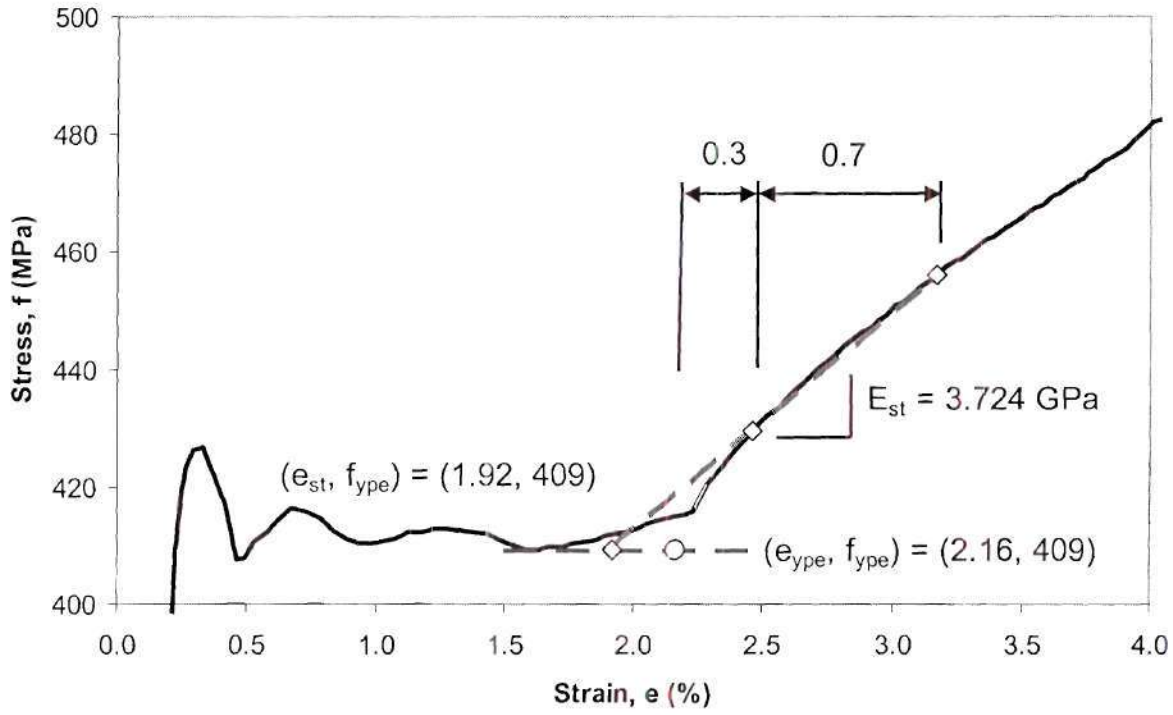

Figure 73 Enlarged view of a typical stress-strain curve for the flange plates of Girders S2 and S2-S illustrating the calculation of e_{st} and E_{st}.

The calulation of e_{st} and E_{st} merits some discussion. Adams et al. (1964) point out that e_{st} depends upon the distribution of inhomogeneities in the tension coupons as well as the amount of prestraining that has taken place in the coupon material before testing. Therefore, the value of this parameter can be highly variable. Adams et al. (1964), ASCE (1971), Alpsten (1972) and Galambos and Ravindra (1978) all indicate considerable variation in values of the strain hardening modulus determined from tension coupon tests, even when the same method of measurement is employed. Also, ASCE (1971) indicates that the value of E_{st} is consistently somewhat higher in compression than in tension. Furthermore, Alpsten (1972) shows that there appears to be some relationship between the strain hardening properties and plate thickness, with E_{st} increas-

ing and e_{st} decreasing with increasing plate thickness. In Table 5, these trends are exhibited in both E_{st} and e_{st} for the S1 and S1-S plates, but only in E_{st} for the S2 and S2-S plates, with no signficant difference between e_{st} for the flanges and web of these girders. Adams et al. (1964) resorted to a special series of tension tests, in which the test was stopped and the specimen held at zero strain rate for a long period of time at and just after the onset of strain hardening, to determine consistent values for E_{st} in their research. Via their special test procedure, they were able to obtain values of E_{st} to within about two percent in 28 of 30 tension coupons. The Adams et al. (1964) tests indicated that the drop in load obtained from static measurements within the strain-hardening region is similar to that within the yield plateau region, and that E_{st} is not sensitive to the time that the specimen is held prior to taking the static measurements. This provides some justification for the use of the e_{st} and E_{st} values determined by the procedures selected in this work along with the measured static F_y values.